REPORT NO. UMTA-MA-06-0025-75-11

WHEEL/RAIL NOISE AND VIBRATION
Volume II: Applications to Control of Wheel/Rail Noise

Paul J. Remington
Michael J. Rudd
István L. Vér

MAY 1975
FINAL REPORT

Prepared for
U.S. DEPARTMENT OF TRANSPORTATION
URBAN MASS TRANSPORTATION ADMINISTRATION
Office of Research and Development
Rail Technology Division
Washington DC 20590

N O T I C E

The contents of this report reflect the views of Bolt Beranek and Newman Inc., which is responsible for the facts and the accuracy of the data presented herein. The contents do not necessarily reflect the official views of the Department of Transportation. This report does not constitute a standard, specification, or regulation.

N O T I C E

The United States Government does not endorse products or manufacturers. Trade or manufacturers' names appear herein solely because they are considered essential to the object of this report.

TECHNICAL REPORT STANDARD TITLE PAGE

1. Report No.	2. Government Accession No.	PB 244 515
UMTA-MA-06-0025-75-11		

4. Title and Subtitle	5. Report Date
WHEEL/RAIL NOISE AND VIBRATION Volume II: Applications to Control of Wheel/Rail Noise	May 1975 6. Performing Organization Code
7. Author(s) Paul J. Remington, Michael J. Rudd, István L. Vér	8. Performing Organization Report No. DOT-TSC-UMTA-75-1.II
9. Performing Organization Name and Address Bolt Beranek and Newman Inc.* 50 Moulton Street Cambridge MA 02138	10. Work Unit No. UM504/R5721 11. Contract or Grant No. DOT-TSC-644-2
12. Sponsoring Agency Name and Address U.S. Department of Transportation Urban Mass Transportation Administration Office of Research and Development Rail Technology Division, Washington DC 20590	13. Type of Report and Period Covered Final Report July 1973 to November 1974 14. Sponsoring Agency Code

15. Supplementary Notes

Under contract to: U.S. Department of Transportation
Transportation Systems Center
Kendall Square
Cambridge MA 02142

16. Abstract Reported here are the final results of a project under the UMTA Urban Rail Supporting Technology Program to develop a basic understanding of urban transit wheel/rail noise control measures. Analytical models of impedance, response, radiation efficiency, and directivity of wheels and rails are presented and compared with field and laboratory measurements. Analytical formulas for the prediction of noise in the three general categories of wheel/rail noise - squeal, impact, and roar - are presented and verified by comparison with laboratory measurements as well as field measurements using a small steel-wheeled personal rapid transit vehicle on a test track. In general, the agreement between the predictions and the measurements is adequate to verify the formulas, although uncertainties in the wheel/rail stick-slip curve and significant variations in roughness across the faces of wheels and rails (measured by a device developed during the program) lead to some uncertainties in the squeal and roar predictions, respectively. A number of new devices for the control of wheel/rail noise are suggested and a number of old techniques are evaluated in light of new information generated during this program. Lastly, testing techniques are suggested for reproducibly evaluating wheel/rail noise control measures. The report is divided into two volumes. The first deals with the theory of wheel/rail noise generation and the second deals with applying the theory to the control of wheel/rail noise.

17. Key Words	18. Distribution Statement
Noise, Transportation Noise, Wheel/Rail Interaction, Noise Control	DOCUMENT IS AVAILABLE TO THE PUBLIC THROUGH THE NATIONAL TECHNICAL INFORMATION SERVICE, SPRINGFIELD, VIRGINIA 22161 PRICES SUBJECT TO CHANGE

19. Security Classif. (of this report)	20. Security Classif. (of this page)	21. No. of Pages	22. Price
Unclassified	Unclassified		

Form DOT F 1700.7 (8-69)

iv

TABLE OF CONTENTS

VOLUME I

TABLE OF CONTENTS *(Cont'd.)*

VOLUME II

TABLE OF CONTENTS *(Cont'd.)*

TABLE OF CONTENTS *(Cont'd.)*

TABLE OF CONTENTS *(Cont'd.)*

LIST OF FIGURES

VOLUME I

LIST OF FIGURES *(Cont'd.)*

LIST OF FIGURES *(Cont'd.)*

LIST OF FIGURES *(Cont'd.)*

VOLUME II

LIST OF FIGURES *(Cont'd.)*

LIST OF FIGURES *(Cont'd.)*

LIST OF FIGURES *(Cont'd.)*

LIST OF FIGURES *(Cont'd.)*

3. VERIFICATION OF PREDICTION FORMULAS FOR WHEEL/RAIL NOISE

In this section we describe measurements of wheel/rail noise that were performed at the Champ Carry Technical Center test track of Pullman Standard (P-S) in Hammond, Indiana, as well as a number of scale-model impact noise measurements made at BBN. We compare both sets of measurements with predictions based on the analytical/empirical formulas of Sec. 2. At P-S, we measured the noise produced by the interaction of the steel wheels of a small PRT (personal rapid transit) vehicle with the rails of the test track. Ideally, we would have been able to perform measurements on a full-scale transit system, but the magnitude of the costs and the complexity of the logistics involved discouraged us from taking that approach at this stage. In fact, since the PRT vehicle has flanged steel wheels and the test track has steel rails basically the same, except for size, as those in a full-scale transit system, the wheel/rail interaction and noise production mechanisms should be essentially the same in both cases. Consequently, if our predictions agree with the measurements of noise and vibration from the PRT vehicle on the test track, there is strong reason to believe that predictions based on the analyses in Sec. 2 will also agree with measurements on full-scale transit systems. Similar arguments apply to the scale-model impact noise measurements.

3.1 Description of P-S Tests

3.1.1 The PRT vehicle

As mentioned above, P-S operates a small PRT vehicle on a test track at their Champ Carry Technical Center. This vehicle, originally fabricated as an engineering test model, is shown in Fig. 3.1-1. The PRT has four 14 in. (35.5 cm) diameter steel

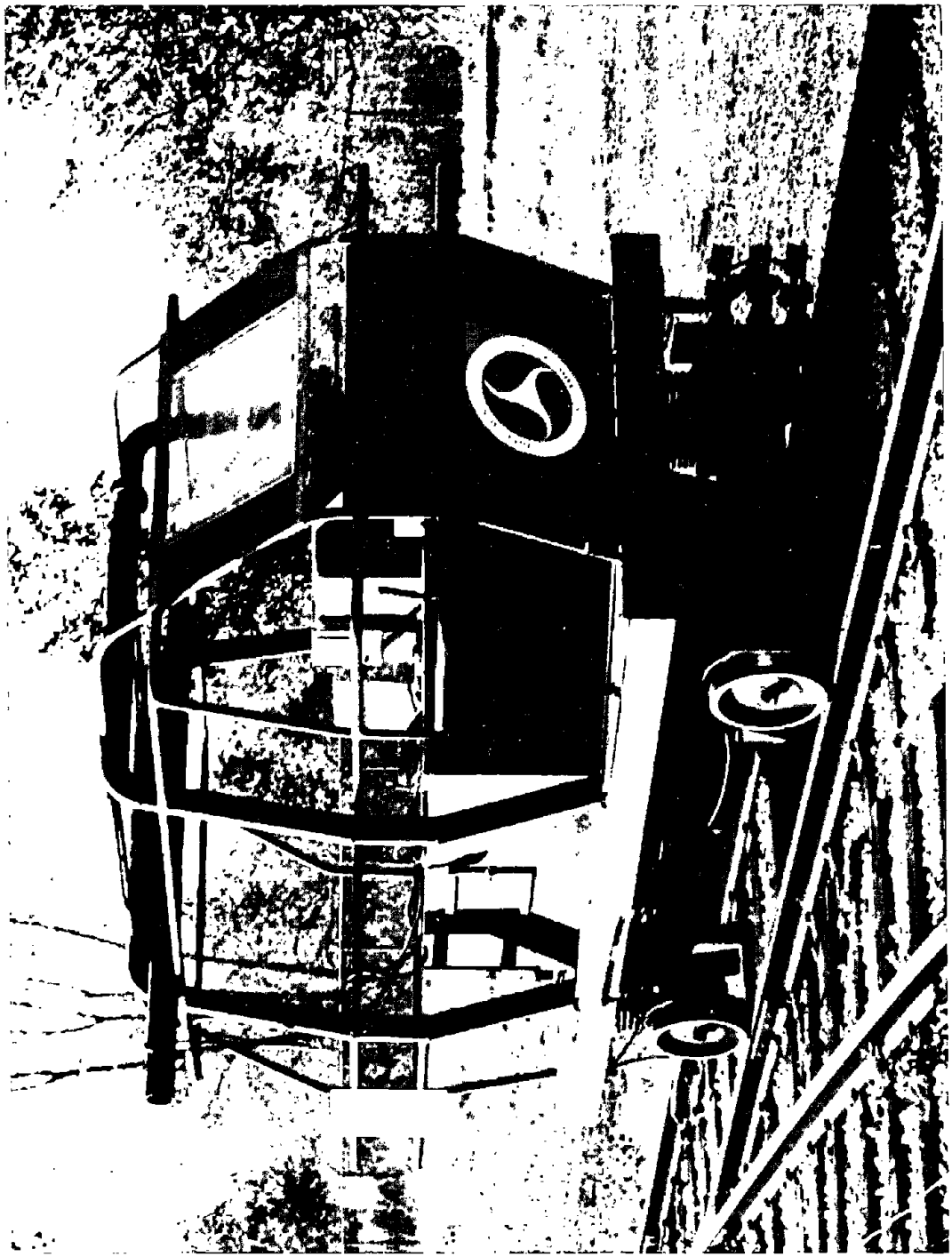

FIG. 3.1-1. PRT VEHICLE AT PULLMAN STANDARD.

wheels, each of which is individually powered by a hydraulic motor. The forward and aft bolsters (metal frames containing the two hydraulic motors and the associated wheel bearings) are each suspended independently on four coil springs with hydraulic dampers. Figure 3.1-2 shows some details of the suspension system. Specifications for the vehicle are given in Table 3.1-1.

TABLE 3.1-1. VEHICLE SPECIFICATIONS

Vehicle weight	6500 lb (2950 kg)
Wheel base	8 ft (2.43 m)
Width over side sills	4.5 ft (1.38 m)
Length over end sills	12 ft (3.66 m)
Height of the floor above the rail	~2 ft (0.61 m)
Extreme height of vehicle	~7 ft (2.13 m)

3.1.2 Test track

The test track, shown in Fig. 3.1-3, is an oval ~1/3 mile (0.53 m) around with a spur leading to two successive 30 ft (9.2 m) radius curves. The oval contains 70 ft (21.4 m), 80 ft (24.3 m), and 90 ft (27.4 m) radius curves and both welded and bolted ASCE 60 lb/yd (30 kg/m) steel rail at 42 in. (1.07 m) gauge. The rail is laid on wood ties 4 in. × 6 in. × 6 ft (10 cm × 15.2 cm × 1.83 m) on crushed limestone ballast. A three-phase power rail is located on the inner side of the oval and on the westerly side of the spur.

FIG. 3.1-2. CLOSE-UP OF THE WHEEL AND SUSPENSION OF THE PRT VEHICLE SHOWING THE BOOM MICROPHONE AND WHEEL VIBRATION TELEMETRY INSTRUMENTATION.

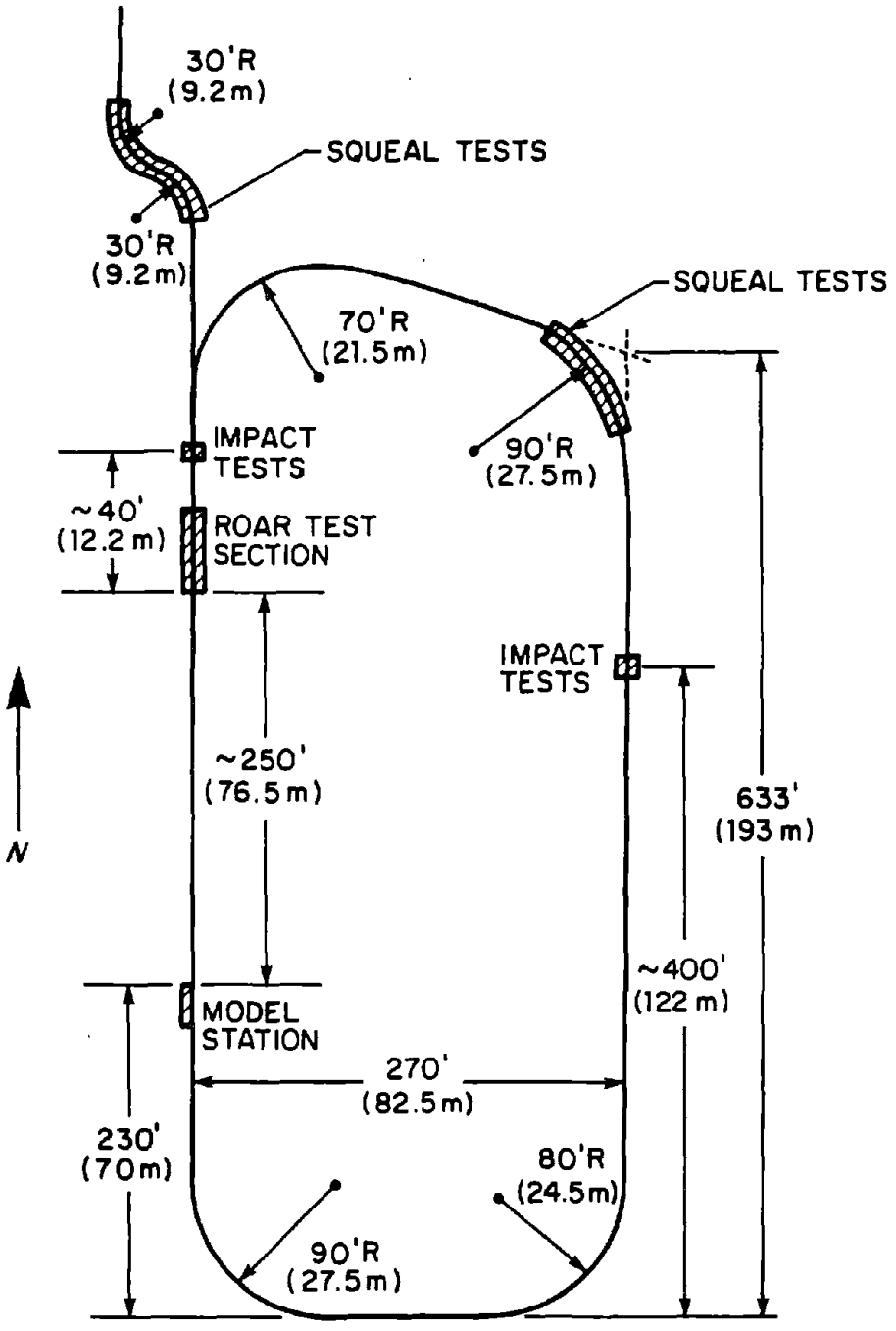

FIG. 3.1-3 PULLMAN STANDARD TEST TRACK

Measurements of squeal noise were made on the 30 ft (9.2 m) and 90 ft (27.4 m) radius curves as shown in Fig. 3.1-3. A section of tangent welded rail north of the station on the west leg of the oval was selected for measurements of roar noise. Two points, one just north of the roar noise section and one on the east leg of the oval, were selected for impact noise measurements.

3.1.3 Test wheels

Noise and vibration measurements were made for three wheel types – standard, resilient, and damped.* The standard wheel was a 14 in. (35.5 cm) running tread diameter flanged steel wheel weighing approximately 140 lb (63.5 kg) and made by United States Steel. A half section of the wheel is shown in Fig. 3.1-4. In order to fit the wheel onto the taper-lock attachment on the vehicle axle, the hub of the wheel was faced down to approximately the dotted line in the figure.

After testing the vehicle fitted with the standard wheels, we removed the wheels and applied damping treatment to them* as shown in Fig. 3.1-5. A 1/4 in. (0.63 cm) thick layer of damping material (Lord Corporation LD-400) was glued to the side of the tread. We then glued a steel ring on top of the damping material as shown in Fig. 3.1-5. The result was a contrained damping layer designed to give the wheel a loss factor of between 5 and 10% for axial vibration of the wheel. According

*Note that at the completion of the standard wheel tests, an accident occurred in which the vehicle sustained considerable damage. This damage, combined with modifications made to the power rail for the purpose of obtaining clearance for the wider tread on the resilient and damped wheels, necessitated a 2-month delay between standard wheel testing and tests on the resilient and damped wheels.

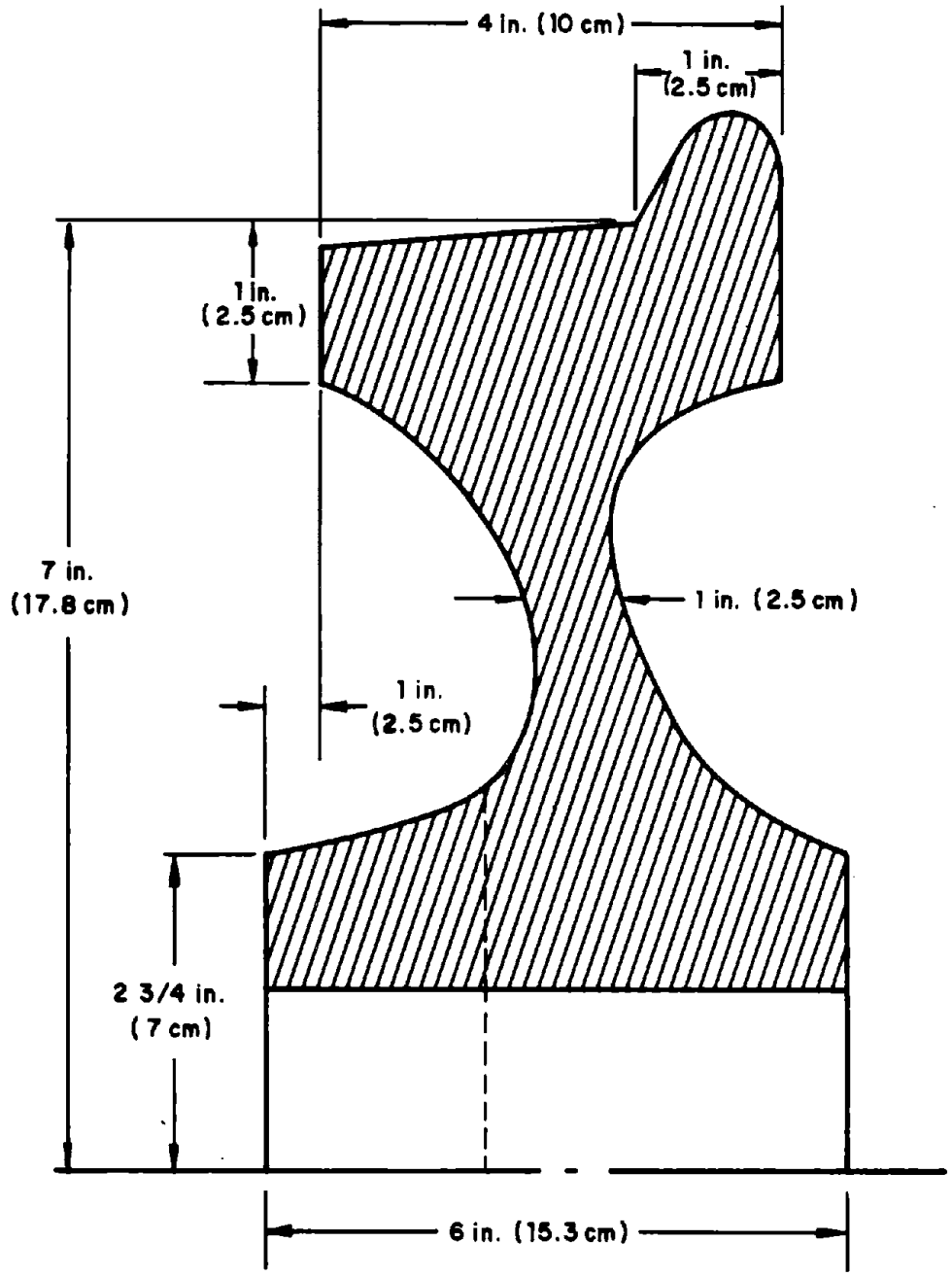

FIG. 3.1-4 STANDARD STEEL WHEEL

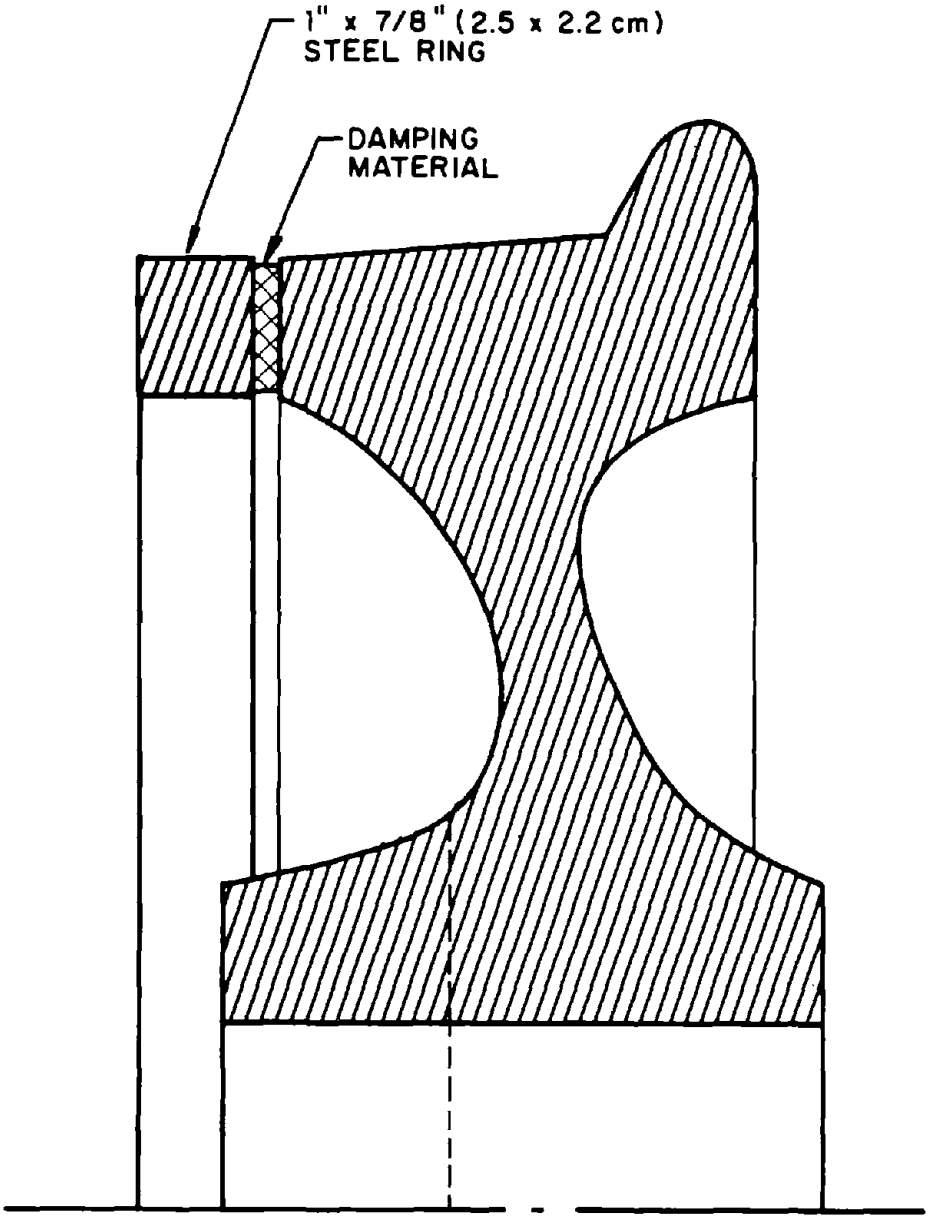

FIG. 3.1-5 DAMPED STANDARD WHEEL

to the predictions in Sec. 2.2, this amount of damping should totally suppress squeal. Before applying the treatment to the PRT wheels, we similarly damped a 14 in. (35.5 cm) diameter wheel* in the laboratory and measured the bandwidth of the wheel resonances before and after the treatment. After the treatment only one resonance at ~1800 Hz could be found; all others had been totally suppressed. This one resonance had a loss factor of 1.3%, somewhat less than expected.

The third type of wheel tested was a 14 in. (35.5 cm) diameter Penn Cushion resilient wheel made by Friedrich Krupp Hüttenwerke A.G. in Germany and marketed in this country by the Penn Machine Co. A half section of the wheel is shown in Fig. 3.1-6. The wheel is steel and weighs 92 lb (42 kg). The tread is isolated from the web by rubber pads spaced at regular intervals around the circumference. There is no published information on the stiffness of the resilient layer, i.e., the deflection of the tread relative to the rim under load. We attempted to determine this stiffness by measuring the wheel deflection under the weight of the PRT vehicle [~1625 lb (736 kg)] per wheel. Unfortunately, the tests were inconclusive, showing only that the deflections were less than 10 mils (0.25 mm) — the lower limit of the calipers we were using for the measurement.

3.1.4 Instrumentation

Both the noise radiated by the wheel/rail interaction and the vibration of the rail and bolster were measured during the roar and impact noise testing. During the squeal noise test,

*The wheel was the same as the PRT wheel except that the hub was not faced.

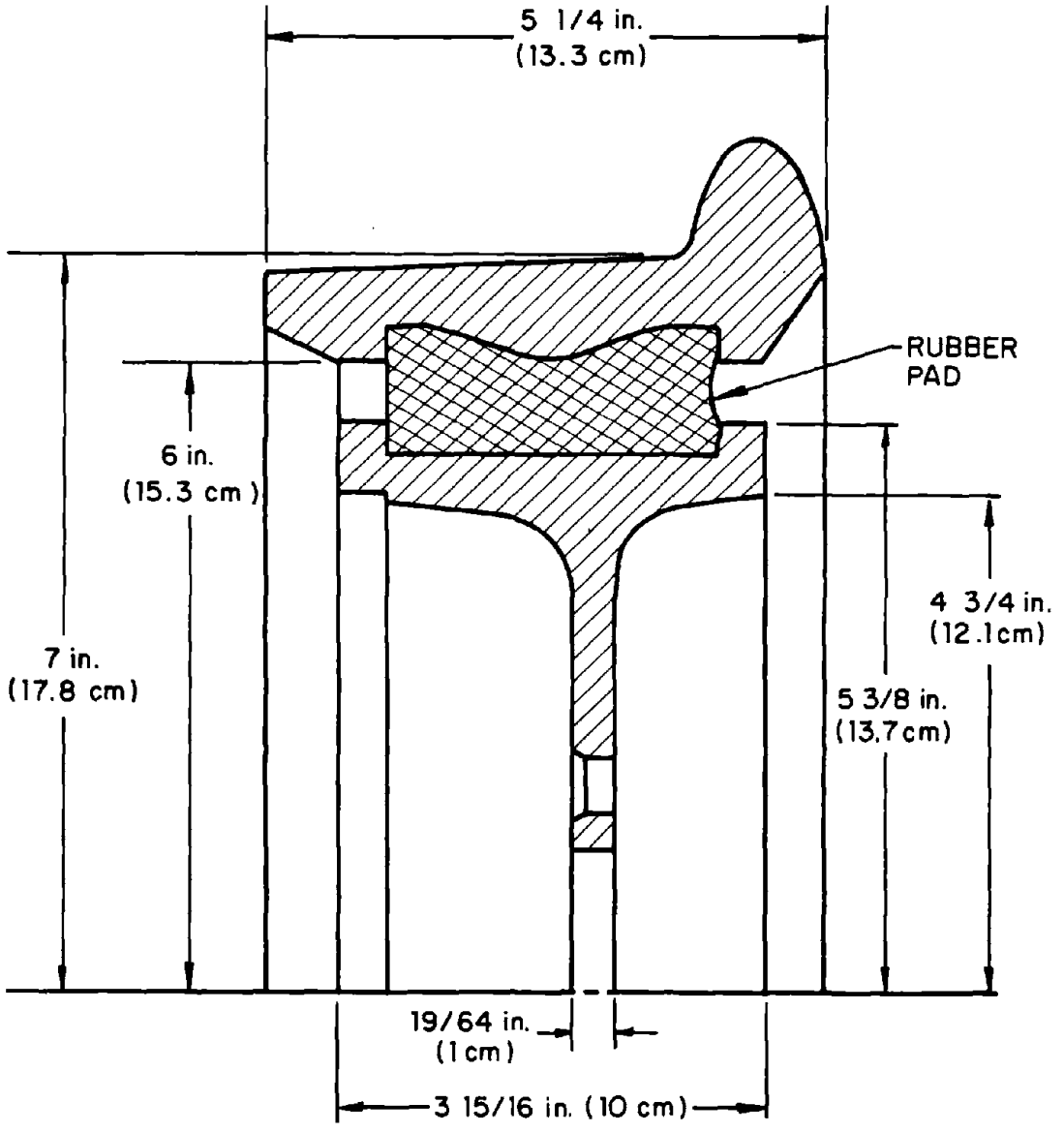

FIG. 3.1-6 PENN CUSHION RESILIENT WHEEL

only the noise radiated by the vehicle was measured, although an attempt was made to telemeter wheel vibration data (see Fig. 3.1-2). Low dynamic range and high electronic noise in the transmitter prevented us from obtaining good data.

The noise was measured by a microphone hung on a boom suspended from the vehicle such that the microphone was 3 ft (0.91 m) from the face of the wheel on the axis of the wheel. The microphone always hung on the opposite side of the vehicle from the power rail. The arrangement of the microphone and boom is shown in Fig. 3.1-2.

The bolster acceleration in the vertical direction was measured with an accelerometer attached to the metal frame forming the bolster. The accelerometer was located near the wheel nearest the boom microphone.

The rail acceleration was measured with two accelerometers, one attached beneath the rail head to measure vertical rail vibration and one attached to the side of the rail head or the center of the web to measure horizontal rail vibration.

The instrumentation chain used for these measurements is shown in Figs. 3.1-7 and 3.1-8. Note that the chain differed slightly between the standard wheel tests and the resilient and damped wheel tests. Also, since no bolster acceleration data were recorded during the sound pressure level measurements of squeal and roar for resilient and damped wheels, a single-track Kudelski Nagra III tape recorder was used to record the sound pressure level data.

3.2 Squeal Model Verification

As described above, squeal noise was measured for the PRT vehicle on curves of 30-ft (9.15 m) and 90-ft (27.4 m) radius. The vehicle was run through the curves at a range of speeds, and the squeal was measured by the boom-mounted microphone.

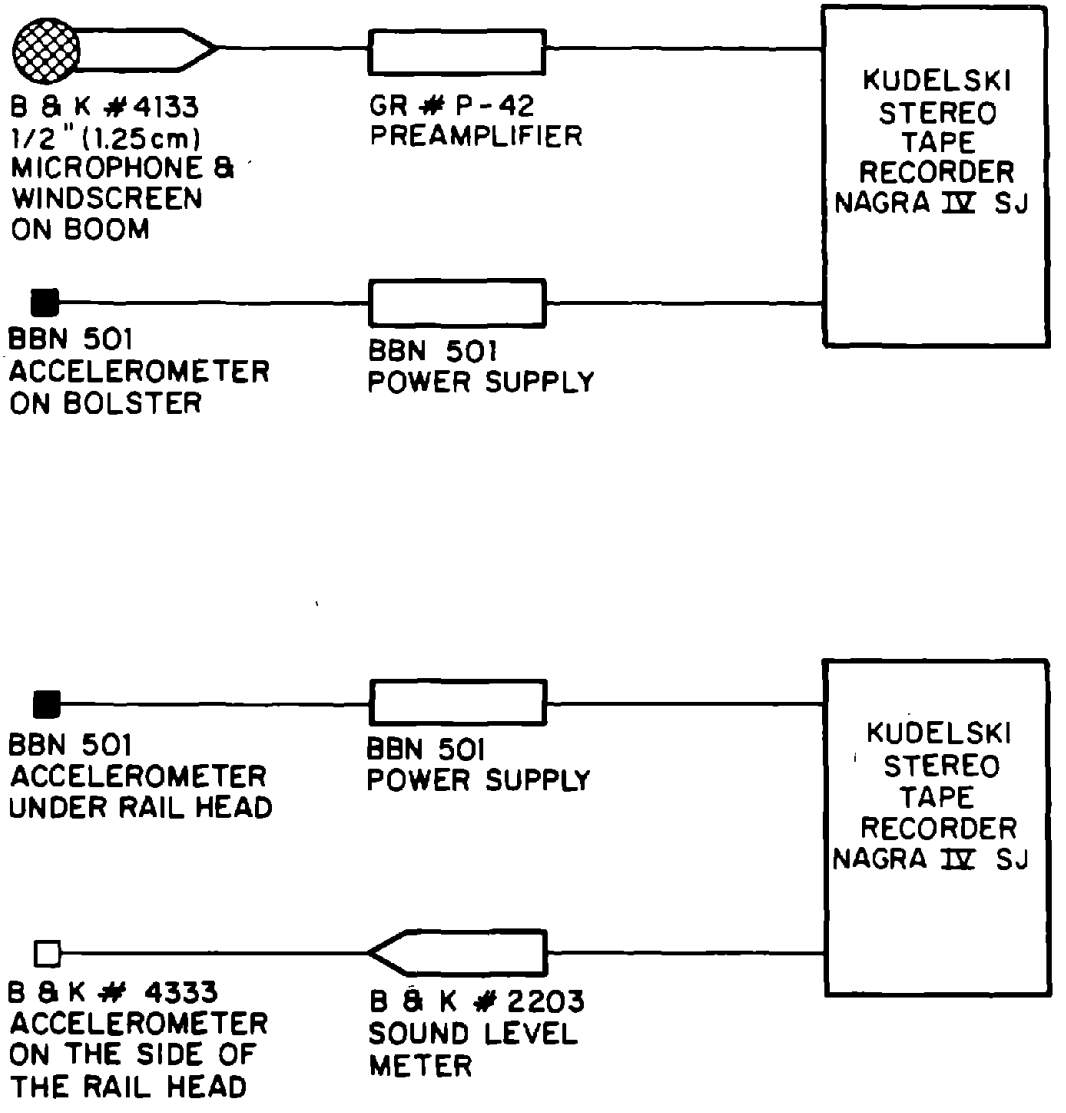

FIG. 3.1-7 INSTRUMENTATION FOR THE STANDARD WHEEL TESTS

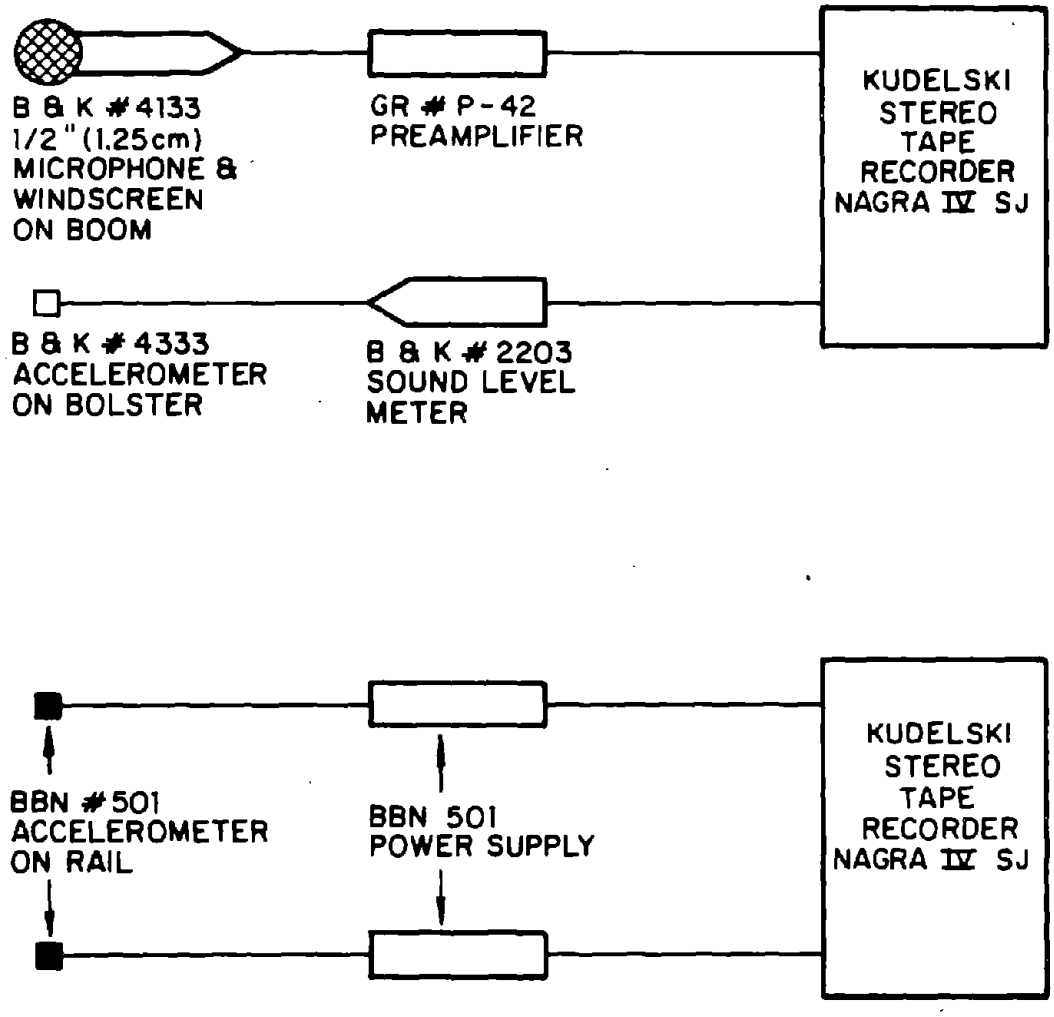

FIG. 3.1-8 INSTRUMENTATION FOR THE DAMPED AND RESILIENT WHEEL TESTS

3.2.1 Sound level of squeal

Figures 3.2-1 and 3.2-2 show the measured sound level of the squeal as a function of vehicle speed in the curve for the 90-ft (27.4 m) and 30-ft (9.15 m) radius curves respectively. The figures also show the theoretical predictions for these conditions. There is considerable scatter in the results which may be caused by the differences in track conditions at different times. However, another, more serious, source of uncertainty is the uncertainty as to which wheel was squealing. These measurements were made with a microphone placed only 3 ft (.915 m) from the side of the car. There is clearly a large difference in level depending upon whether a wheel close to the microphone or one far away is squealing. The predicted levels for all four wheels are plotted in these figures. It seems that the wheel closest to the microphone was rarely the one to squeal. On the 30-ft (9.15 m) curve, the levels for the other wheels are within ±5 dB of most of the measurements. On the 90-ft (27.4 m) curve, the predictions for the wheels other than the closest are about 5 dB higher than the mean measured value. However, bearing in mind the assumptions that had to be made in the model and the uncertainty in the condition of the rail, the investigators consider this agreement to be acceptable.

3.2.2 Squeal frequency

The frequency of each of the squeal events was measured on the 30-ft (9.15 m) and 90-ft (27.4 m) radius curves. The frequency is extremely difficult to measure, since it is generally quite intermittent and conventional analog filters cannot be used. However, using a digital frequency counter, counting over a tenth of a second, and using a sonogram (voiceprint) machine proved successful.

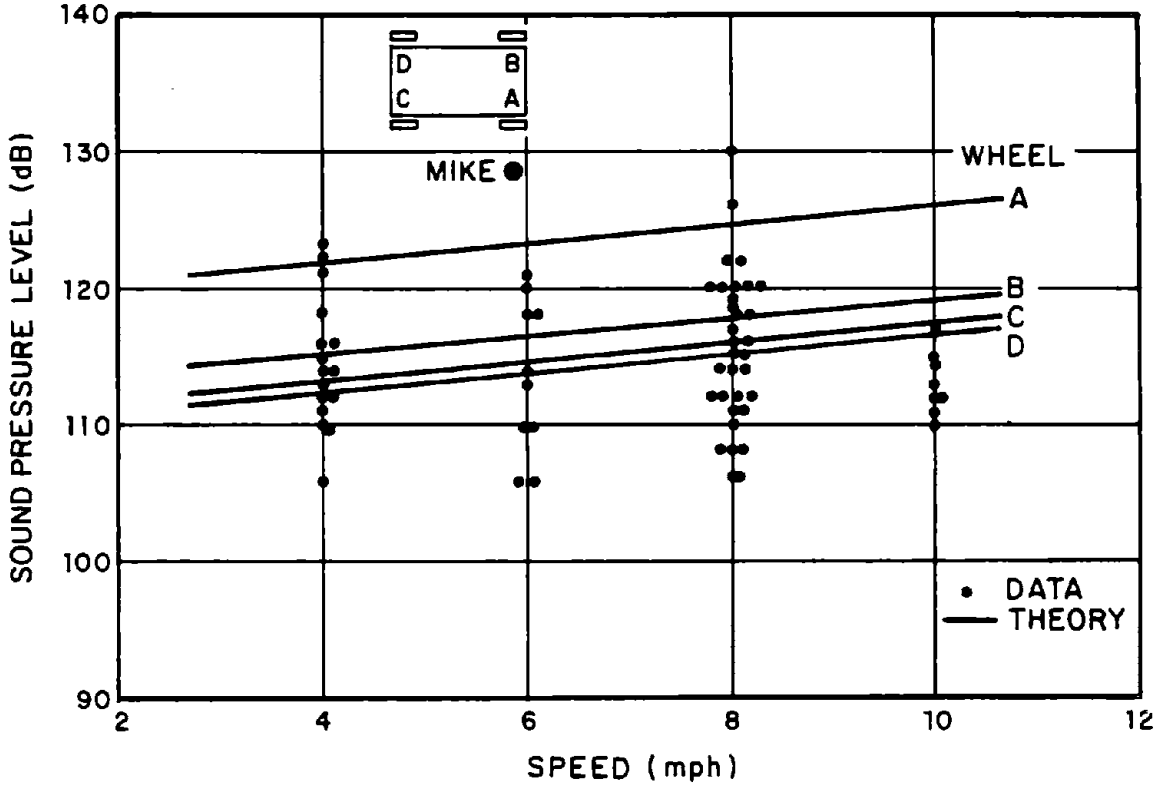

FIG. 3.2-1 SQUEAL SOUND LEVELS VS SPEED ON 30 FT (9.15 m) RADIUS CURVE

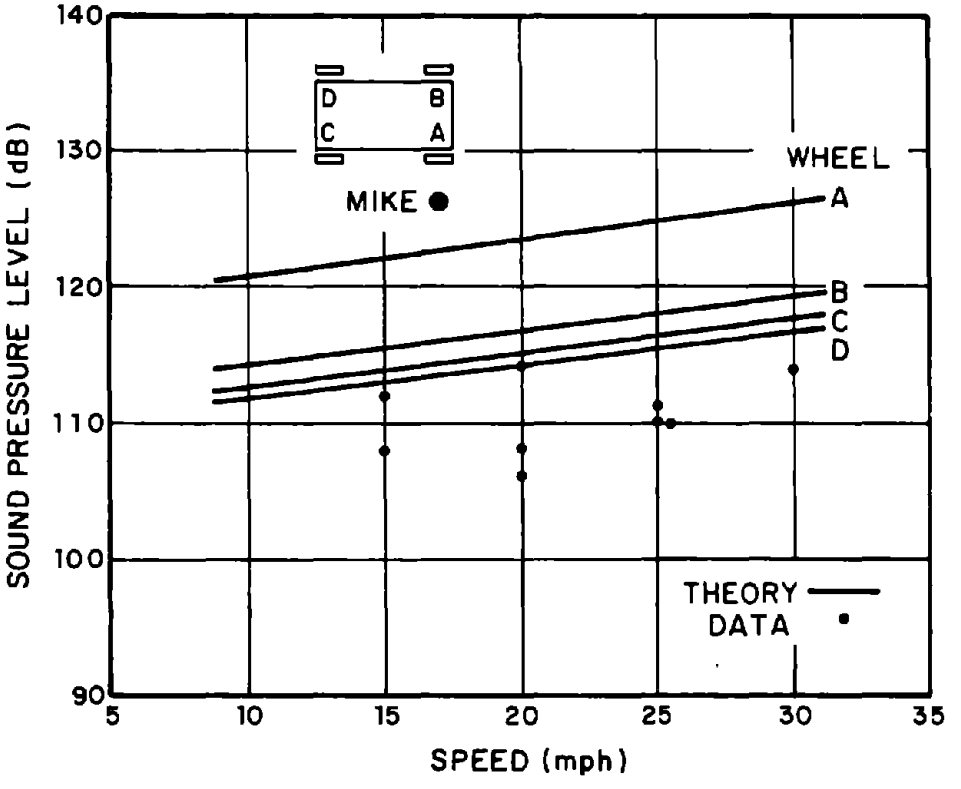

FIG. 3.2-2 SOUEAL SOUND LEVELS VS SPEED ON 90 FT (27.4 m) RADIUS CURVE

The occurrence of squeal in terms of the frequency vs vehicle speed is plotted in Figs. 3.2-3 and 3.2-4 for the 30-ft (9.15 m) and 90-ft (27.4 m) radius curves. There seems to be little relation between the speed and the frequency of the squeal. However, on the 30-ft (9.15 m) radius curve, squeal at 1.75 kHz is much more common than at any other frequency. This is not inconsistent with the model, which states that the mode of lowest frequency will be the most unstable and, hence, most common mode.

The results of the frequency counter measurements for one squeal frequency are shown in Fig. 3.2-5. A significant discrepancy is noticeable. For the squeal mode considered, the natural resonance frequency is 2050 Hz. However, squeal was rarely observed at this frequency, but was lower by about 15%, the squeal frequency varying from 1650 Hz to 1850 Hz. Similar frequency shifts are discovered for other squeal modes. It should be pointed out, however, that the wheel whose resonance was measured was slightly different (Sec. 3.1) from that on the P-S vehicle. This might account for part of the frequency shift, but not the spread in frequencies.

The sonogram analysis showed that even during a particular occurrence, the squeal frequency would vary by discrete steps, with rare occurrences at the natural resonance frequency. This frequency shift is not properly understood at this stage. It is possible that it arises from the loading of the wheel by the rail. The discrete frequency jumps would then occur as the wheel passes over a rail joint. However, the calculated frequency shifts are only about 1% as compared with the 15% observed.

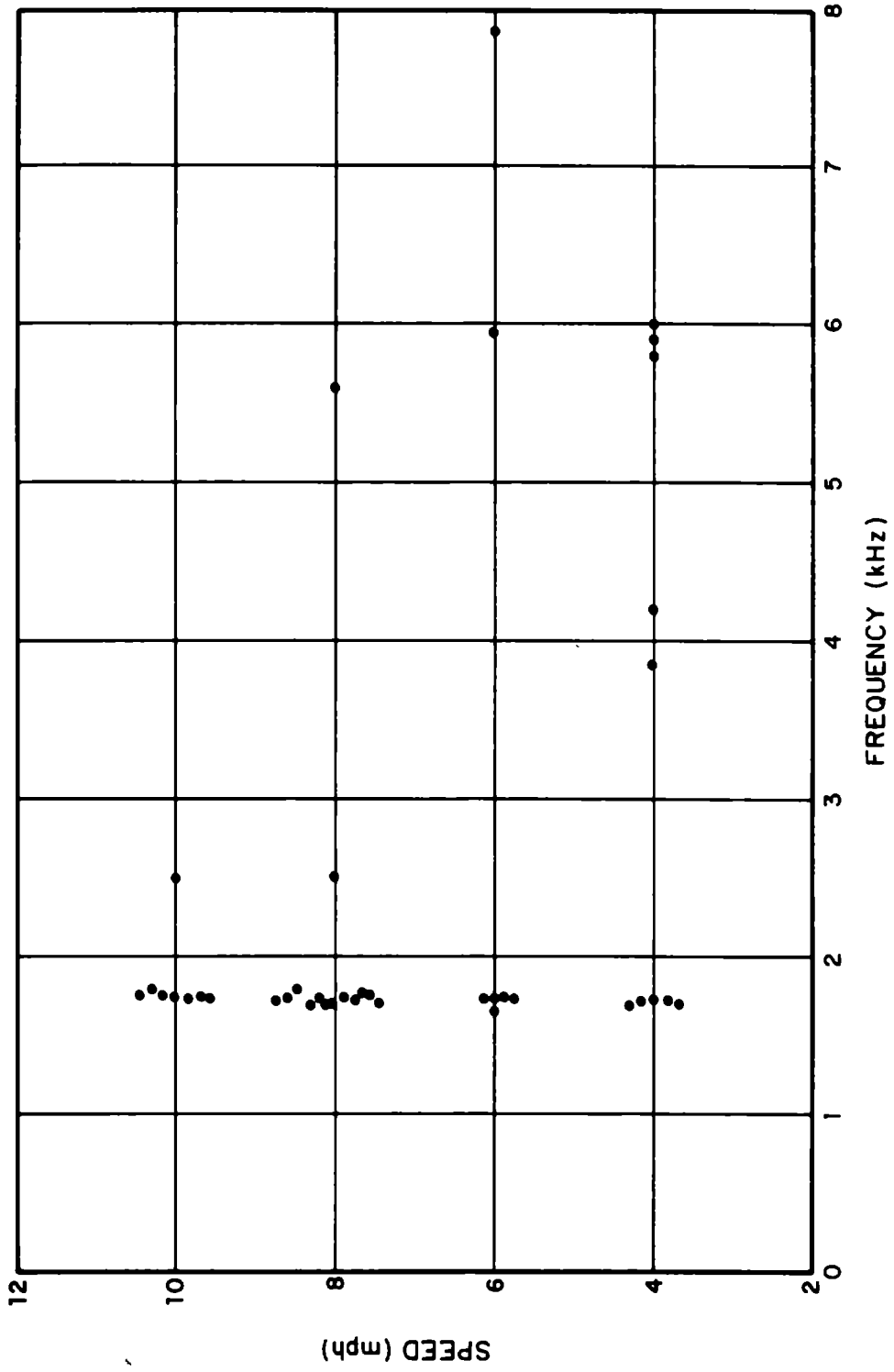

FIG. 3.2-3 OCCURRENCE OF SQUEAL FOR 30-FT (9.15 m) RADIUS CURVE.

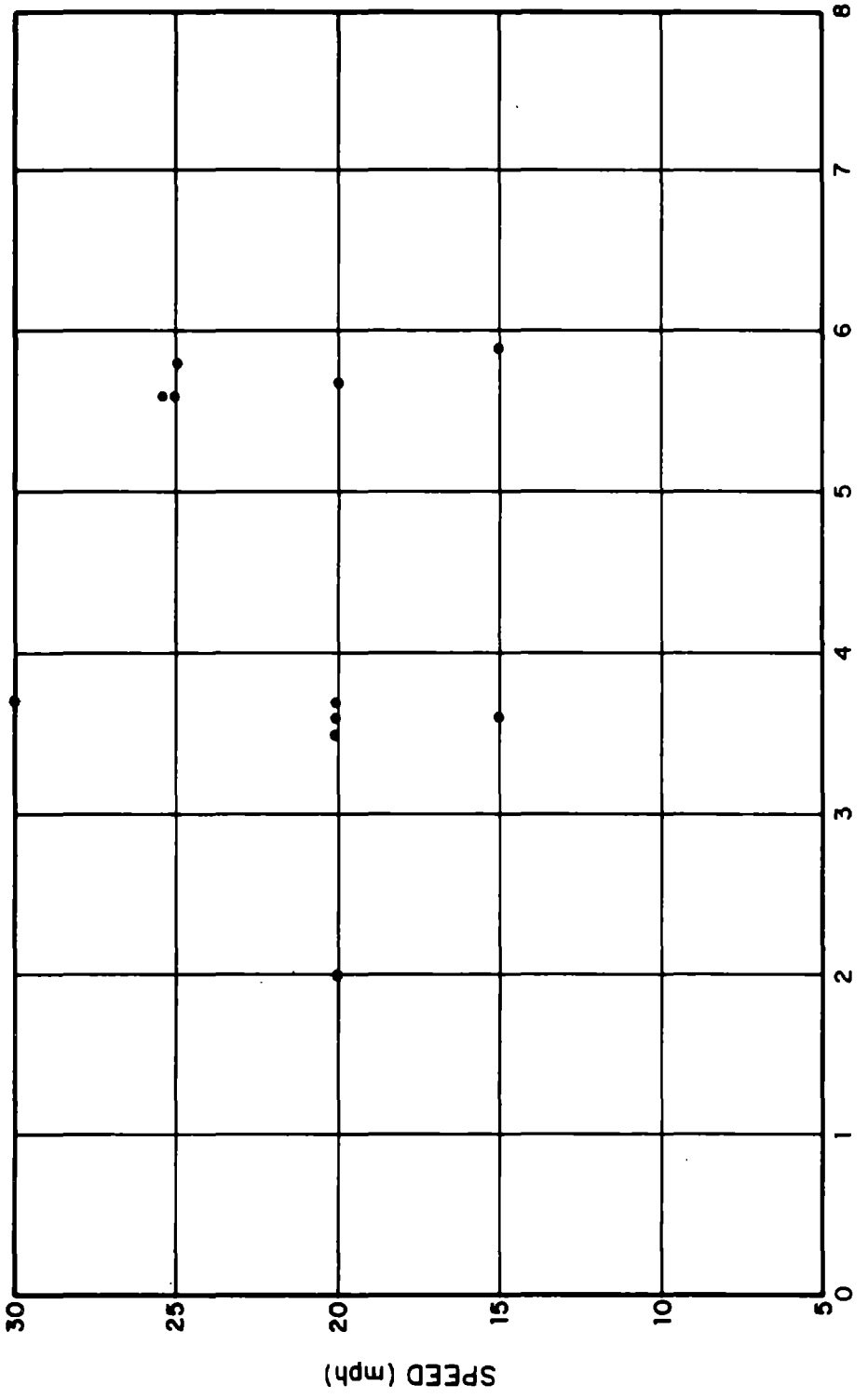

FIG. 3.2-4. OCCURRENCE OF SQUEAL FOR 90-FT (27.4 m) RADIUS CURVE.

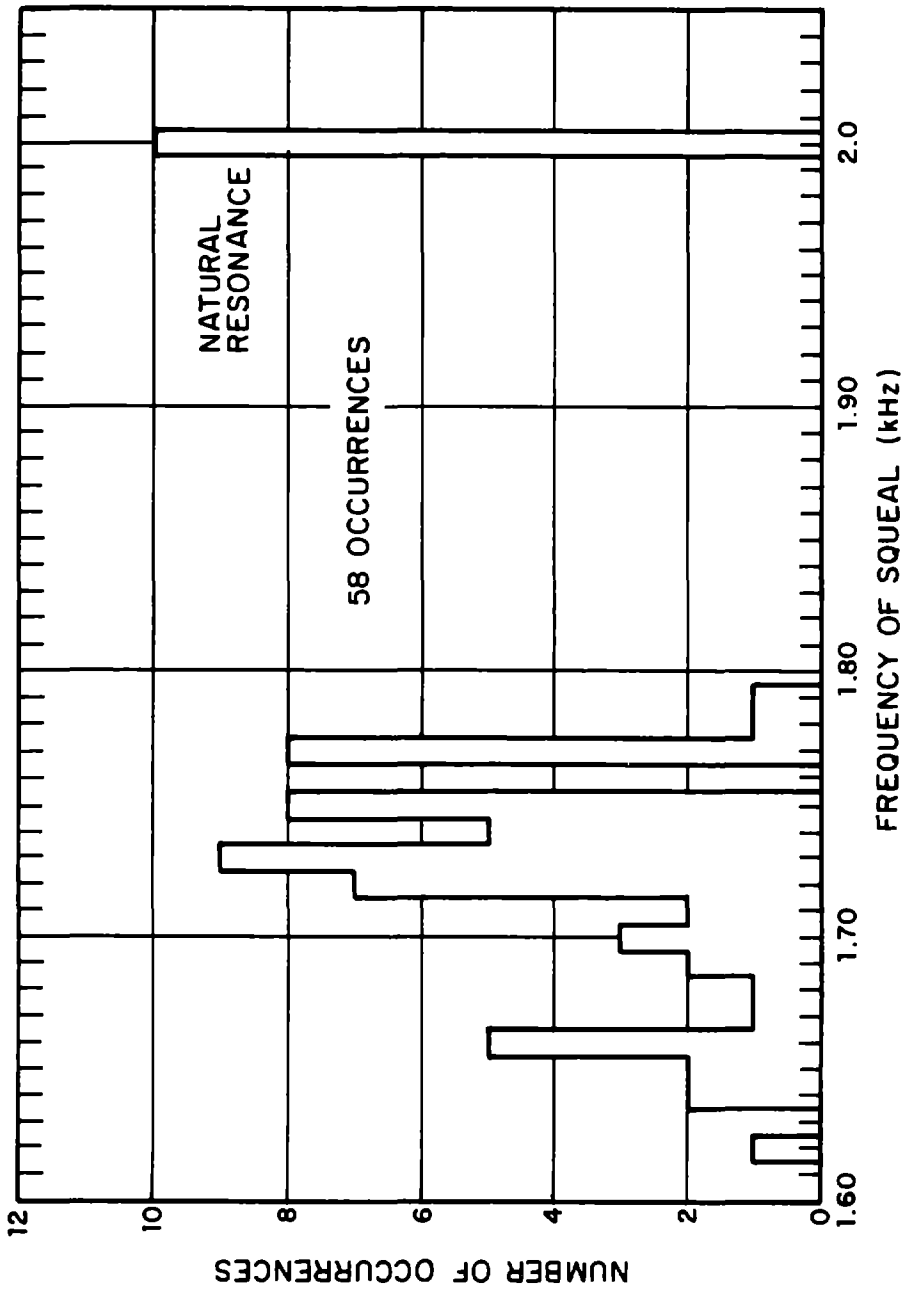

FIG. 3.2-5 HISTOGRAM OF SQUEAL FREQUENCY

3.2.3 Ultrasonic squeal

During the series of tests on the PRT vehicle, we made an unexpected discovery. On the tight, 30-ft (9.15 m) radius curves, squeal was found at a frequency of about 25 kHz, well above the normal range of hearing. The squeal was extremely intense, being 150 to 160 dB, although there was some uncertainty due to uncertainty in the calibration of the recording apparatus. The squeal was so intense that it could be *sensed* as a raspiness in the sound. This ultrasonic squeal could occur alone or in conjunction with an audible squeal. The mode of the squeal appears to correspond to a longitudinal standing wave operating transversly in the wheel tread. The tread sides are nodes, with the center an antinode. It is not known at this stage if the ultrasonic squeal occurs on other transit vehicles, but this does appear to be a very distinct possibility.

3.2.4 Relative sound radiation from wheel and rail

In the model for wheel squeal, it was assumed that the sound was radiated by the wheel. This assumption needed to be verified. For a frequency of 1.75 kHz, we can describe the sound radiated from the wheel or the rail in terms of the acceleration of the surface as follows.

$$\text{Wheel SPL} = 68 + 20 \log(g/R) \quad \text{dB}$$

$$\text{Rail SPL} = 75 + 20 \log(g/\sqrt{R}) \quad \text{dB} ,$$

where g is the mean acceleration of the surface and R is the distance of the observer in meters. Now, the impedance of the rail was measured as 3000 lb sec/ft at 1.75 kHz and the impedance of the wheel at this resonance was measured as 7.5 lb sec/ft. Since equal and opposite forces act between wheel and rail, the

velocity of the wheel at resonance must be 400 times greater than the velocity of the rail. Therefore,

$$\frac{L_p \text{ due to wheel}}{L_p \text{ due to rail}} = 19 - 10 \log R \text{ dB} .$$

Thus, for distances close to the track, the wheel radiation dominates over the rail radiation. However, as we move further away, the noise due to the rail decays less rapidly than that due to the wheel, since the rail behaves like a line source at high frequency and the wheel like a point source. However, when we go more than about one rail length [34 ft (10.3 m)] away from the track, the rail will no longer behave like a line source, because the vibrations cannot propagate across a rail joint. Thus, even far from the track, the wheel radiated sound will dominate over the rail radiated sound. Hence, the assumption in the model that the sound is radiated from the wheel is justified.

3.2.5 Testing of treated wheels

The standard wheels on the Pullman PRT vehicle were replaced by a set of resilient wheels (Penn Cushion) manufactured by Penn Machine Co. and a set of damped wheels made by BBN. The effectiveness of both wheels at reducing or eliminating squeal was investigated. The model of wheel squeal gives the following expression for the damping required to eliminate squeal:

$$\eta_{int} > \frac{P v_{max}}{m \omega_{min} V} .$$

For the PRT vehicle, P = 1500 lb (6700 N), m = 50 lb (22.7 kg), and $\omega_{min} = 10^4$ rad/sec. Thus, to avoid squeal

$$\eta_{int} > \frac{\nu_{max}}{10V} ,$$

with V in ft/sec. There is great uncertainty in the value of ν_{max}, the peak slope of the stick-slip curve. Values can range from 2 to 30. If we take an arbitrary value of ν_{max} of 10, then we will not expect squeal for speeds of

$$V > 1/\eta_{int} \text{ ft/sec} .$$

For the Penn Cushion wheels, when squeal occurred, the observed levels were lower than with a standard wheel by about 10 to 15 dB. In fact, the squeal was comparable to the roar noise and, hence, difficult to measure. The loss factor of the wheels was measured and found to be 8% (±2%). Thus, on the argument presented above, we would not expect squeal at speeds above 8 mph (13 km/h). On the 30-ft (9.15 m) radius curve, a weak squeal was indeed heard only at speeds up to 8 mph (13 km/h). However, on the 90-ft (27.4 m) radius curve, weak squeal was heard up to 20 mph (32 km/h). This may be due to a larger value of ν_{max} on the larger radius curve.

The BBN damped wheels also substantially reduced the level of squeal, when squeal occurred. Indeed, squeal was never heard on the 90-ft (27.4 m) radius curve at any speed and only at 4 and 6 mph (6.4 and 9.8 km/h) on the 30-ft (9.15 m) curve.

The loss factor of the damped wheel was generally too large to be measured by the resonant amplication technique employed, except at 1850 Hz. This means that the loss factor was generally well in excess of 10% except at 1850 Hz where it was only 1.3%.

In conclusion, it appears that both the resilient wheel, with its significant loss factor, and the damped wheel do significantly reduce or eliminate the wheel squeal.

3.3 Experimental Verification of the Impact Noise Model

Limited scale-model experiments at BBN and full-scale experiments at Pullman Standard were carried out to give some preliminary verification of the analytical model developed in Sec. 2.3. These experiments and their results are discussed briefly in the following two subsections.

3.3.1 Scale-model experiments

To validate experimentally the analytical model of impact noise generation caused by rail discontinuities, we performed a scale-model study using BBN's 1:8-scale-model railway facility. The facility consists of a 1:8-scale three-axle steel locomotive bogie and aluminum magnesium alloy rails. Both the bogie and the rail are precise geometric scale models of an actual locomotive truck and rail. Since the experimental program was restricted to evaluation of the dependence of the impact noise on train speed and on the height difference of the joint, no attempt was made to scale exactly the dynamic properties of a full-scale bogie and track.

The bogie frame, shown in Fig. 3.3-1, is made of cast iron and the wheels and axles are made of steel. The suspension of the wheel set consists of brass leaf springs bearing on the journal boxes, which are free to move in the vertical direction but are restrained in the horizontal direction.

The important parameters of the scale-model facility are:

Total weight of bogie:	62.9 lb (28.5 kg)
Weight of a wheel set (axle plus two wheels):	6.37 lb (2.9 kg)
Weight of bogie frame:	43.75 lb (20 kg)

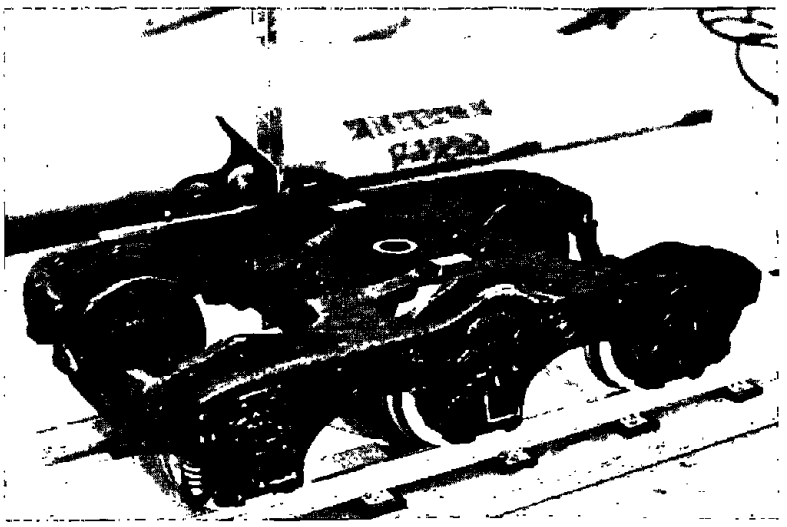

FIG. 3.3-1. PHOTOGRAPH OF THE 1/8-SCALE-MODEL BOGIE.

Spring constant of a single leaf spring:	1175 lb/in. ($2.07 \cdot 10^5$ N/m)
Nominal wheel radius:	2.2 in. (5.6 cm)
Track gauge:	7.25 in. (18.5 cm)

The rail fastening arrangement, as shown in Fig. 3.3-2, consists of model tie plates spaced 5 in. (12.7 cm) apart and nailed through a rubber pad onto a composition board. At the test rail joint, the two adjacent fasteners on either side of the joint were replaced by vertically oriented bolts separated from the rail by rubber pads. The height of the rail could be adjusted by turning the bolts. This arrangement is shown in Fig. 3.3-3.

The 15-ft (4.6 m) long test track was positioned near the center of a semianechoic room. A 1/2-in. (1.27 cm) diameter condenser microphone (B&K Type 4133) was placed 4.5 in. (11.4 cm) to the side of the rail and at the height of the rail head at the joint. The ground in the vicinity of the joint and the microphone was covered by a highly absorptive layer of fiberglass mat to avoid ground reflections which would interfere with the direct sound. For certain runs the vertical acceleration of the run-on rail was also measured by a miniature accelerometer mounted on the underside of the rail. Both the impact sound and acceleration signals were displayed as a function of time on the screen of a calibrated oscilloscope and photographed by a properly triggered camera. The block diagram of the instrumentation used in these scale-model experiments is shown in Fig. 3.3-4.

The truck was accelerated to the required speed by an initial manual push and was running free by the time it reached the portion of the track that contained the experimental rail

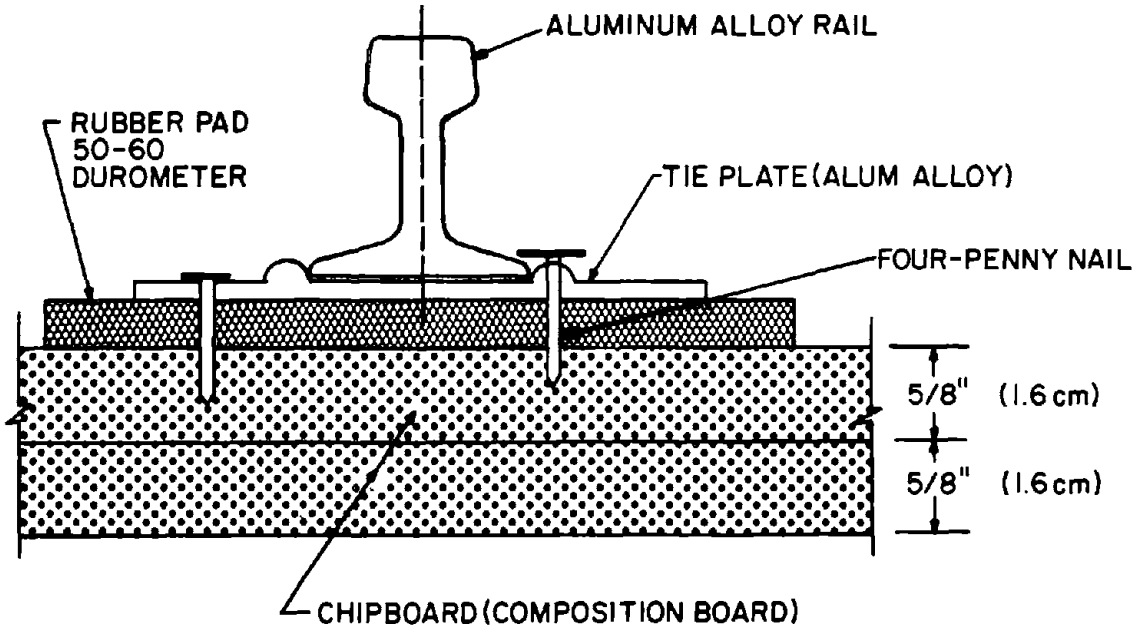

FIG. 3.3-2. SKETCH OF THE 1/8 SCALE MODEL RAIL FASTENING ARRANGEMENT.

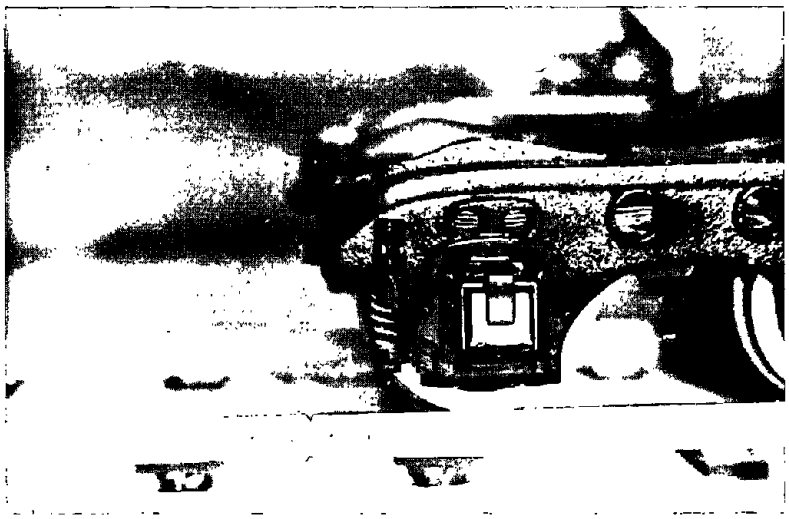

FIG. 3.3-3. PHOTOGRAPH OF THE EXPERIMENTAL 1/8 SCALE MODEL RAIL JOINT, WITH HEIGHT ADJUSTING BOLTS, AND BOGIE, SHOWING DETAILS OF WHEEL SUSPENSION.

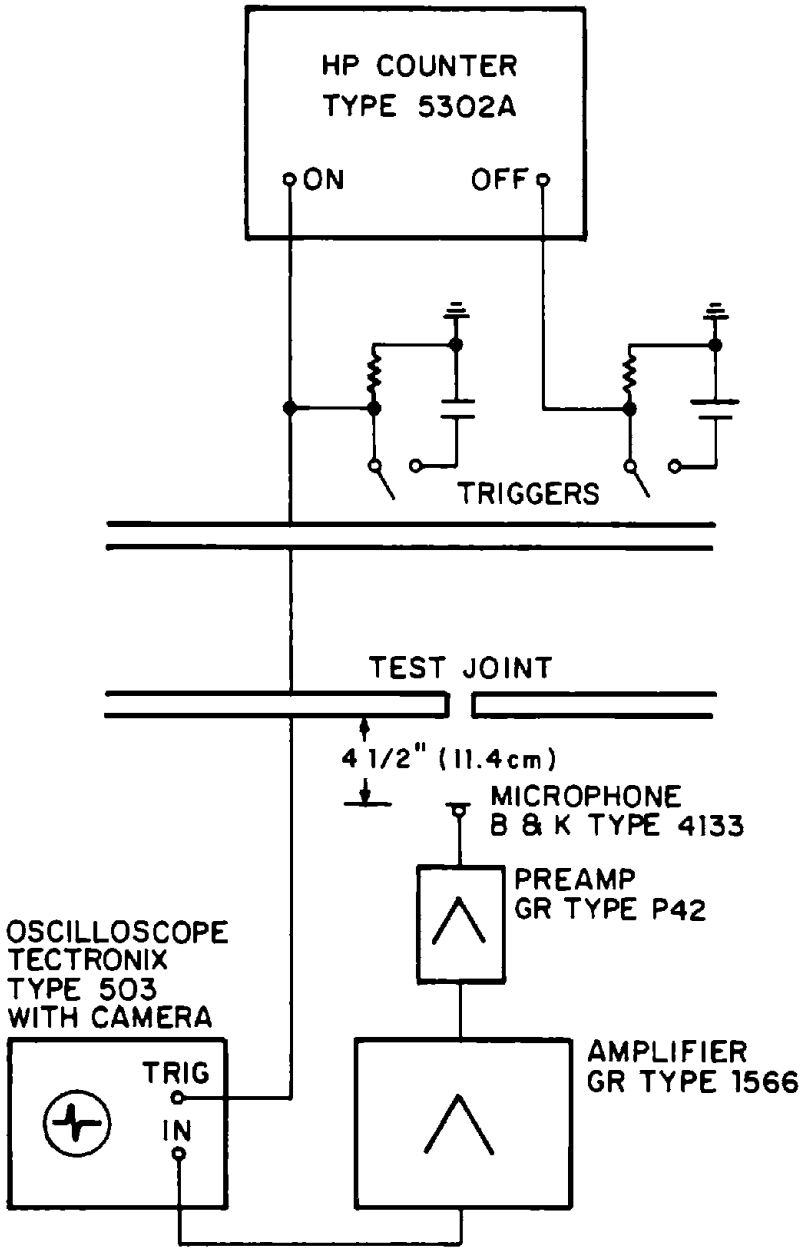

FIG. 3.3-4. BLOCK DIAGRAM OF THE EXPERIMENTAL SETUP.

joint. The train speed was measured by means of two closely spaced stationary switches located alongside the track, which were triggered by a beam that was rigidly attached to the moving truck. The first switch started an electronic counter and also provided the triggering signal for starting the horizontal sweep of the oscilloscope. The second switch provided a short electronic pulse used to stop the counter.

Rail Joint with Height Difference

The speed dependence of the peak impact sound pressure was evaluated for a rail joint with height difference h = 0.039 in. (0.1 cm) for travel in both the step-up and step-down directions. Figure 3.3-5 shows the results of this test. For travel in the step-up direction, the peak sound pressure level increases monotonically with increasing train speed, with a characteristic slope of 20 dB for a tenfold increase in train speed. This behavior is in accordance with the speed dependence predicted by Eq. 2.3-33.

For travel in the step-down direction, the peak sound pressure level at low speeds coincides with that obtained for the step-up direction, as predicted by Eqs. 2.3-29 and 2.3-33. However, above 50 in./sec (4.27 m/sec) train speed, the SPL vs speed curve levels off, thereby confirming the existence of a critical train speed, as predicted by Eq. 2.3-12, above which the wheel separates from the rail. The critical train speed calculated by inserting the appropriate wheel radius, wheel mass, and axle load into Eq. 2.3-12 is V_c = 52.8 in./sec (1.32 m/sec), which is confirmed by the experimental data. Since Eq. 2.3-12 is applicable to the rigid rail case, the agreement between the measured and predicted critical speed indicates that the experimental scale-model track can be considered essentially rigid.

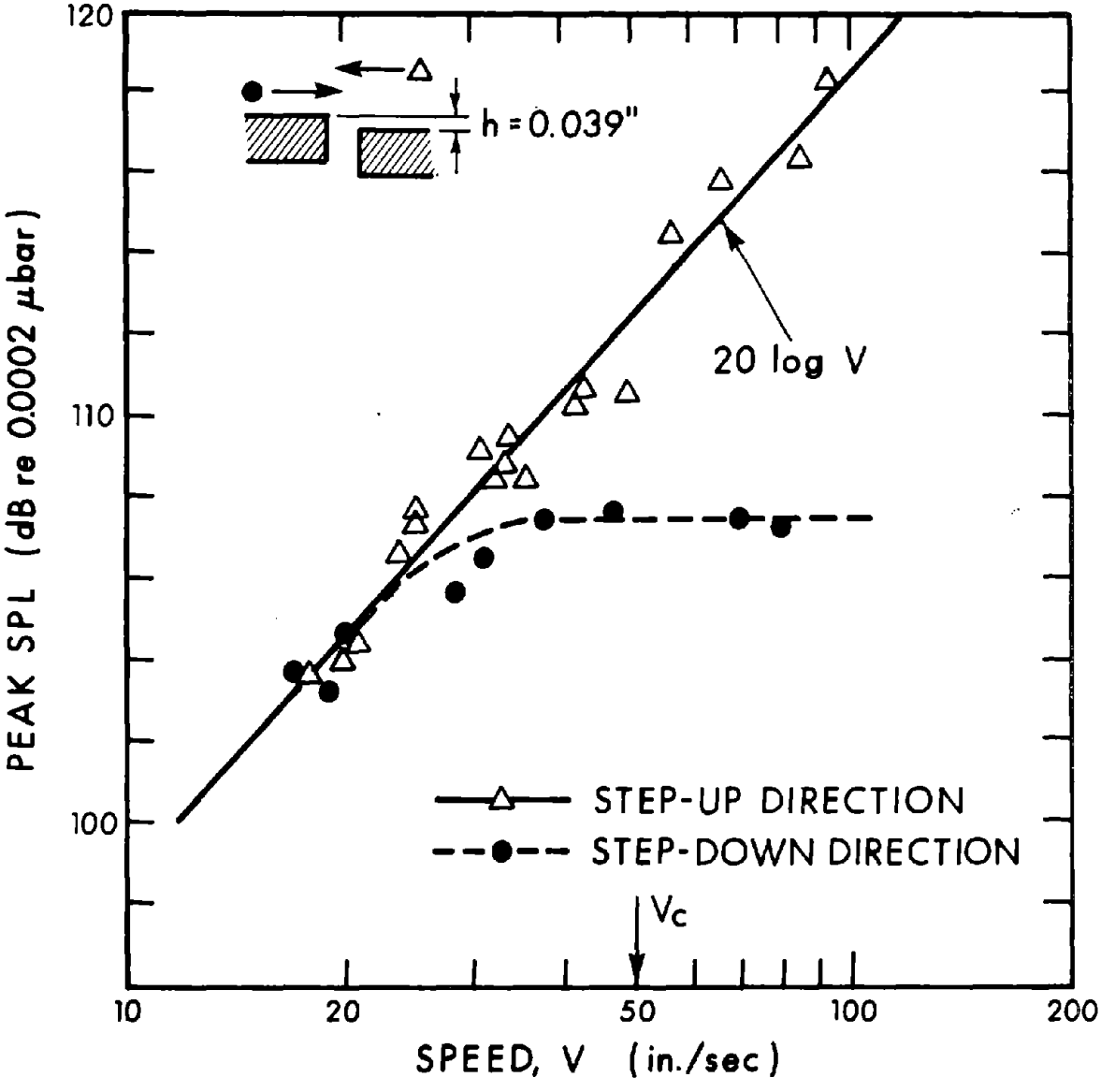

FIG. 3.3-5. PEAK SPL VS 1/8 SCALE MODEL BOGIE SPEED OBTAINED FOR A RAIL JOINT WITH HEIGHT DIFFERENCE h = 0.039 in. (0.1 cm) AND STANDARD SCALE MODEL WHEEL.

Figure 3.3-6 presents the experimental results obtained for a rail joint with a smaller height difference of h = 0.023 in. (.056 cm). Here again, the SPL vs train speed curves obtained for travel in both the step-up and step-down directions follow the characteristic speed dependence predicted by Eqs. 2.3-29 and 2.3-33. Comparing Fig. 3.3-5 with Fig. 3.3-6, one notes that the rail joint with the smaller height difference generates consistently lower impact sound levels for both directions of travel as compared to the rail joint with the larger height difference. Equation 2.3-33 predicts a sound pressure level difference of $\Delta SPL = 10 \log(h_1/h_2) = 10 \log (0.039/0.023) = 2.3$ dB, which is smaller than the difference indicated by the measured data. It is believed that the reason for this discrepancy is the lack of accuracy in the measurement of small height differences.

Time history of the pressure pulse

Figure 3.3-7 is a photograph of the oscilloscope trace of the time history of the sound pressure as obtained for a step-down rail joint. The left-hand side of the trace corresponds to the rolling noise before impact. The impacting wheel generates an intense short-duration pressure pulse with a peak amplitude much higher than the amplitude of the rolling noise. The short pulse width of approximately 1.5 msec indicates that the intense dynamic interaction between wheel and rail must take place during a similar time period.

An important finding of the experimental study is that the duration of the pressure pulse seems to be practically invariant with train speed and joint height difference. Because of the special triggering arrangement, the photograph of the oscilloscope trace did not have sufficient time resolution to

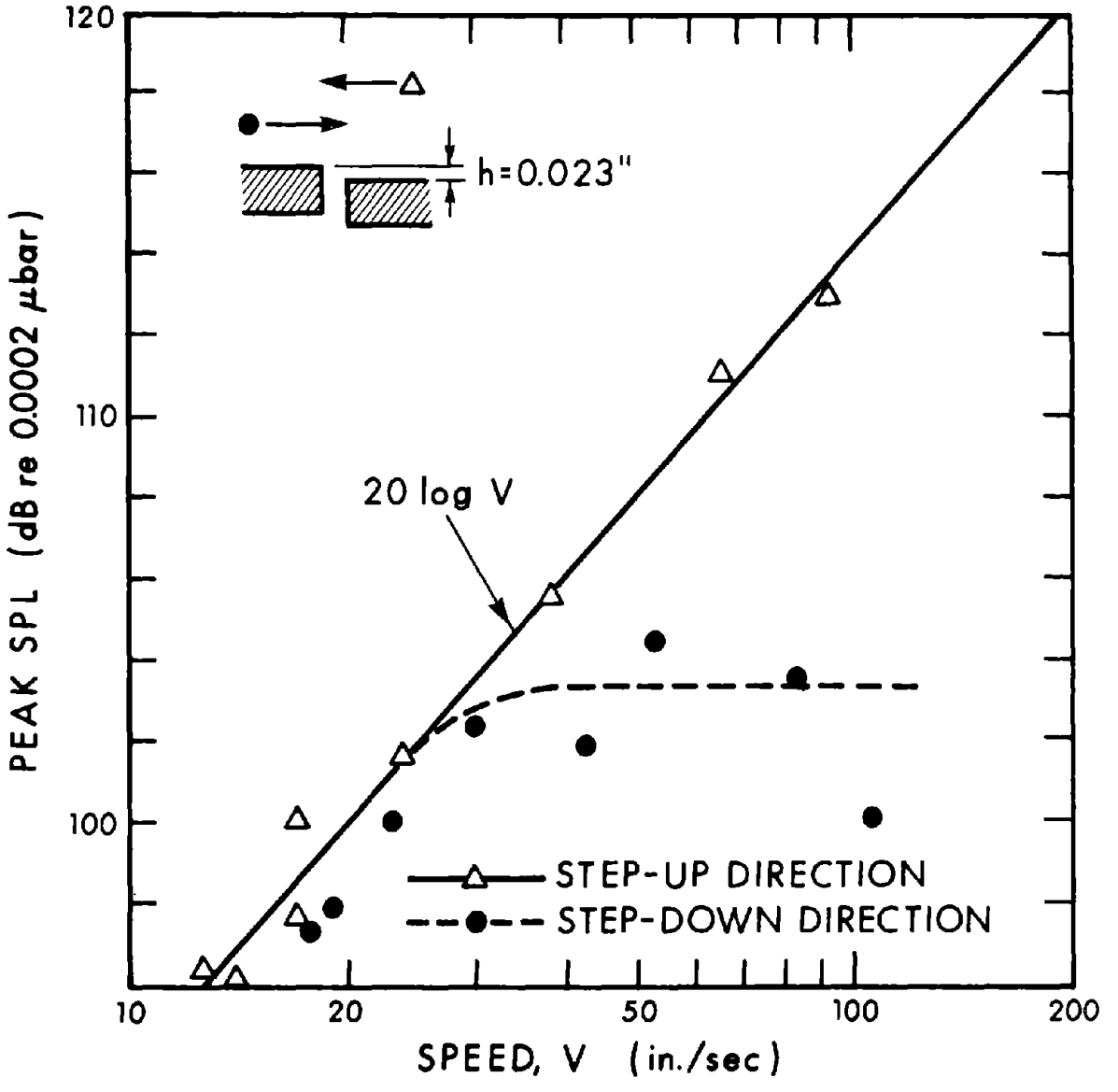

FIG. 3.3-6. PEAK SPL VS 1/8 SCALE MODEL BOGIE SPEED OBTAINED FOR A RAIL JOINT WITH HEIGHT DIFFERENCE h = 0.023 in. (0.056 cm) AND STANDARD SCALE MODEL WHEEL.

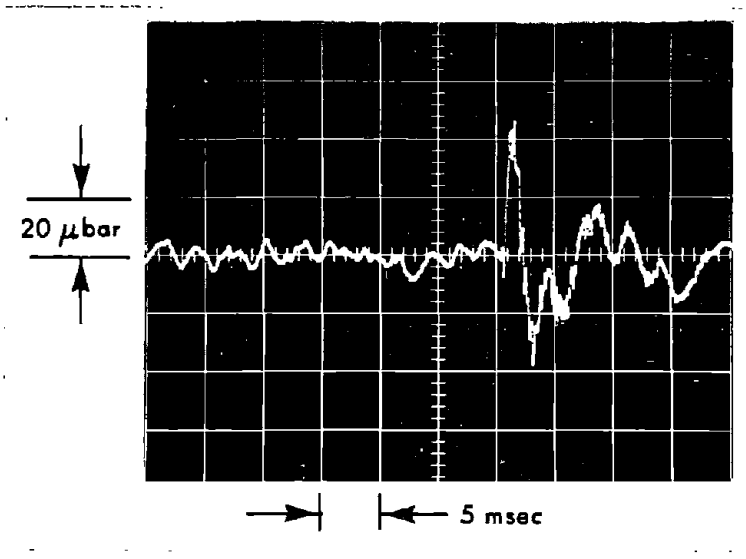

FIG. 3.3-7. TYPICAL TIME HISTORY OF THE SOUND PRESSURE CAUSED BY THE IMPACT OF A STANDARD SCALE MODEL WHEEL.

reveal small variations in the time duration that may be caused by nonlinear Hertzian contact stiffnesses. Identification of the major parameters which determine the pulse duration requires further detailed studies.

Dependence on axle load

To explore the effect of static axle load on the peak impact sound pressure generated by a train passing over a non-level rail joint, runs were made with and without added load. The added load consisted of a 61.8 lb (28 kg) lead brick attached to the center of the bogie frame. Figure 3.3-8 shows the results obtained for passages in the step-up direction; they indicate that for this direction of travel the peak impact sound generated does not depend on axle load. This is because the wheel is dynamically decoupled from the bogie, and the impact force is essentially the inertia force created by forcing the wheel to move on a path dictated by the rail joint geometry. Both the independence of the peak impact sound on axle load and the 20 dB/decade slope of the SPL vs train speed curve in Fig. 3.3-8 are in accordance with the analytical results presented in Eq. 2.3-33.

For travel in the step-down direction, the wheel is in contact with the rail below critical speed and the static axle load does not influence the impact noise. Above critical speed, where the wheel separates from the rail, the increased axle load, which produces a higher downward acceleration of the wheel, increases the impact speed and the corresponding peak impact sound pressure level. The experimental data presented in Fig. 3.3-9 confirm this characteristic dependence. According to Eq. 2.3-25, the increase in peak impact sound pressure level above critical train speed should be given by

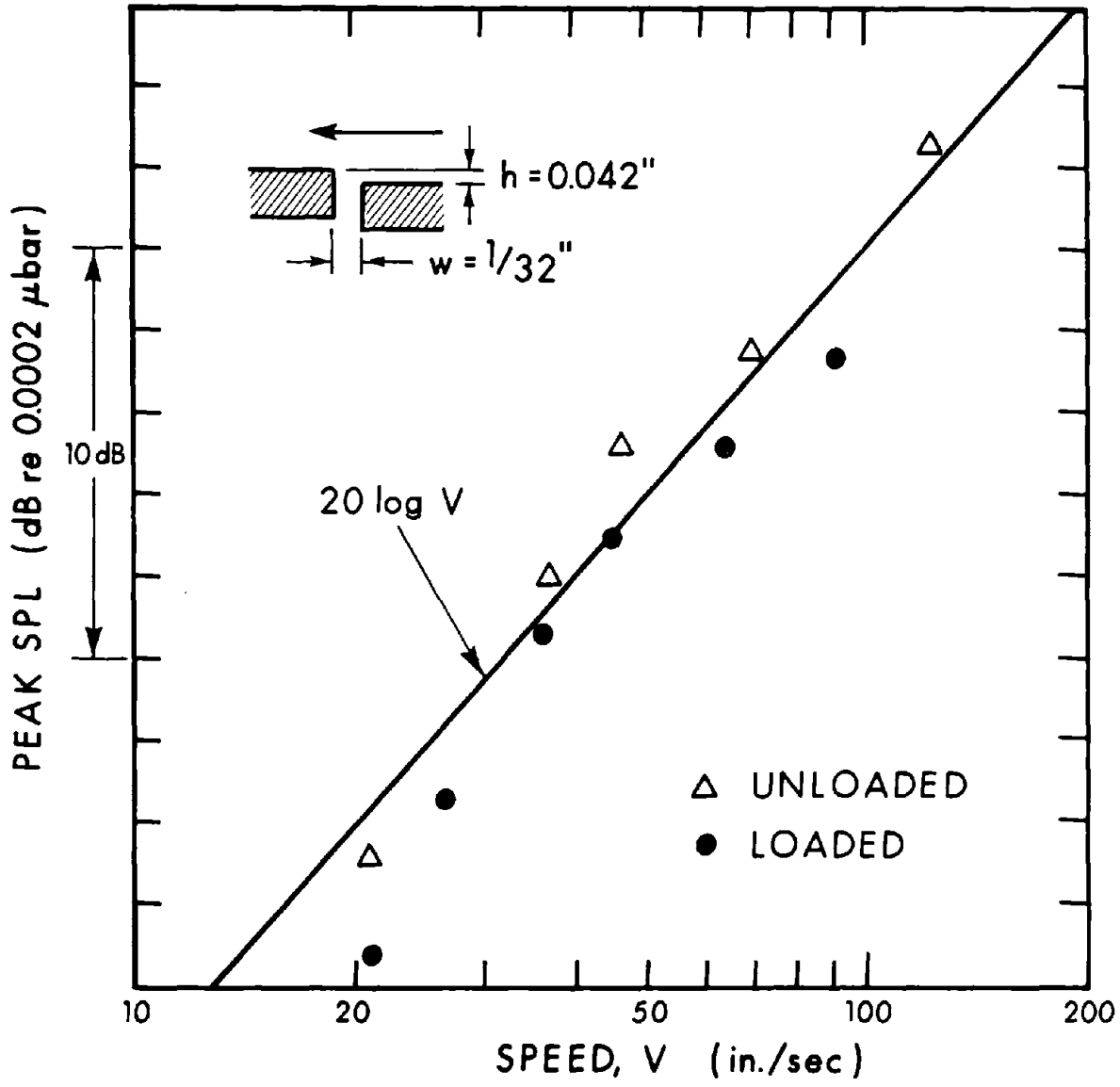

FIG. 3.3-8. EFFECT OF STATIC AXLE LOAD ON PEAK IMPACT SOUND PRESSURE LEVEL FOR TRAVEL IN THE STEP-UP DIRECTION; AXLE LOAD RATIO M/M' = 2.4; STANDARD SCALE MODEL WHEEL.

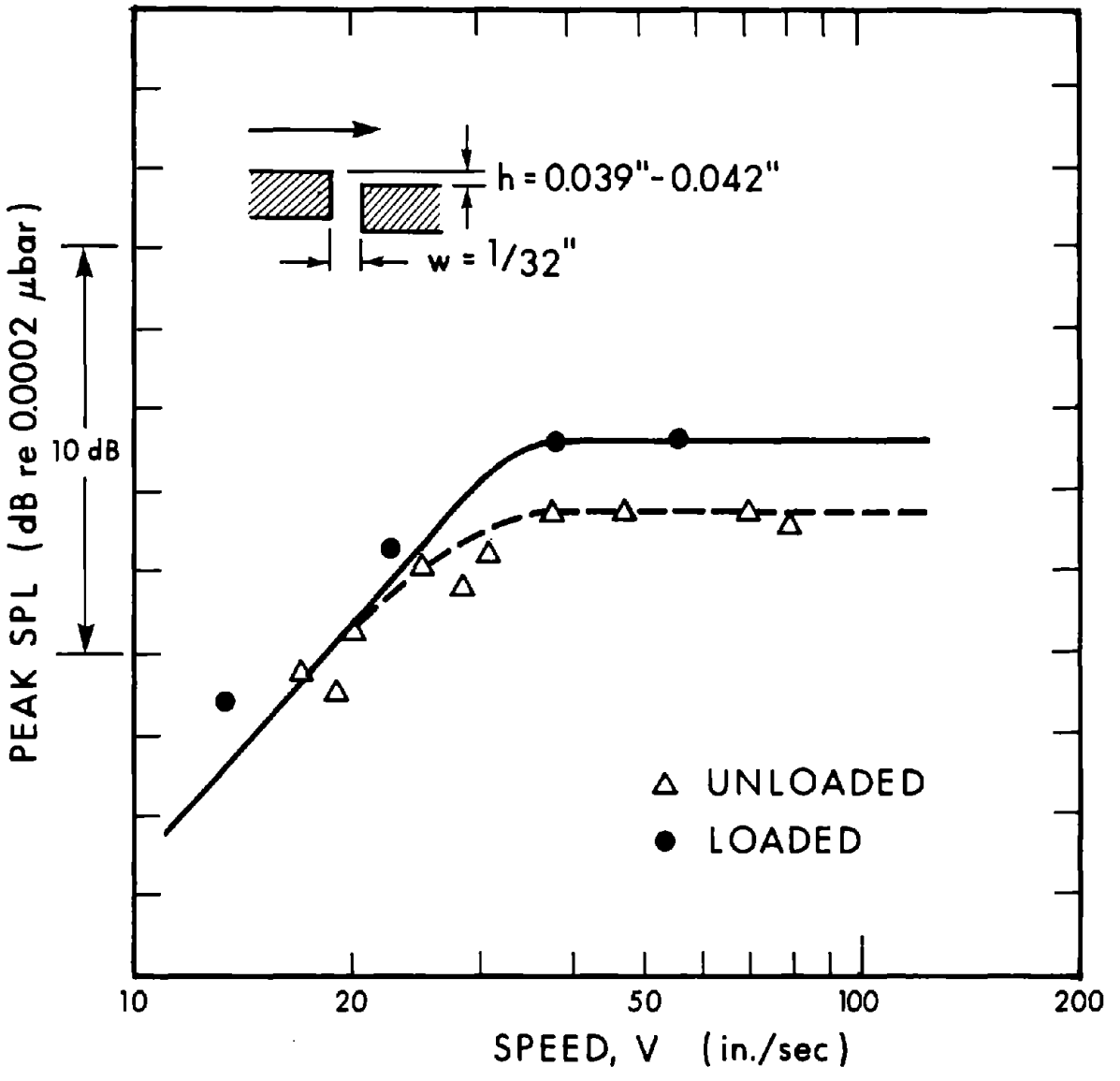

FIG. 3.3-9. EFFECT OF STATIC AXLE LOAD ON PEAK IMPACT SOUND PRESSURE LEVEL FOR TRAVEL IN THE STEP-DOWN DIRECTION; AXLE LOAD RATIO M/M' = 2.4; STANDARD SCALE MODEL WHEEL.

$\Delta SPL = 10 \log[(1+M/m)/(1+M'/m)]$, which would yield a 3-dB increase in our case, instead of the 2-dB increase indicated by the experimental data presented in Fig. 3.3-9. The 1-dB discrepancy between the predicted and measured increase is within the overall accuracy of the experiment.

Speed dependence of wheel acceleration

The peak wheel acceleration as a function of train speed was investigated by attaching a miniature accelerometer to the underside of the journal box and running the experimental vehicle in both the step-up and step-down directions over a rail joint with height difference. As shown in Fig. 3.3-10, the journal box acceleration level has the same characteristic speed dependence as the corresponding peak sound pressure level shown in Figs. 3.3-5 and 3.3-6.

Level Rail Joint

With the addition of a new fishplate, the horizontal gap between the adjoining rails was widened and the height difference was, as much as practically possible, eliminated. Figure 3.3-11 shows the characteristic speed dependence of the peak sound pressure level generated by the passage of the experimental vehicle over the level rail joint. The slope of the SPL vs train speed curve is 20 dB/decade, as predicted by Eq. 2.3-17. Note that the peak impact noise level does not depend on the direction of travel, indicating that the joint was indeed level.

The analytical formulas presented in Eqs. 2.3-17 and 2.3-33 indicate that, for the same train speed, the difference in peak sound pressure level obtained for a step-up joint with

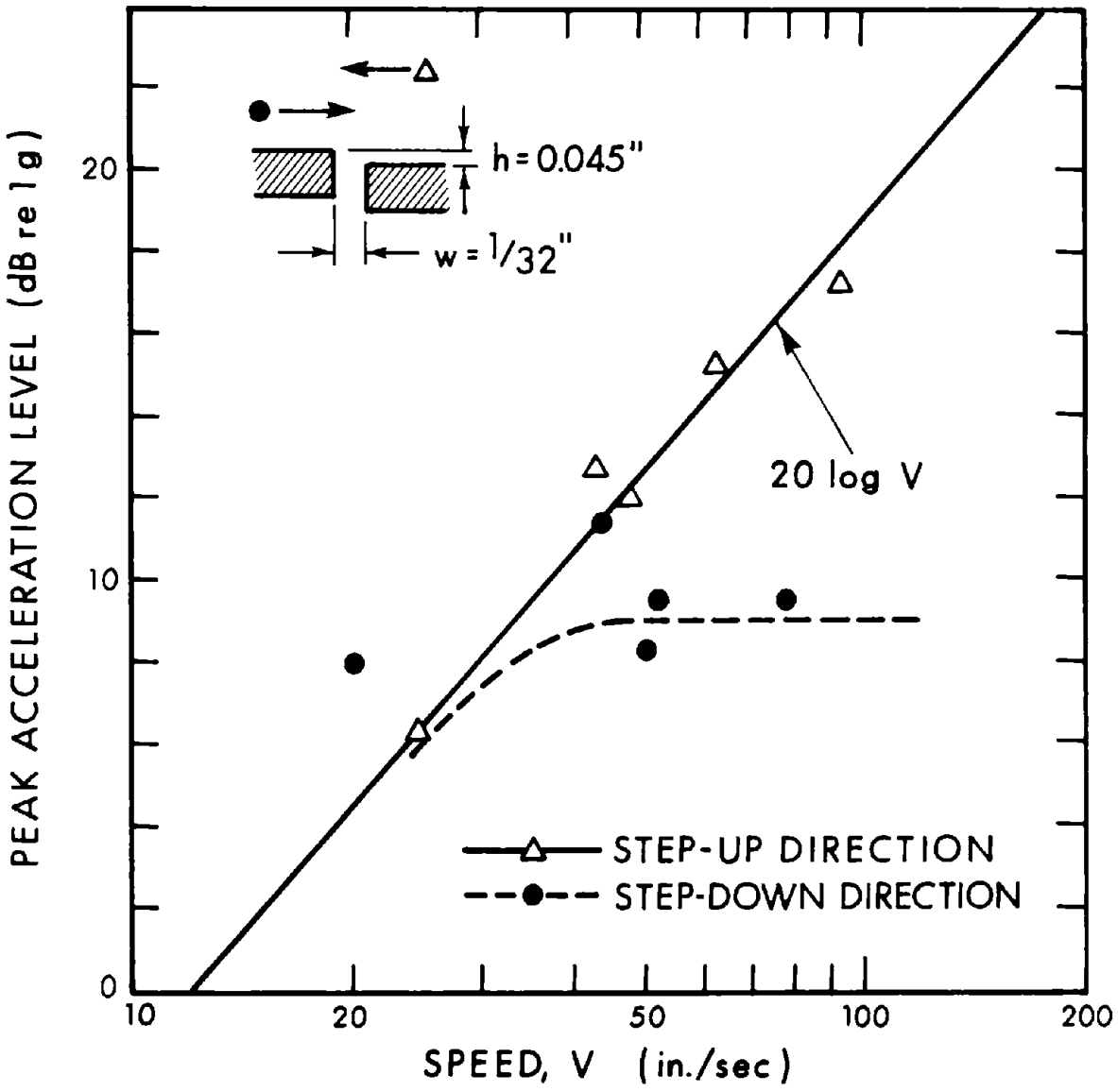

FIG. 3.3-10. SPEED DEPENDENCE OF THE PEAK JOURNAL BEARING ACCELERATION LEVEL DURING WHEEL PASSAGE OVER A RAIL JOINT WITH HEIGHT DIFFERENCE; STANDARD SCALE MODEL WHEEL.

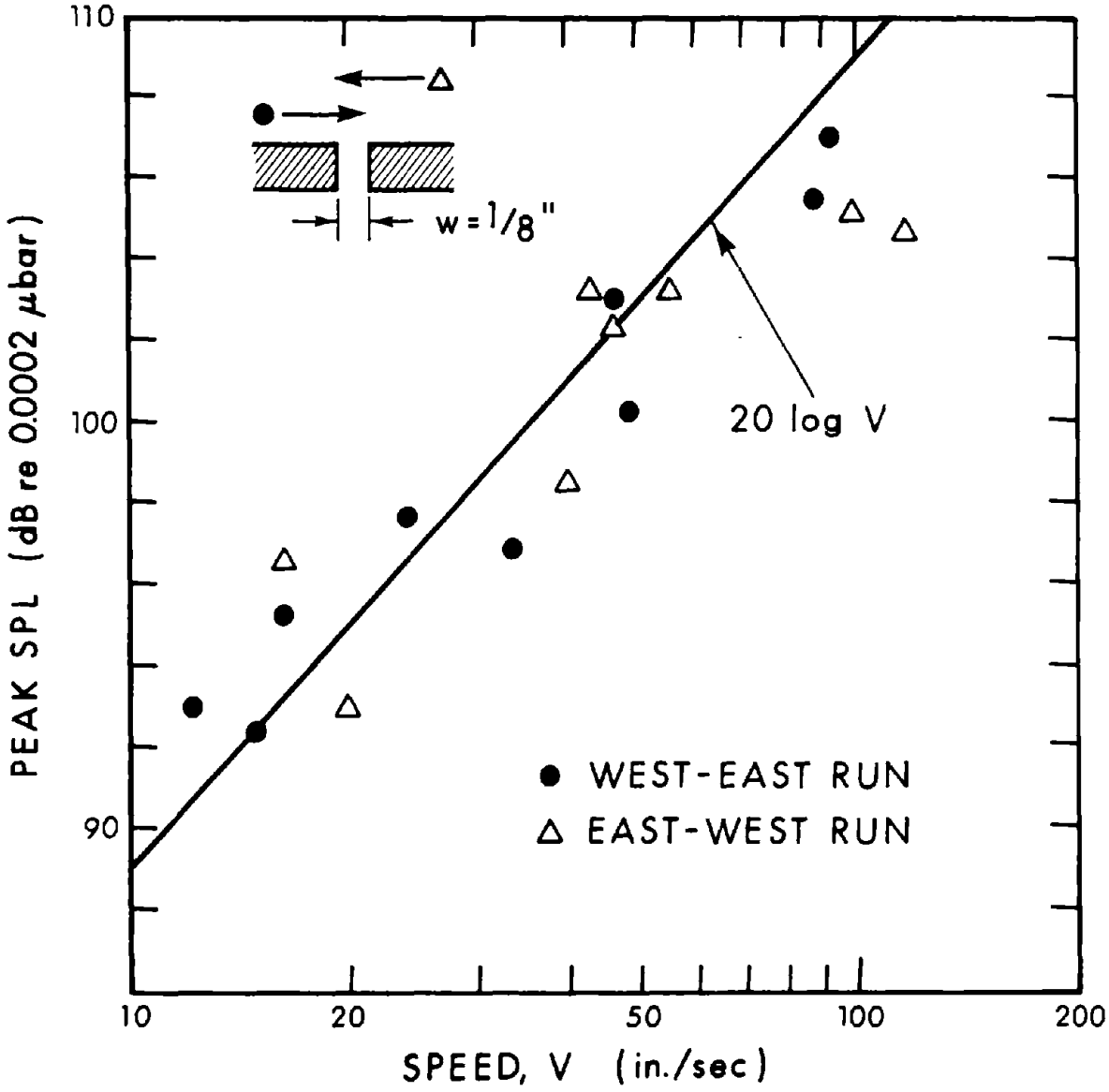

FIG. 3.3-11. PEAK SPL VS TRAIN SPEED CURVES OBTAINED FOR A LEVEL RAIL JOINT j = 0; w = 0.125 IN. (0.318 cm); STANDARD SCALE MODEL WHEEL.

height difference h and that obtained for a perfectly level joint with a horizontal gap of w is given as $\Delta SPL = 20 \log (2\sqrt{2ah}/w)$. For a = 2.2 in. (5.6 cm), h = 0.039 in. (0.1 cm), and w = 0.125 in. (0.318 cm), the analytically predicted difference in peak sound pressure level would be $\Delta SPL \approx 16.5$ dB. The ΔSPL determined by comparing the data presented in Figs. 3.3-5 and 3.3-11 is only 10 dB. The cause for this discrepancy is primarily the presence of rolling noise, which for a level rail joint is the same order of magnitude as the impact noise. This point became evident during evaluation of the oscilloscope traces, when the impact noise generated by the level joint was hard to separate from the rolling noise.

Since the impact noise generated by level rail joints is negligible compared with the impact noise generated by rail joints with even the smallest height difference and is only slightly higher than the continuously emitted rolling noise, one can conclude that the level rail joint plays only a very minor role in the generation of railway noise.

Wheel Drop Test

To study the generation of wheel/rail impact noise free of the rolling noise, we removed a wheel set from the bogie and carried out a wheel drop test. In this test, the wheel set was positioned on the track and while one wheel retained contact with the rail the other was lifted up to various heights above the rail head and let free to drop on it. The time history of the sound pressure caused by the impacting wheel was again displayed on the screen of the oscilloscope and photographed to obtain a measurement record for later evaluation. The drop experiments were performed in the immediate vicinity of the rail joint and also farther down the track at the midpoint

between two successive rail fastening points. The relative location of the microphone for these tests was the same as that used in the previously reported experiments.

Figure 3.3-12 shows the peak impact sound pressure level as a function of the drop height for the two locations. Since the wheel velocity at the instant of impact is proportional to the square root of the falling height, the peak sound pressure level should increase by 10 dB for each tenfold increase of the falling height; this behavior is confirmed by the experimental data. The peak SPL obtained away from the experimental rail joint is 6 dB higher than that obtained near the joint. This difference may be attributable to larger bending stiffness and larger equivalent impact mass of the rail at locations away from the rail joint. Additional, more detailed, experimental and analytical studies would be needed to explain this behavior in a quantitative manner.

To test whether or not the peak sound pressure levels obtained by the wheel drop test and those obtained for a step-down joint above critical train speed are compatible, we have extrapolated the peak sound pressure level from Fig. 3.3-12 down to a height of h = 0.039 in. (0.1 cm), obtaining 102 dB. Considering now that, in the case of a step-down rail joint of the same height difference, the impact speed of the wheel is larger by the factor of $(1 + M/m)^{\frac{1}{2}}$, because of the additional acceleration provided by the spring force acting on the wheel, the 102-dB impact sound pressure level predicted from the drop test must be increased by $10 \log(1 + M/m) = 10 \log(1 + 7.29/3.19) = 5.2$ dB. Accordingly, the peak impact sound pressure level predicted for a step-down rail joint with height difference h = 0.039 in. (0.1 cm), is 107.2 dB at train speeds in excess of the critical train speed. Since we have directly measured the

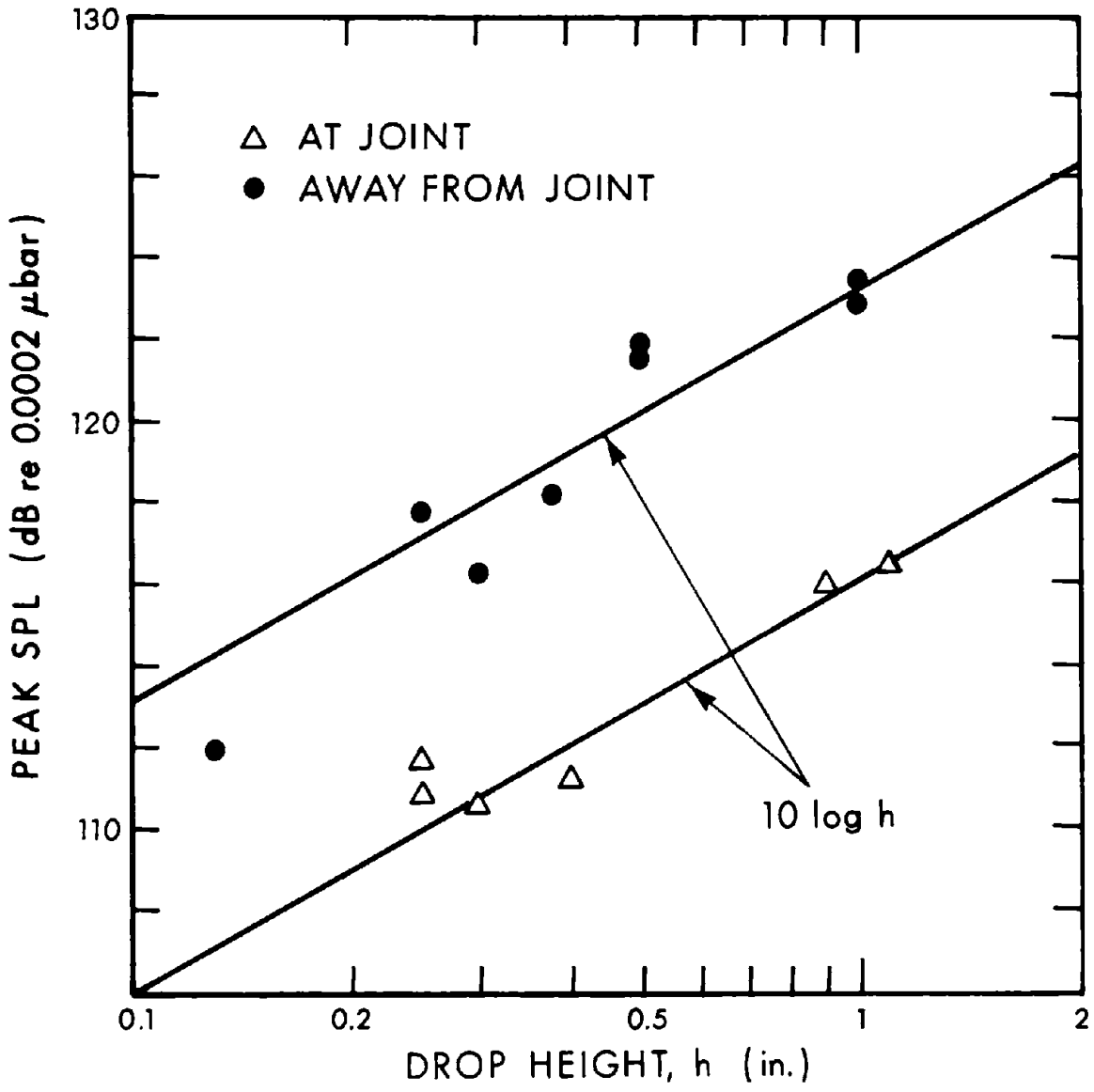

FIG. 3.3-12. PEAK SPL VS DROP HEIGHT FOR STANDARD SCALE MODEL WHEEL.

peak SPL of the step-down joints under the above conditions, we can check the accuracy of our prediction by comparing the predicted level of 107.2 dB with the 107.5 dB obtained from Fig. 3.3-5.

This excellent agreement between the data predicted from the wheel drop test and the data directly measured on a rail joint suggests that the wheel drop test performed at full-scale can be used with the analytical models of Sec. 2.3 to predict the impact noise generated by wheel and rail discontinuities.

Comparison of Impact and Roar Noise

The relative importance of the impact and roar noise was determined from photographs of the oscilloscope traces. The photographs were used to evaluate both the rms value of the roar noise just prior to the impact and the peak impact sound pressure produced by the standard wheel traveling over a step-up rail joint with a height difference h = 0.023 in. (.059 cm). Figure 3.3-13 shows the difference of the peak impact sound pressure level and the estimated rms-based sound pressure level of the rolling noise as a function of the train speed.

The data in Fig. 3.3-13 indicate that: (1) for this particular rail joint, wheel roughness, and rail roughness, the peak impact sound pressure level caused by the rail joint is, on the average, 14 dB above the level of the overall rolling noise; (2) both the peak impact noise and the overall rolling noise have the same speed dependence – namely, both increase by 20 dB for each tenfold increase in train speed.

It should be noted that the 20 log V dependence of the overall sound pressure level of the rolling noise and the 30 log V dependence of the A-weighted sound pressure level of

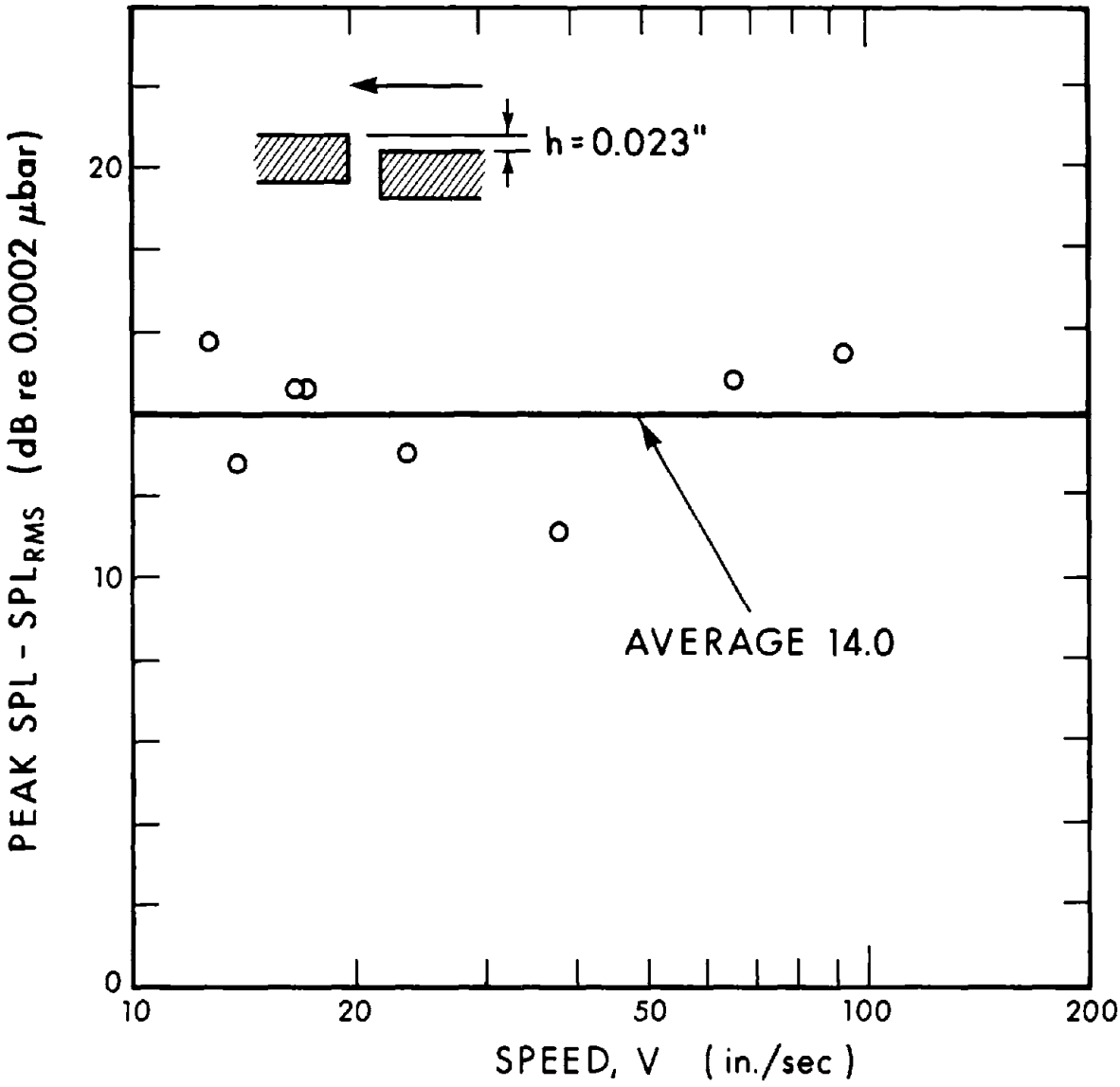

FIG. 3.3-13. DIFFERENCE IN THE LEVEL OF THE PEAK IMPACT SOUND AND RMS ROLLING NOISE AS A FUNCTION OF 1/8 SCALE MODEL BOGIE SPEED; STANDARD SCALE MODEL WHEEL; STEP-UP JOINT, h = 0.023 in. (0.056 cm).

the rolling noise are compatible.

Resilient Wheel

A limited program of scale-model experiments was undertaken to determine what effect, if any, the use of resilient wheels has on the noise generated by the impact between wheel and rail at a rail joint. This work supplements the formerly described experiments employing a standard "rigid" wheel.

A single wheel of the six-wheel truck was modified to accommodate resilient mounts that dynamically decouple the wheel rim from the hub. Mounts with different spring constants were used to evaluate the effect of mount stiffness on noise radiation. The impact noise and vertical rail acceleration caused by this wheel in rolling over selected rail joints were measured as a function of the rolling velocity of the truck.

A sketch of the resilient wheel is shown in Fig. 3.3-14. The hub portion of a standard cast iron wheel (same as used in the rigid wheel experiments) was machined out, leaving only the rim. The hub was replaced by an aluminum disk fastened to the axle inboard of the rim. Rubber vibration isolation units, arranged symmetrically around the periphery of the disk, support the rim. These units, acting in shear, provide the resiliency in the wheel.*

Tests were carried out both with four and with eight rubber-in-shear units in place, thereby providing two values of wheel spring rate. The shear units used are manufactured

---

*This arrangement is similar in concept to the SAB resilient wheel.

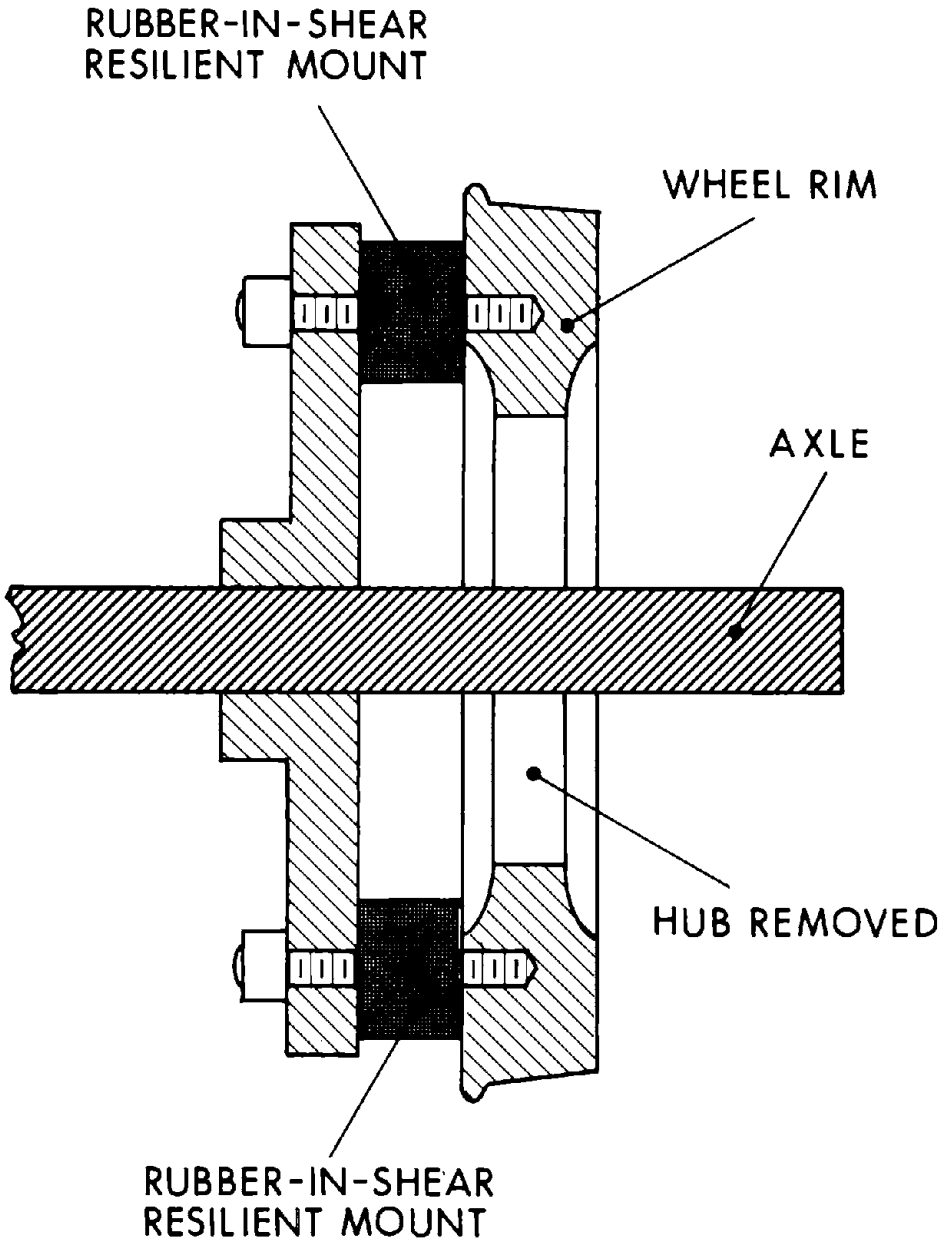

FIG. 3.3-14. CROSS-SECTIONAL VIEW OF SCALE MODEL RESILIENT WHEEL.

by the Barry Corporation (Serial No. A21-041). They have a nominal spring rate in shear of 120 lb/in. ($2.12 \cdot 10^4$ N/m), so that the wheel spring rates obtained are roughly 480 and 960 lb/in. ($8.5 \cdot 10^4$ and $1.7 \cdot 10^5$ N/m). The larger of these two rates provides a scaled static deflection (under scale loading) comparable to the values published for the SAB resilient wheel.

The truck, with the resilient wheel always mounted on the leading axle, was rolled at various speeds and in both directions over two rail joints. One joint had a vertical rail misalignment of 0.039 in. (1 mm) and a negligible, but nonzero, horizontal gap. The second joint had no measurable vertical rail misalignment and a horizontal gap of 0.125 in. (3.18 mm).

For the sound pressure level measurements, the microphone was placed about 4.5 in. (11.4 cm) from the track, on the near side, level with the rail head. Vertical acceleration of the impacted rail (the rail downtrack from the joint) was measured by mounting an accelerometer on the underside of the rail immediately adjacent to the joint. The instrumentation used for both sound pressure level and acceleration measurements was identical to that employed for the corresponding tests involving a standard wheel.

Figure 3.3-15 shows the peak sound pressure levels measured at the rail joint having a 0.039 in. (1 mm) vertical misalignment for the resilient wheel with eight resilient mounts. Repeating the runs with the same wheel but with four resilient mounts yielded practically identical results, indicating that the wheel hub is dynamically decoupled from the rim, even for the stiffer construction containing eight of the resilient mounts. The shape of the peak SPL vs train speed curves obtained for the resilient wheel is similar to that obtained with standard wheels.

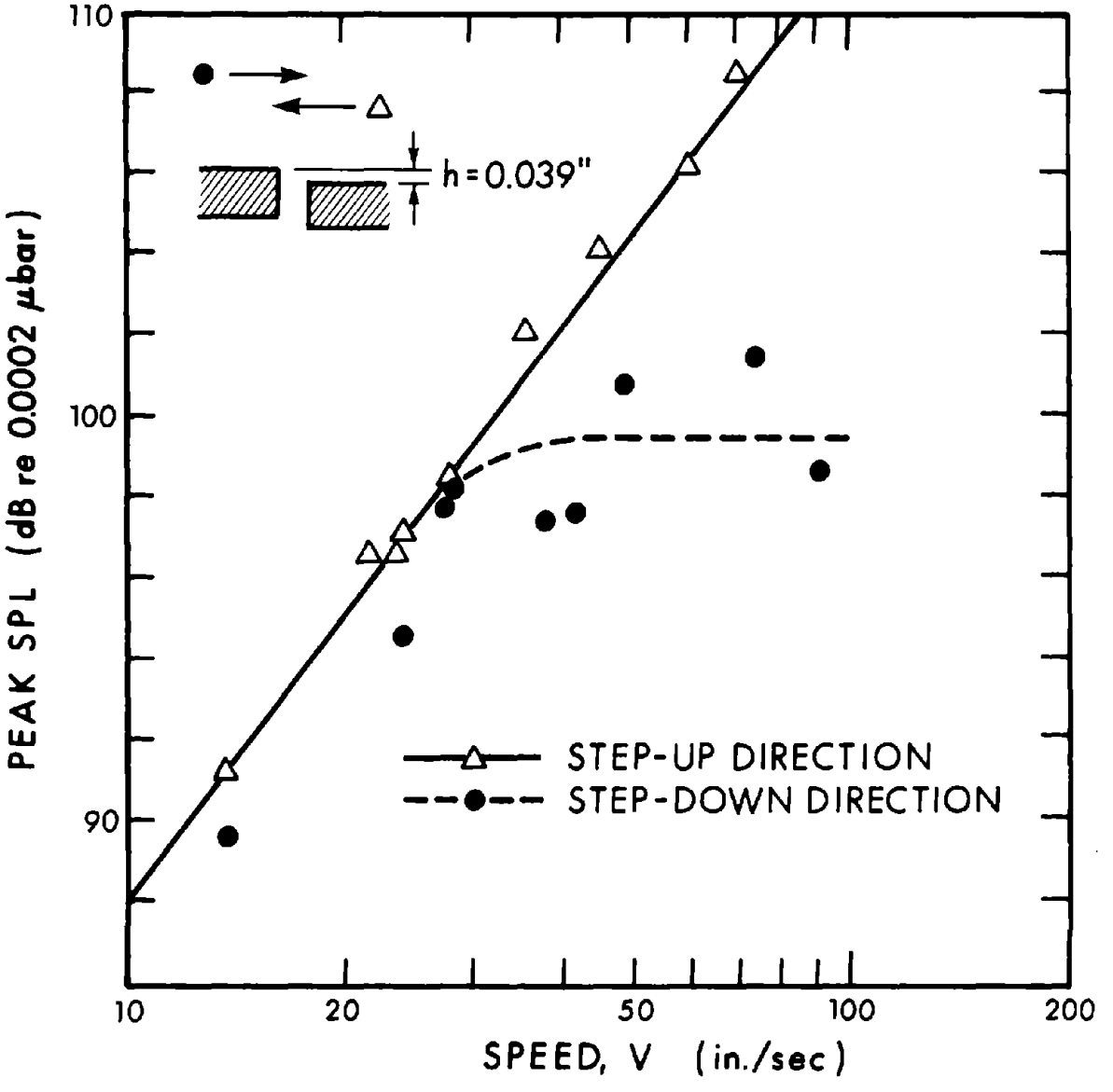

FIG. 3.3-15. PEAK SPL VS 1/8 SCALE MODEL BOGIE SPEED CURVES OBTAINED FOR A RAIL JOINT WITH h = 0.039 in. (0.1 cm) HEIGHT DIFFERENCE AND SCALE MODEL RESILIENT WHEEL WITH 8 RUBBER-IN-SHEAR MOUNTS.

In Fig. 3.3-16, the data of Fig. 3.3-5 are shown along with comparable data obtained previously for a standard rigid wheel. The resilient wheel produces about 8 dB less noise at all velocities. If one assumes that the rim of the resilient wheel is dynamically decoupled from the hub (so that the hub and axle are not disturbed by the joint), then the effective moving mass for the resilient wheel would be that of the hub alone. The corresponding quantity for the rigid wheel would be the wheel mass plus one-third of the axle mass, or nearly one-half the mass of an axle set. At any given truck velocity, the impulsive loadings between wheel and rail at the joint are proportional to these masses. If the acoustic radiation is proportional to the impulsive loading, then we get for the reduction in SPL:

$$\Delta SPL = 20 \log \frac{m_{wheel}}{m_{rim}} = 20 \log \frac{3.19}{1.34} \approx 7.5 \text{ dB} ,$$

which agrees well with the experimental data.

A rather limited number of data were collected for the level joint; that is, the rail joint with no discernible vertical misalignment but with a horizontal gap of 0.125 in. (3.2 mm). These data seem to indicate a $30 \log_{10} V$ variation in peak SPL with train speed. No explanation for this is offered at present.

Some measurements of rail acceleration were also made. These showed the same qualitative behavior as the SPL data, although with considerably more scatter.

On the basis of the data obtained, we conclude the following:

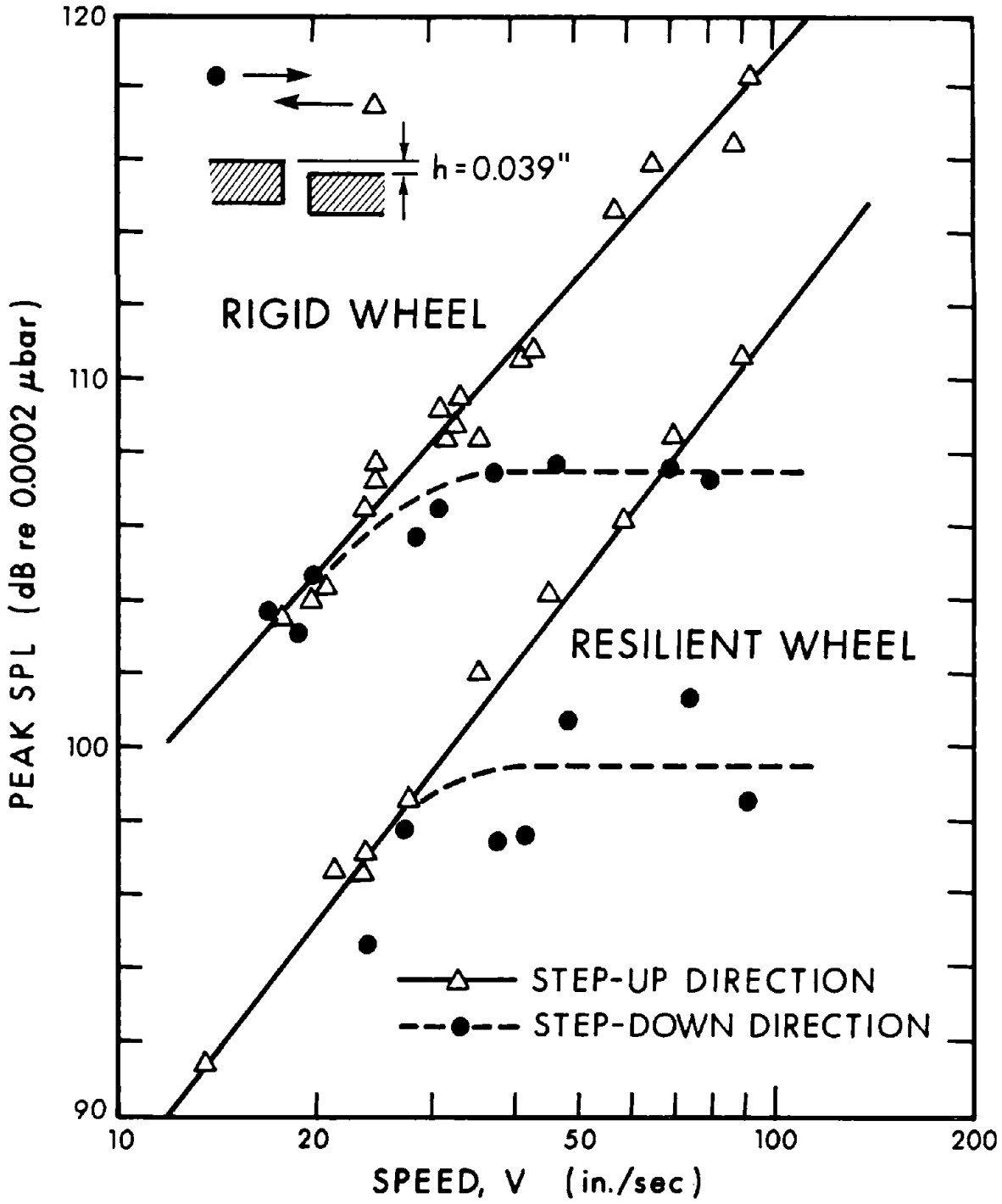

FIG. 3.3-16. COMPARISON OF THE PEAK SPL VS 1/8 SCALE MODEL BOGIE SPEED OBTAINED FOR A STANDARD SCALE MODEL HARD WHEEL AND A SCALE MODEL RESILIENT WHEEL.

1. Compared with the scale model hard wheel, the scale model resilient wheel provides a substantial reduction of the peak sound pressure level observed when the rail rolls over a nonlevel rail joint.

2. The extent of the reduction of the peak sound pressure is substantially independent of the direction of travel and forward speed and for essentially rigid rails is proportional to the ratio of the respective effective masses of the impacting wheel (i.e., total wheel mass/rim mass).

3. Practically no difference is observed between peak sound pressure levels obtained with scale model resilient wheels containing four as compared to eight rubber-in-shear mounts, indicating that the wheel hub was effectively decoupled from the rim even for the stiffer construction containing the eight mounts.

3.3.2 P-S tests

Impact testing was performed at the Pullman Standard Champ Carry test track using the PRT vehicle. The test track and vehicle are described in detail in Sec. 3.1. Our series of experiments involved taking measurements similar to those of the scale-model study with the PRT vehicle fitted with standard steel wheels.*

The data acquisition system was that described in Sec. 3.1 and illustrated in Fig. 3.1-7. The tape recorded transients were later reduced using the transient capture capabilities of a Federal Scientific Corp. UA-500 real-time analyzer.

---

*Although measurements were taken with the PRT vehicle fitted with damped and resilient wheels, funding and time limitations have prevented our reducing, analyzing, and presenting that impact data here.

Figure 3.3-17 shows the peak impact sound pressure level vs train speed data obtained on the experimental rail joint for travel in both step-up and step-down directions. The joint represented in Fig. 3.3-17 had a height difference of 0.17 in. (4.3 mm) and was situated above the center of a tie. The joint was apparently rigid, since neither rail end was visibly deflected as the vehicle passed over the joint and transferred the load from one rail end to the other. Both the 20 $\log_{10} V$ dependence of the peak SPL and the existence of a critical speed for travel in the step-down direction are evident from the experimental data. Actually, the critical train speed indicated by the experimental data agrees closely with the value of 15.5 mph (24 km/h) calculated from Eq. 2.3-12 using the appropriate parameters of the experimental vehicle.

In conclusion, the results of the full-scale and scale-model experiments strongly suggest that the analytical model developed for predicting the dependence of the impact noise on train speed, geometry, and the dynamics of the suspension system is basically sound.

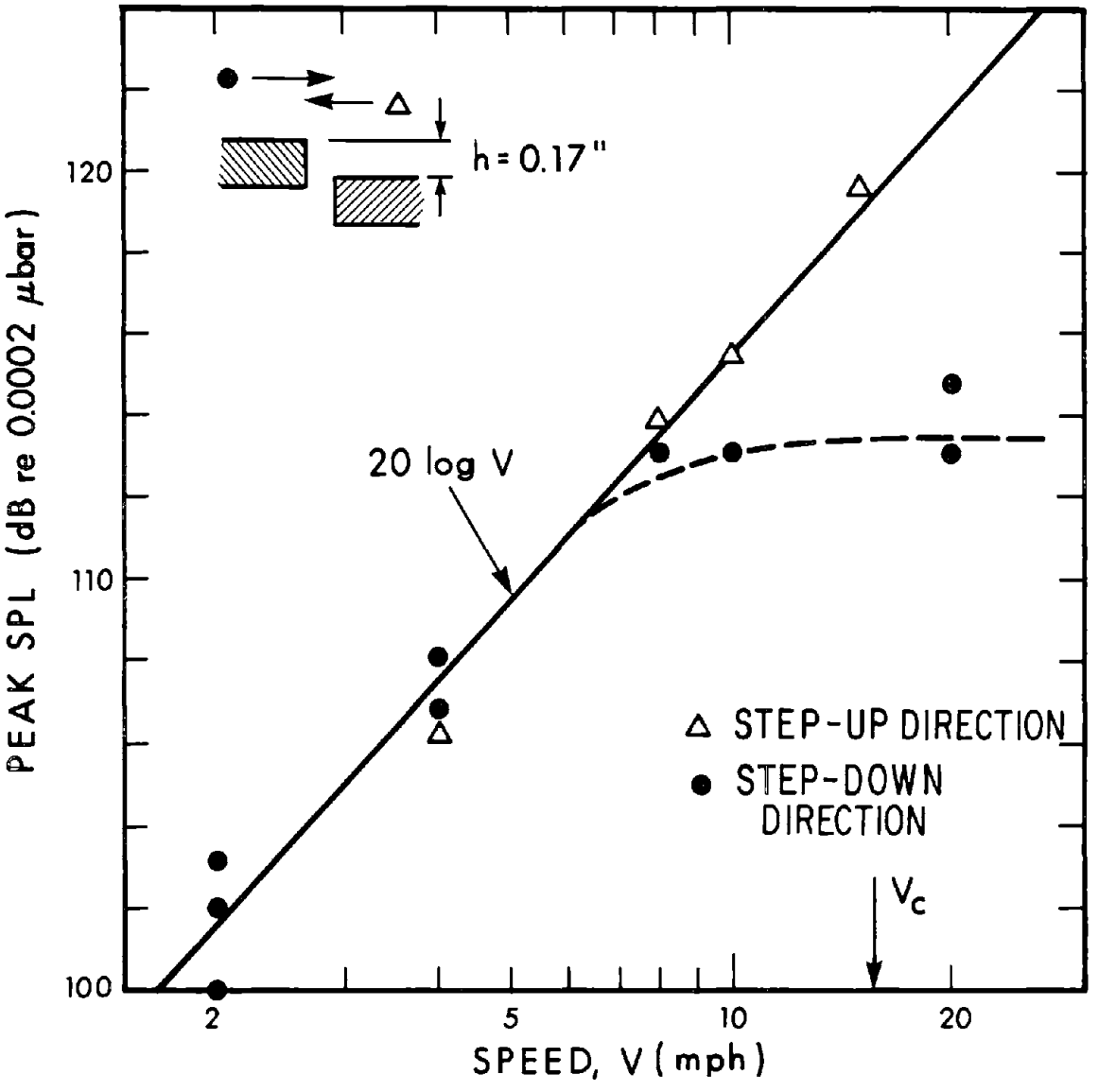

FIG. 3.3-17. PEAK SPL VS VEHICLE SPEED OBTAINED WITH THE PULLMAN STANDARD PRT VEHICLE; RAIL JOINT HEIGHT DIFFERENCE h = 0.17 in. (0.43 cm); STANDARD WHEEL.

3.4 Comparison of Roar Noise Predictions with Measured Data

We here compare analytical predictions of roar noise based on the analytical formulas developed in Sec. 2.4 with measurements of noise from the P-S PRT vehicle on a welded section of the P-S test track. The PRT vehicle was equipped with three different types of wheels: standard 14 in. (0.35 m) diameter steel wheels, 14 in. (0.35 m) diameter Penn Cushion resilient wheels, and damped wheels modified from the standard wheels as described in Sec. 3.1. We discuss below the measurements, the analytical noise predictions, and the agreement between the two for each of these wheels.

3.4.1 Standard wheels

Measurements

We conducted several tests on the PRT vehicle equipped with standard 140 lb (63.5 kg), 14 in. (0.35 m) running tread diameter steel wheels. Noise and vibration measurements were taken as the vehicle passed over a welded section of the test track at P-S (see Sec. 3.1). Approximately one month before these measurements, we measured the roughness of the rail section using the roughness measuring device described in Sec. 2.4.

The rail section measured was 10 ft (3.1 m) long and situated ~250 ft (76 m) north of the terminal just before the switch onto the S curve. We measured the roughness of two parallel strips, or lines of contact between the wheel and the rail, on the outside rail. The 1/3-octave band wavenumber spectra of the

two strips are shown in Fig. 3.4-1. There is considerable difference in roughness at high wavenumber between them. Since it is not possible to know at all times exactly where the wheel contacts the rail, the spread in rail roughness will lead to a band of uncertainty in our predictions of roar noise.

In addition to measuring rail roughness, we also measured the roughness of one of the standard wheels using a setup similar to the one described in Sec. 2.4. The wheel was mounted in a lathe and measured for roughness before and after it was turned smooth. Figure 3.4-2 compares the roughness spectra before and after turning. The turned wheel is considerably smoother and, in fact, is sufficiently smoother than the rail that for all practical purposes its roughness can be neglected.

The remaining three standard wheels were also turned smooth and mounted on the PRT vehicle. A microphone and a wind screen were then mounted on a boom and attached to the vehicle 3 ft (0.91 m) from the face of the lead wheel, in line with its axis, as shown in Fig. 3.4-3. The microphone was used to measure roar noise when the vehicle entered the test section where the rail roughness had been measured. Its output along with the acceleration of the bolster was recorded as described in Sec. 3.1. At the same time that roar noise and bolster vibration from the moving PRT were being recorded, two accelerometers mounted to the rail in the center of the test section recorded the rail vibration as described in Sec. 3.1. Bolster accelerations were typically 10 dB below rail acceleration and will therefore be considered no further here.

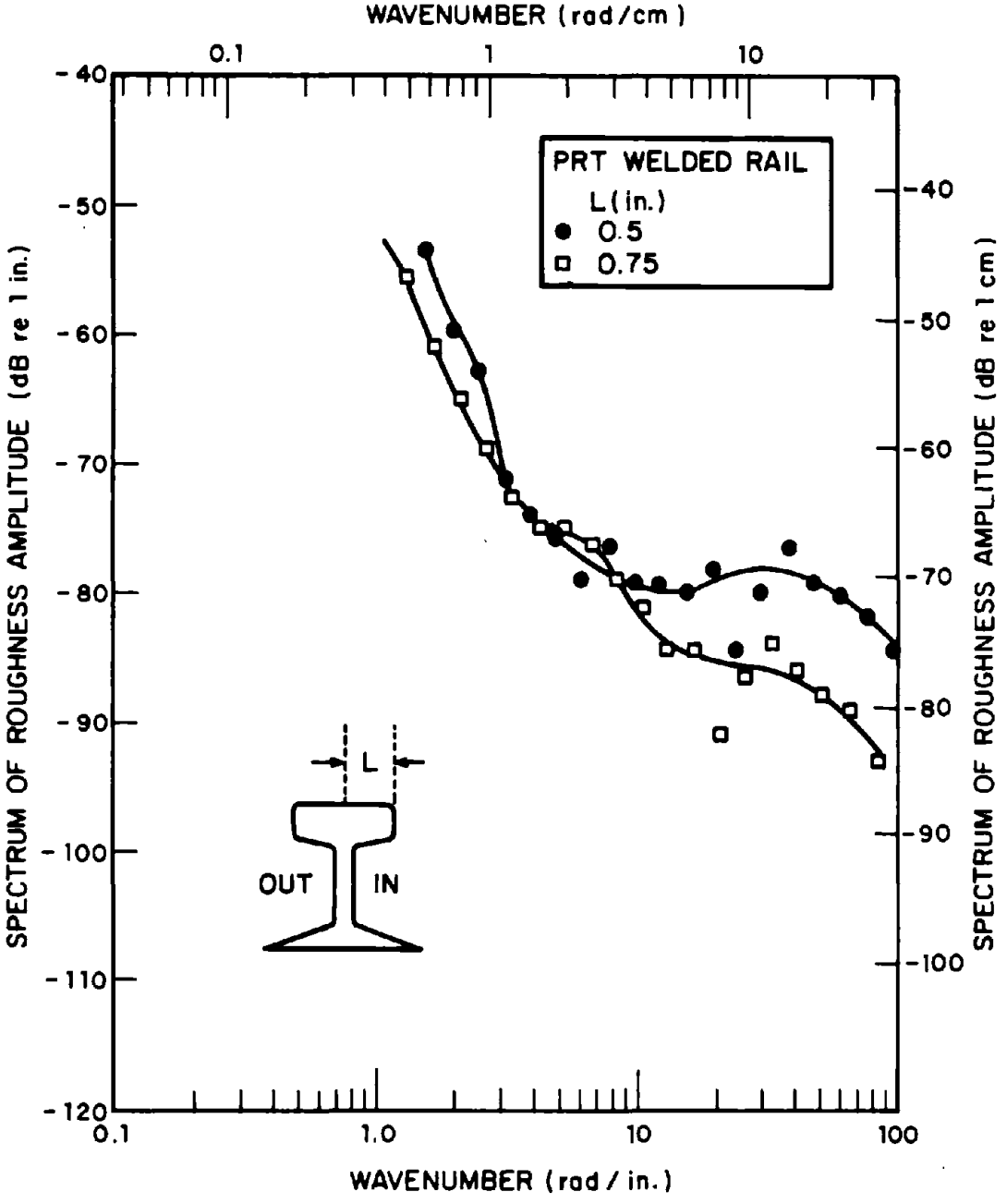

FIG. 3.4-1 RAIL ROUGHNESS ON THE PULLMAN STANDARD TEST TRACK

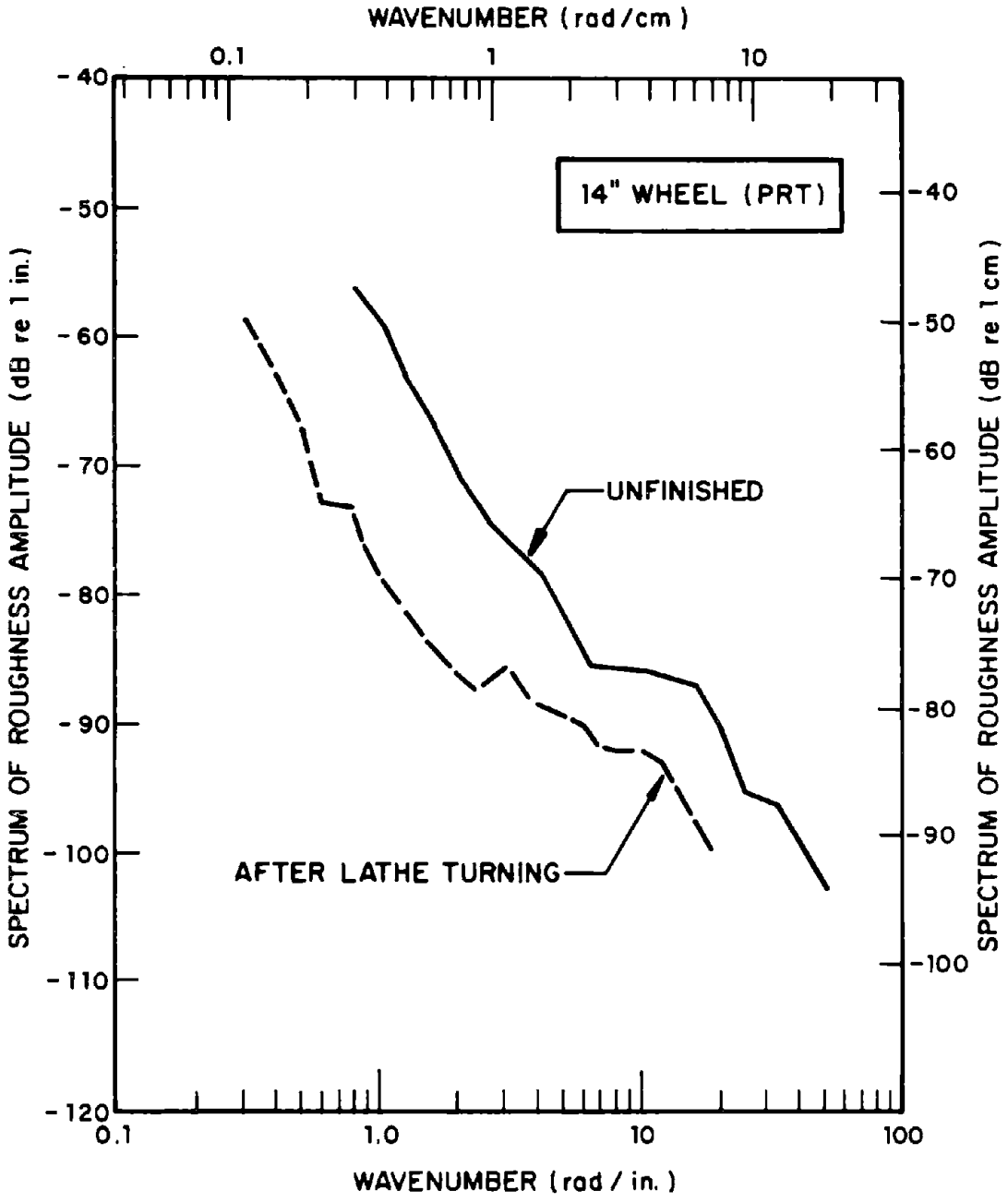

FIG. 3.4-2 ROUGHNESS SPECTRA OF 14 IN. (35.5 cm) DIAMETER PRT STANDARD WHEELS

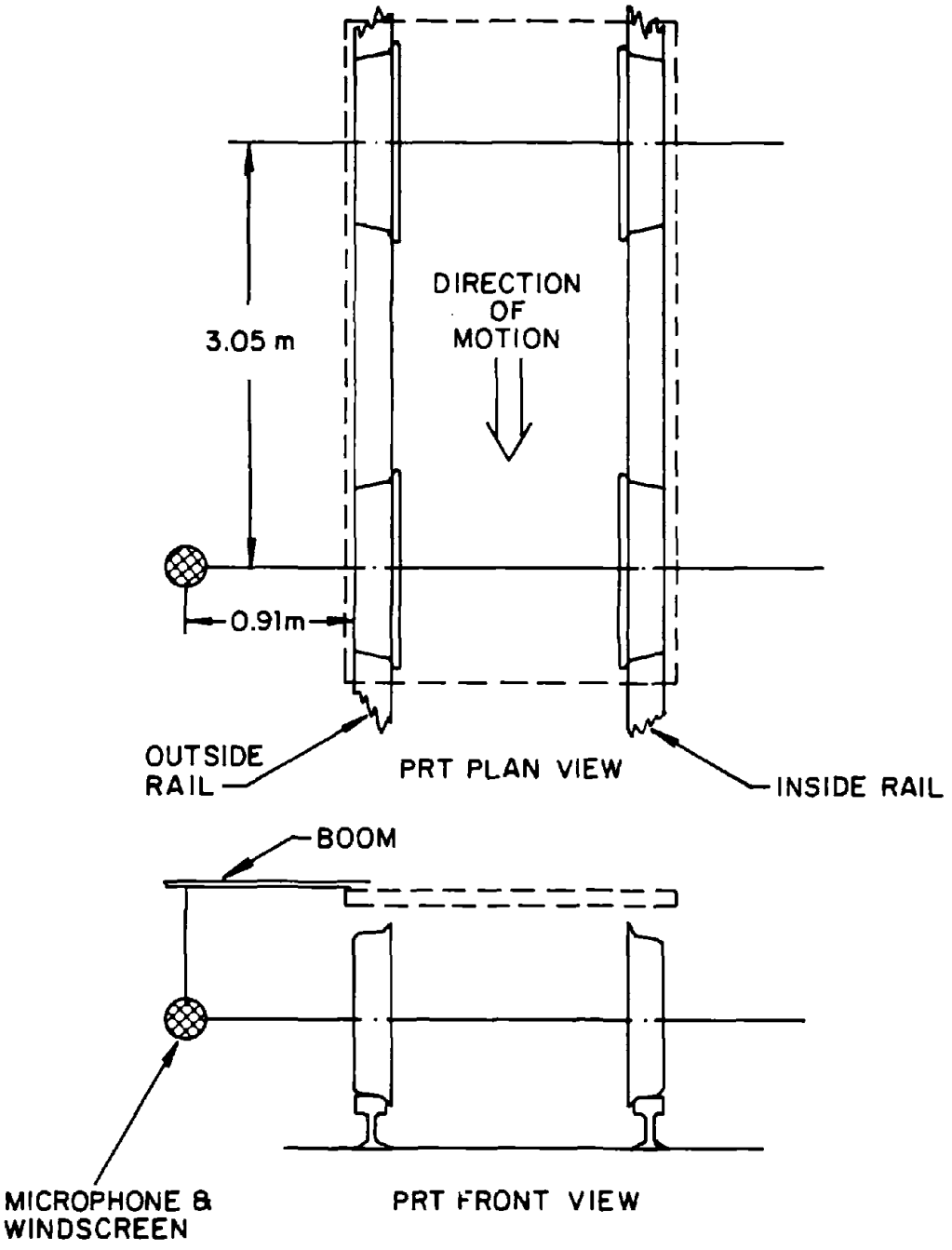

FIG. 3.4-3 CONFIGURATION FOR NOISE MEASUREMENTS AT PULLMAN STANDARD

For the noise and vibration tests, the PRT vehicle was driven over the test section in both directions at 10, 20, and 25 mph (16, 32, and 40 km/h). A mark was placed on the voice track of both the tape recorders as the vehicle reached the center of the test section. In the laboratory we reduced the data to 1/3-octave band spectra by passing the recorded signals through a General Radio real-time analyzer. We will compare these data with predictions in the following sections.

Analytical Predictions

Using the analytical formulas of Sec. 2.4, we can predict the SPL at the wayside due to passage of the PRT vehicle through the test section for comparison with our measured data. This SPL is composed of radiation from the rail excited by each of two wheels on one side of the vehicle and radiation from each of these two wheels.*

For the ASCE 60 lb/yd (30 kg/m) rail of the P-S test track, the width of the head is 2-3/8 in. (6 cm) and the width of the foot is 4-1/4 in. (10.8 cm). The wheels are 14 in. (0.35 m) in diameter. These parameters yield the following expressions for the SPL radiated by the rail due to excitation by a single wheel,

$$SPL_R = -12.5 + 10 \log \sigma_R + 10 \log \left| \frac{Z_W}{Z_W+Z_R} \right|^2 + 10 \log \left| H_{cp}(k) \right|^2$$

$$+ 10 \log \left[\left(\frac{\rho c \omega}{p_0} \right)^2 \Phi_{mR}(k) \Delta k \right] + G(\eta R, \eta L) \qquad (3.4\text{-}1)$$

*We are neglecting radiation from the wheels and rail on the opposite side of the vehicle. Because the microphone is so close to the wheels and rails on one side, this should result in at most a 1 or 2 dB error in our predictions.

and the SPL radiated by a single wheel,

$$SPL_W = -12 + 10 \log \left| \frac{Z_R}{Z_W+Z_R} \right|^2 + 10 \log \left| H_{cp}(k) \right|^2$$

$$+ 10 \log \left[\left(\frac{\rho c \omega}{p_0} \right)^2 \Phi_{mR}(k) \Delta k \right] - 20 \log \frac{R'}{3} \quad , \qquad (3.4\text{-}2)$$

where R' is the distance from the observer to the wheel of interest.

It will also be useful to compare predictions of rail response with measured response. The rail acceleration level AL_R due to the excitation of a single wheel is easily obtained from the results of Sec. 2.4 as

$$AL_R = 10 \log \left| \frac{Z_W}{Z_R+Z_W} \right|^2 + 10 \log \left| H_{cp}(k) \right|^2$$

$$+ 10 \log \left[\frac{\omega^4}{g^2} \Phi_{mR}(k) \Delta k \right] - 4.36 \eta L \quad , \qquad (3.4\text{-}3)$$

where the term $4.36\eta L$ includes the fact that the wheel and the measurement point on the rail may be separated by distance L.

The wheels each weigh ~140 lb (64 kg) and have a tread cross section (neglecting the flange) of 4 in. × 1 in. (10 cm × 2.5 cm). The 60 lb/yd (30 kg/m) rail has a radius of gyration of 1.57 in. (4 cm). Using the analytical formulas of Sec. 2.1.1, we can estimate the wheel and rail impedances. The estimates are shown in Fig. 3.4-4, where (based on impedance measurements of the 14 in. (.35 m) diameter wheel) the frequency at which the wheel impedance drops has been chosen to be 1600 Hz.

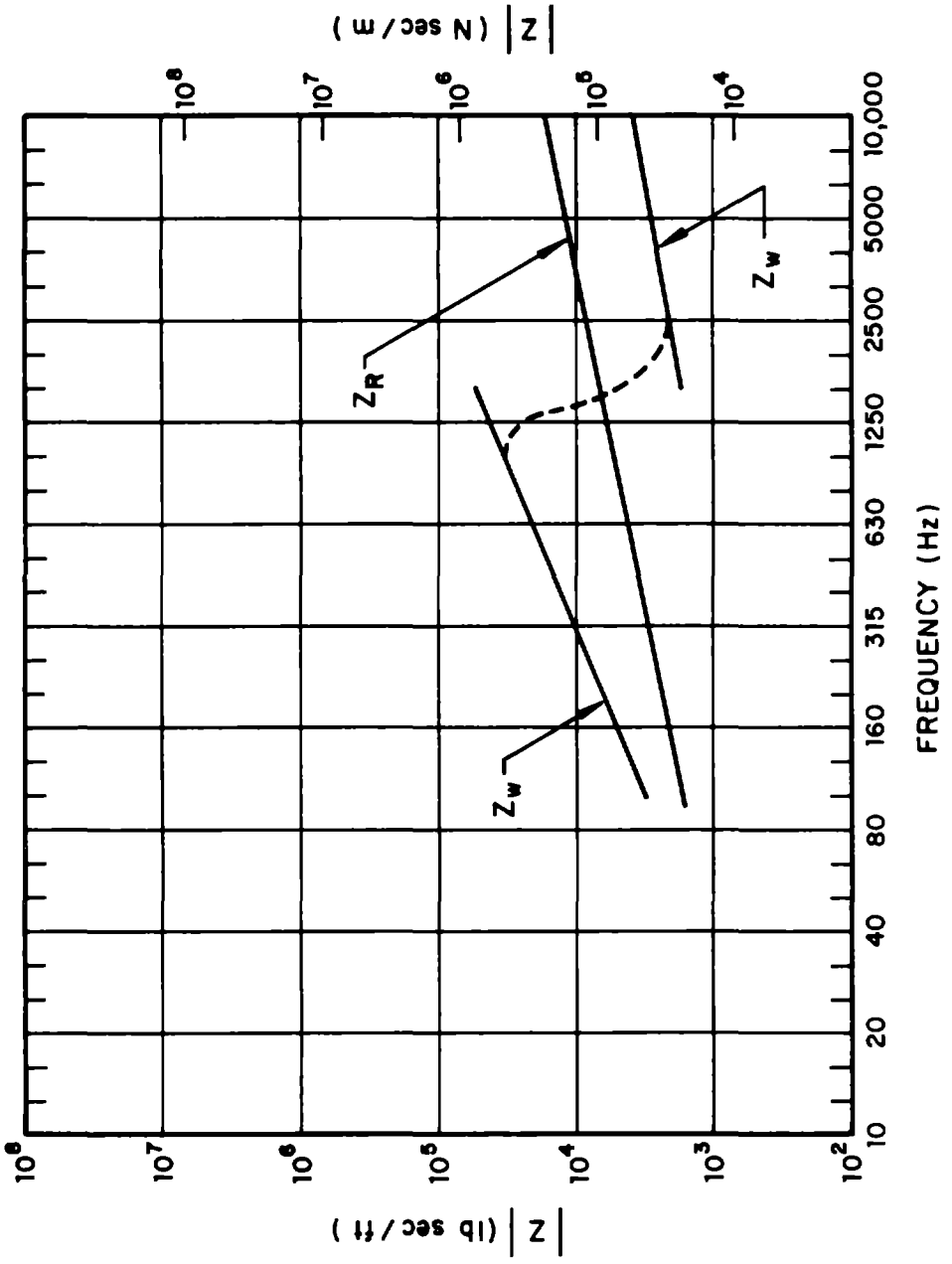

FIG. 3.4-4 WHEEL AND RAIL IMPEDENCE ESTIMATES FOR PULLMAN STANDARD TESTS

In fact, because of some uncertainty as to just where the break occurs, we will assume that from 1250 to 2000 Hz, $Z_W \approx Z_R$ such that

$$\left|\frac{Z_R}{Z_W+Z_R}\right|^2 \cong \left|\frac{Z_W}{Z_R+Z_W}\right|^2 \cong \frac{1}{4} \quad .$$

The weight of the PRT vehicle is ~7000 lb (3180 kg), which gives 1750 lb (7700 N) load applied to each wheel. The radius of the rail head is given as 12 in. (0.31 m). The contact patch then is an ellipse with major and minor axes of length 0.12 in. × 0.23 in. (3 mm × 5.9 mm). As before, we will approximate this by a circle having a radius b of

$$b = \frac{1}{2}\sqrt{(0.12)(0.23)} = 0.083 \text{ in. } (2.1 \text{ mm}) \quad .$$

The contact patch wavenumber filter can then be estimated from Fig. 2.4-2 of Sec. 2.4. Using the estimate for the contact patch wavenumber filter and the rail roughness data of Fig. 3.4-1*, we obtain Fig. 3.4-5, which displays the dimensionless roughness excitation applied to the wheels and rails at 10, 20, and 25 mph (16, 32, and 40 km/h).

The wheelbase of the PRT vehicle is 8 ft (2.45 m). Equation 3.4-2 demonstrates that only the radiation from the wheel opposite the microphone is significant, and from Sec. 2.4 it can be shown that below 2000 Hz only the excitation in the rail produced by that wheel is significant in causing the rail to radiate sound. Above 2000 Hz both wheels cause the rail to radiate equally.

---

*The turned wheels are much less rough than the rails.

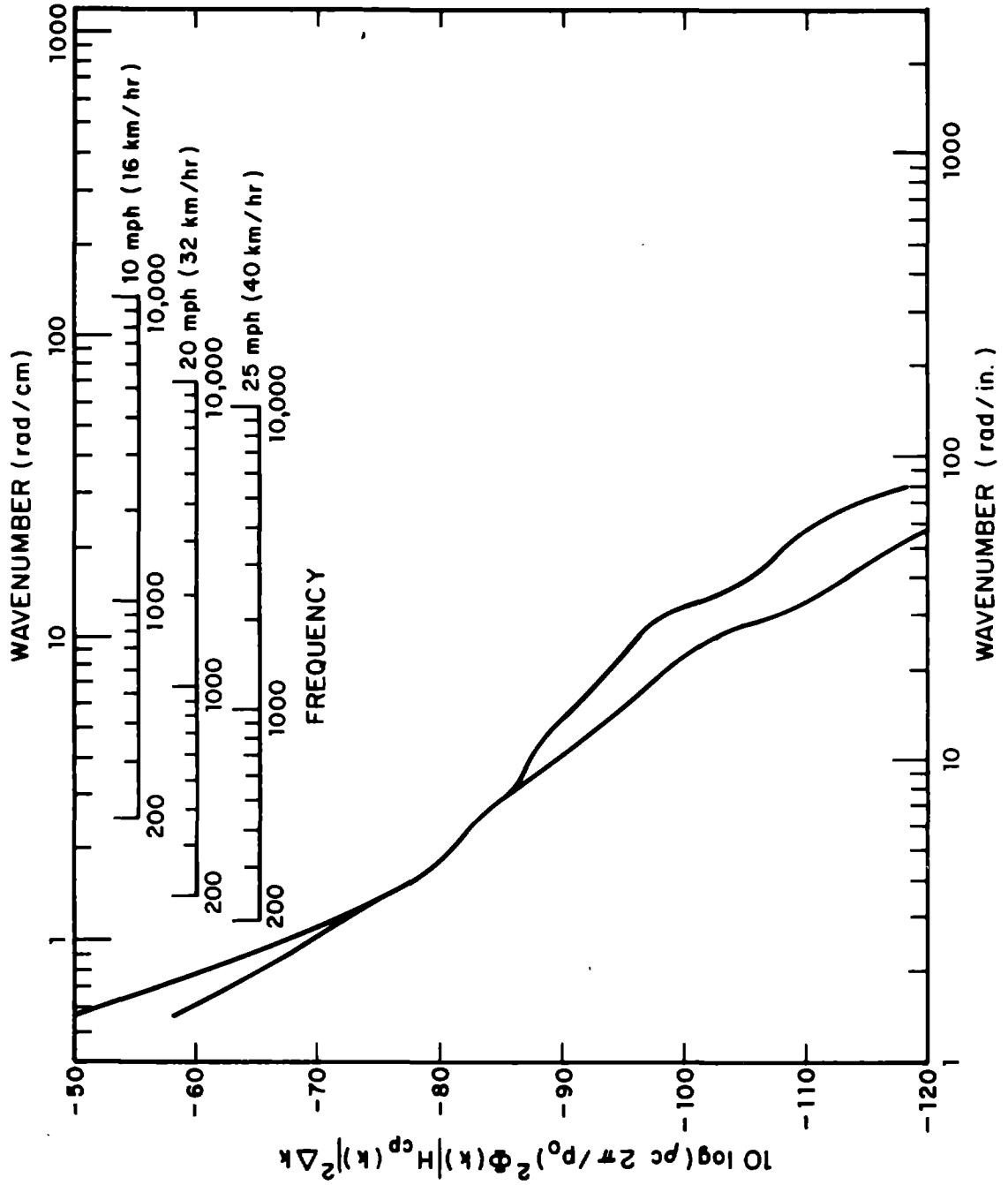

FIG. 3.4-5. FILTERED RAIL ROUGHNESS.

Comparisons of measured and predicted radiated sound and rail vibration are shown in Figs. 3.4-6 through 3.4-11. In general, the agreement is quite good except that at low frequencies we tend to underpredict the radiated sound.* If we had included the local Hertzian stiffness, these low-frequency levels would have been raised approximately 3 dB (see Appendix C), which would certainly improve the agreement. However, within the limits of the approximate models used to develop the predictions, the agreement is as good as could be expected. The major conclusions to be drawn from the results are that the wheel dominates the sound radiation at low frequencies (<315 Hz) and high frequencies (>2000 Hz) and that the rail dominates in the mid frequencies (400 Hz to 1600 Hz). At low frequencies the wheel impedance is only slightly larger than the rail impedance, implying that response levels are comparable. However, the rail is an inefficient radiator at these low frequencies, which results in wheel radiation dominating. In the mid frequencies, the rail impedance is much less than the wheel impedance, implying higher rail response levels; since the rail is an efficient radiator, the sound radiation from the rail dominates. At high frequencies the wheel impedance drops below the rail impedance, resulting in higher wheel response and, hence, higher sound radiation levels.

Figures 3.4-9 through 3.4-11 show measured vs predicted vertical rail acceleration levels at three speeds. Rail acceleration is well predicted at 25 mph (40 km/h) but overpredicted at 20 mph (32 km/h) and 10 mph (16 km/h). Part of the discrepancy

*Previous measurements of the propulsion noise from the vehicle [Gramse and Spence (1974)] made with the vehicle jacked up showed that the vehicle was 15 to 20 dB(A) noisier when running on the rails at 10 to 25 mph (16 to 40 km/hr) than when jacked up, providing at least one indication that wheel/rail noise dominates propulsion noise.

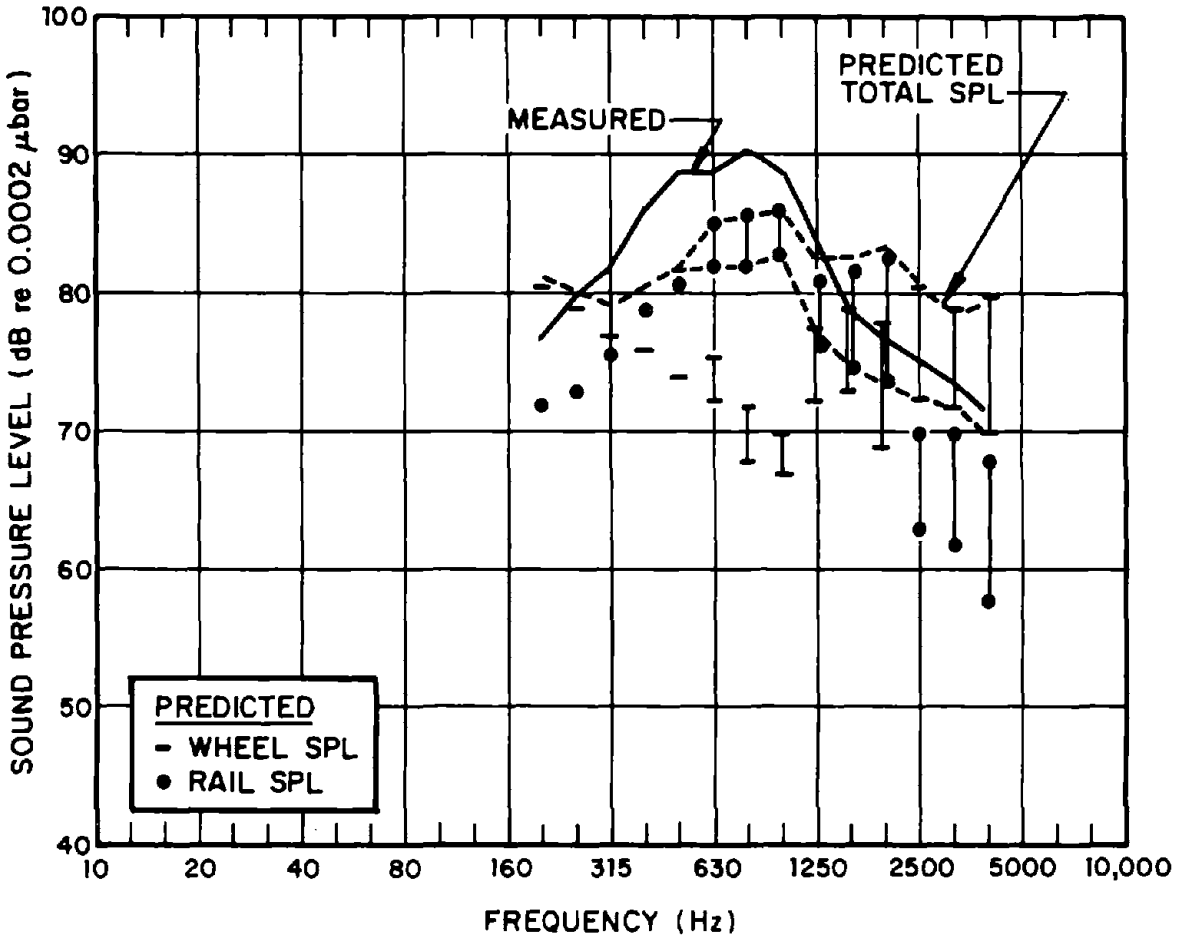

FIG. 3.4-6 WHEEL/RAIL NOISE AT 25 MPH (40 km/h) AT 3 FT (0.91 m) FROM THE WHEEL

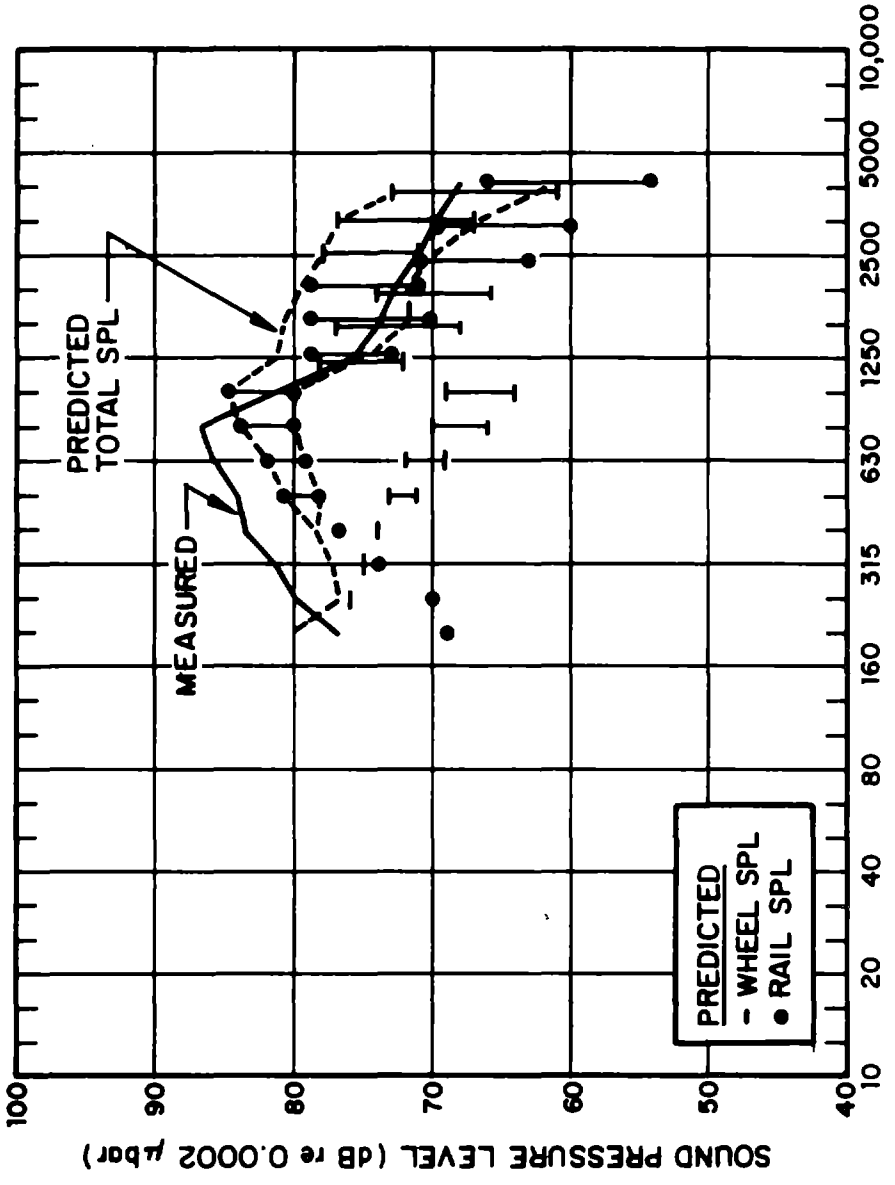

FIG. 3.4-7 WHEEL/RAIL NOISE AT 20 MPH (32 km/h) AT 3 FT (0.91 m) FROM THE WHEEL

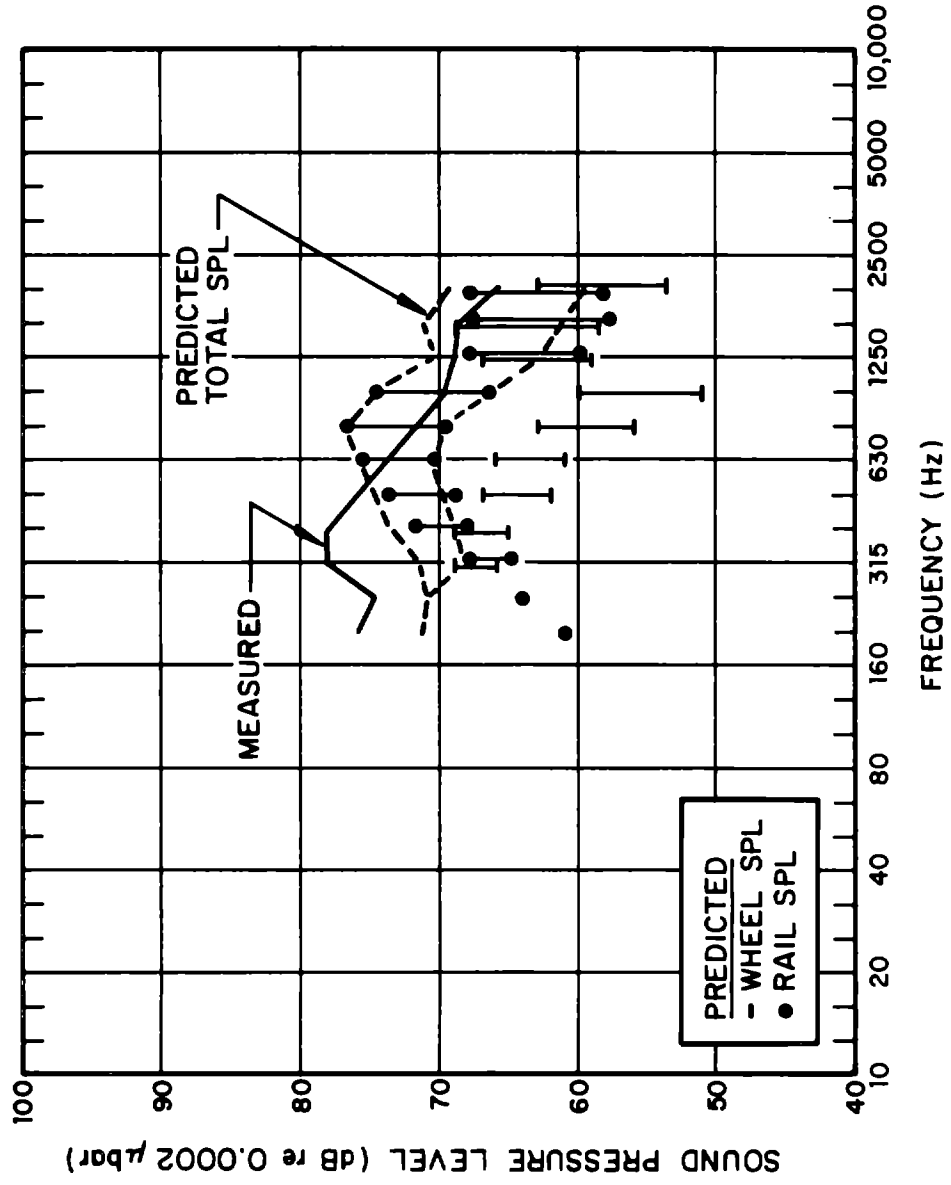

FIG. 3.4-8 WHEEL/RAIL NOISE AT 10 MPH (16 km/h) AT 3 FT (0.91 m) FROM THE WHEEL

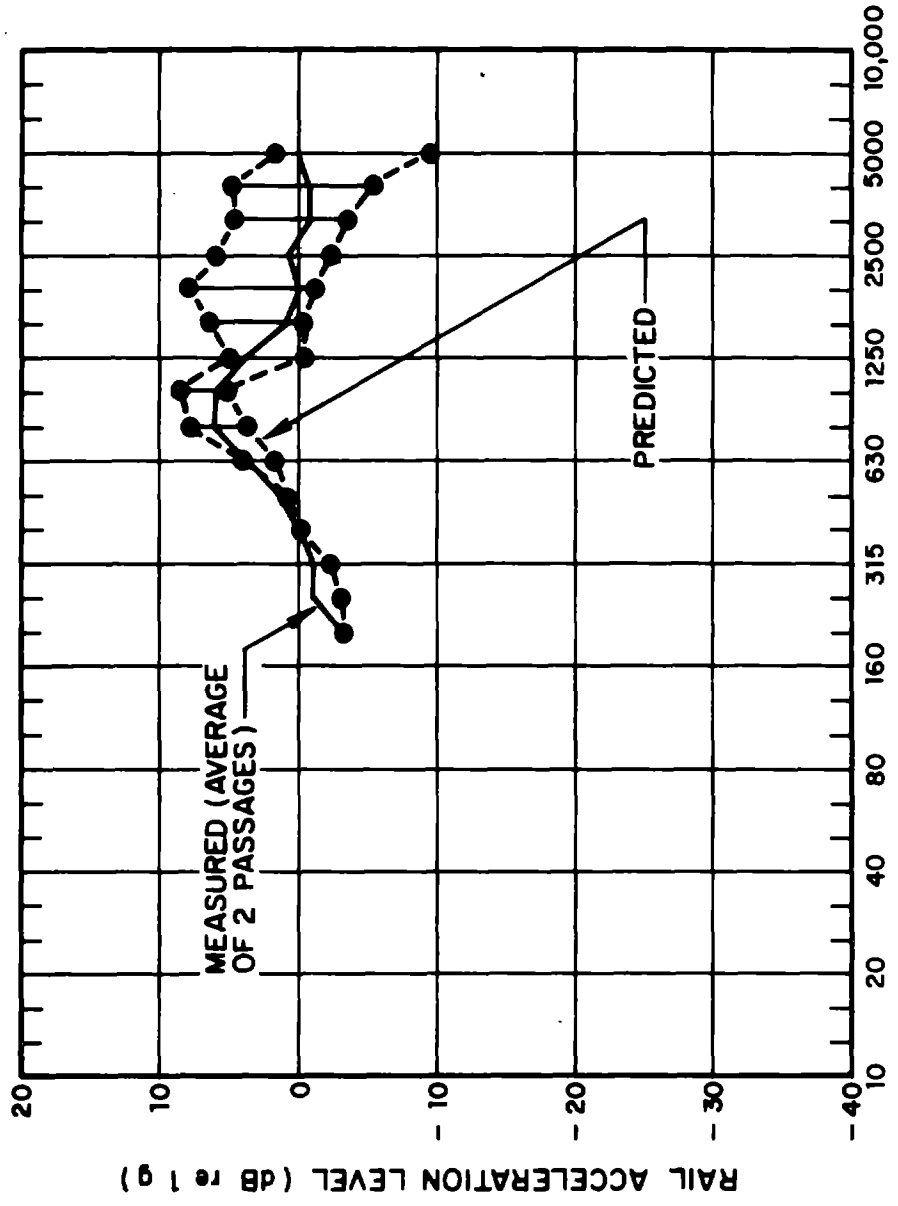

FIG. 3.4-9 VERTICAL RAIL ACCELERATION AT 25 MPH (40 km/h)

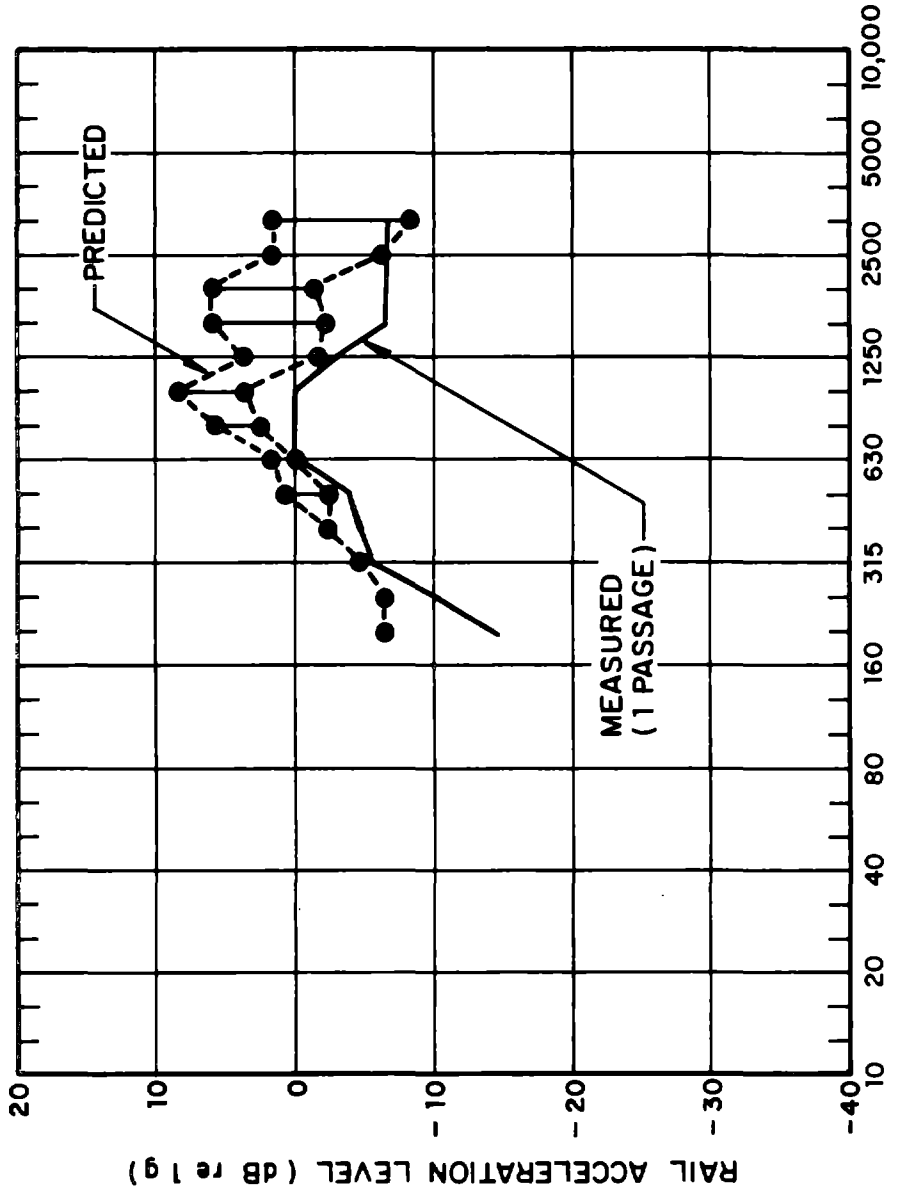

FIG. 3.4-10 VERTICAL RAIL ACCELERATION AT 20 MPH (32 km/h)

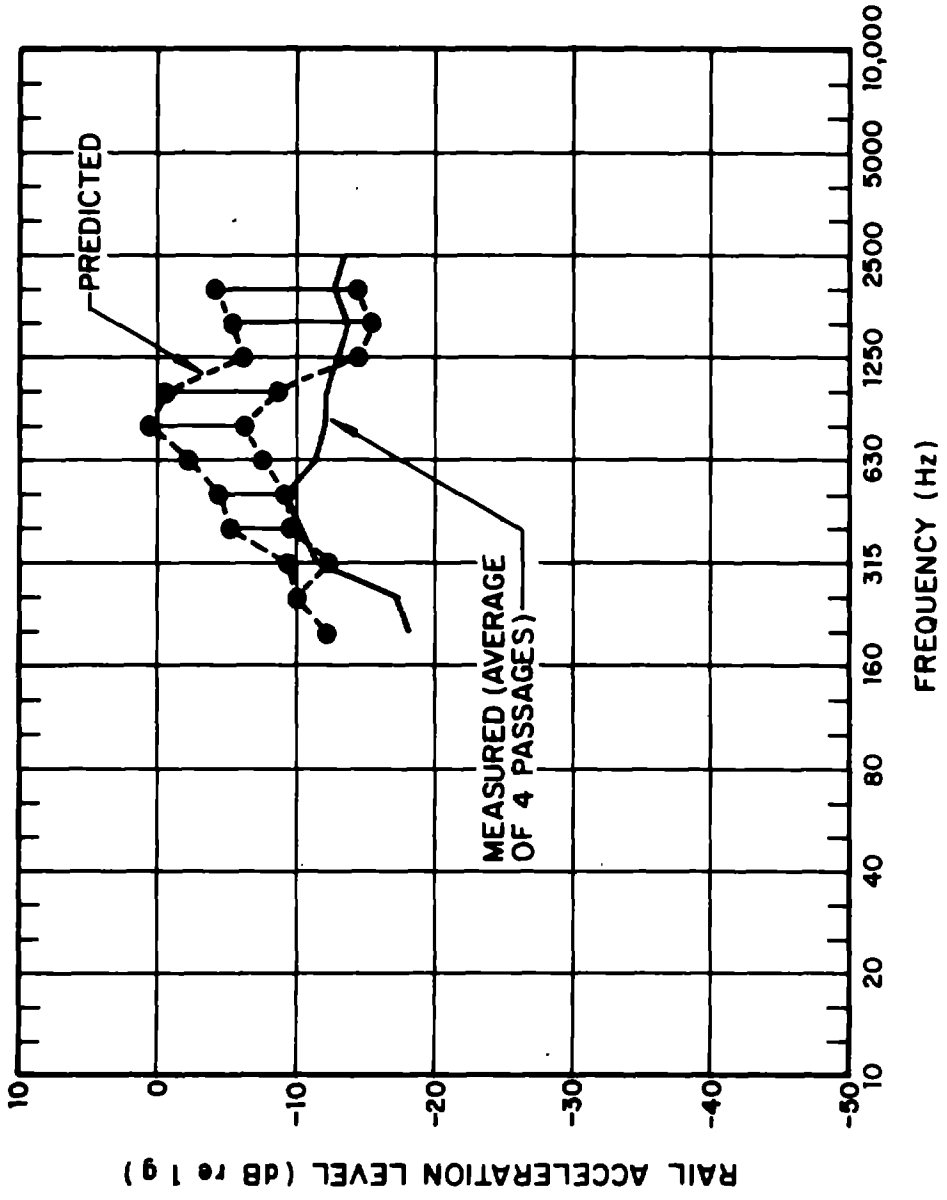

FIG. 3.4-11 VERTICAL RAIL ACCELERATION AT 10 MPH (16 km/h)

may result from the fact that one-half second averages were used to obtain the rail vibration data in Figs. 3.4-9 through 3.4-11. A mark on the voice track of the recording tape indicated when the wheel was directly over the accelerometers in the center of the rail test section. Unfortunately, because of the rapid decay of vibration along the rail, at some frequencies the averaged measured levels can be considerably lower than the peak levels when the wheels are directly above the accelerometers. We have tried to correct for this effect in the predictions by assuming that the averaging begins when the vehicle is centered over the accelerometer and that the mean square rail vibration decays like $e^{-\eta x}$ where η is given in Sec. 2.1.3. The predictions are then corrected by

$$\frac{e^{-\eta L/2}(1-e^{-\eta d})}{\eta d} + \frac{1-e^{-\eta(d-L/2)}+1-e^{-\eta L/2}}{\eta d} ,$$

where L is vehicle wheelbase, 8 ft (2.45 m), and d is the distance the vehicle travels during the averaging time. Unfortunately, small errors in putting the time mark on the tape or in beginning integration of the data during data reduction can result in considerably reduced acceleration levels. These may be two of the causes for the measured acceleration levels falling below the predictions.

3.4.2 Damped wheels

For the damped wheel tests, damping was applied to the standard wheels, which were turned smooth before the tests began (see Sec. 3.1 for description of damping treatment). The data were gathered in the same manner as for the standard wheel tests. According to the analytical models of Sec. 2.4,

we would expect no change in roar noise to result through the use of damped wheels, since under radial forcing the wheel response is primarily nonresonant. This expectation is confirmed by Figs. 3.4-12 through 3.4-14, which compare the wayside SPL from the damped wheels to the noise from the standard wheels for three speeds. In general, the levels are comparable.

3.4.3 Resilient wheels

According to our model, resilient wheels should modify wheel/rail noise in two ways. First, the wheel impedance will change, which will affect the relative levels of wheel and rail response. Second, if the web on the wheel is effectively vibration isolated from the tread, then wheel radiation should be reduced.

Using the device described in Sec. 2.4, we measured the roughness of one of the Penn Cushion resilient wheels described in Sec. 3.1. The 1/3-octave band spectrum of roughness amplitude is shown in Fig. 3.4-15. Note there is some scatter in the data with rotation speed. The solid curve that follows the data from the lowest rotation speed is the one that will be used in the following predictions. The wheel roughness below k = 10 rad/in. (4 rad/cm) is much less than the rail roughness. However, above that value of k, wheel and rail roughness become comparable.* Combining this data with the rail roughness data described in Sec. 3.4.1, we obtain Fig. 3.4-16. This figure plots the dimensionless wheel/rail roughness, including the filtering effect of the contact patch (the same filter characteristic that applies for the standard wheels).

---

*This is in contrast to the standard wheels which after turning were everywhere less rough than the rail roughness.

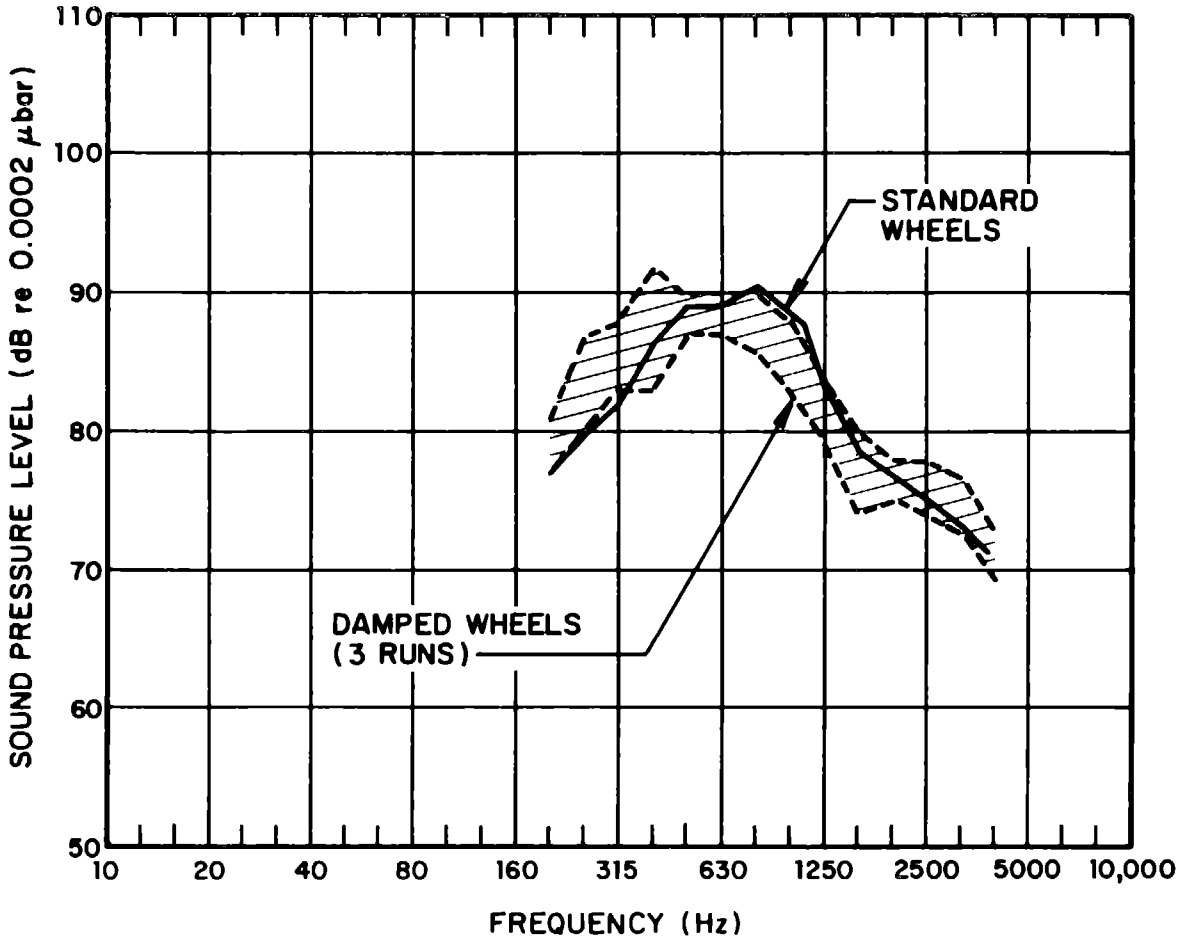

FIG. 3.4-12 WHEEL/RAIL NOISE, STANDARD AND DAMPED WHEELS AT 25 MPH (40 km/h) AT 3 FT (0.91 m) FROM THE WHEEL

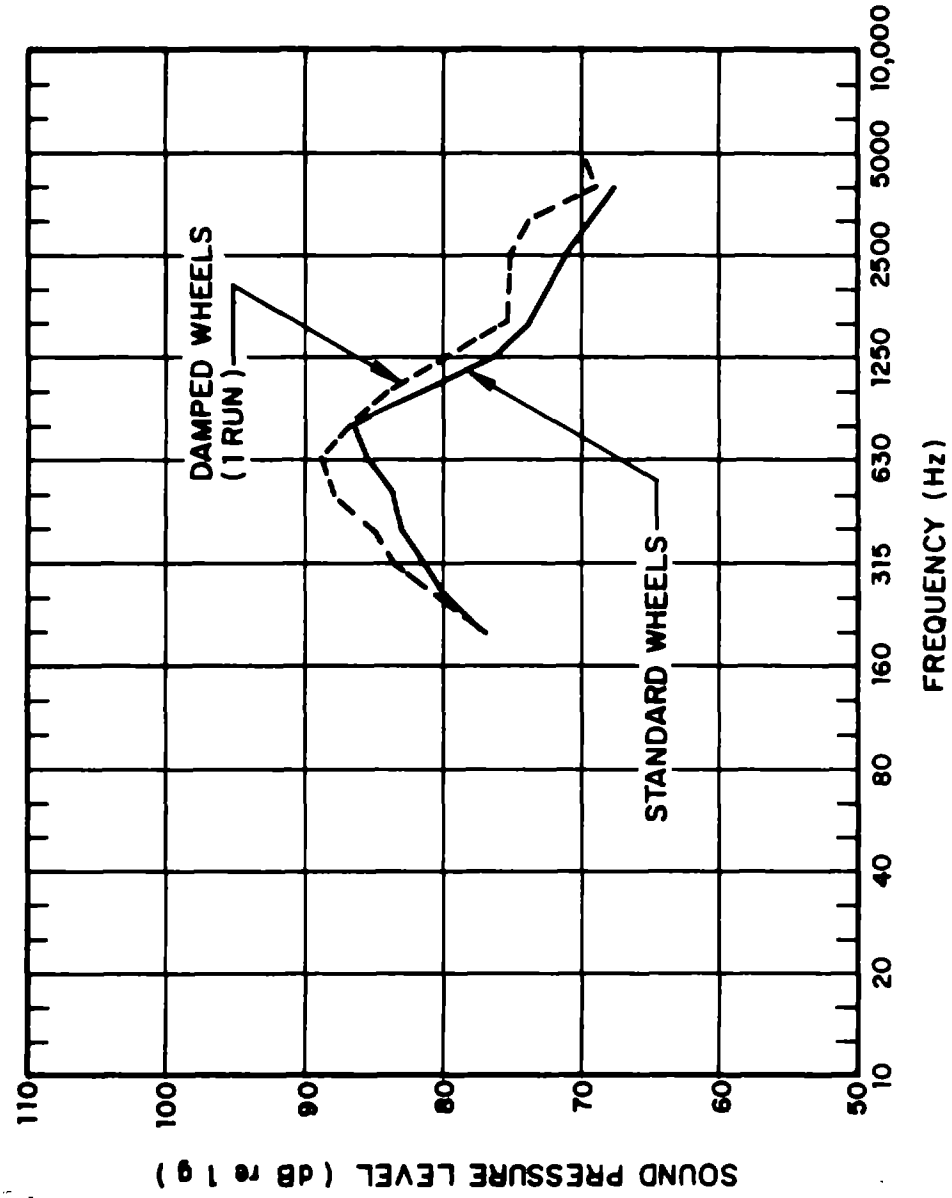

FIG. 3.4-13 WHEEL/RAIL NOISE, STANDARD AND DAMPED WHEELS AT 20 MPH (32 km/h) AT 3 FT (0.91 m) FROM THE WHEEL

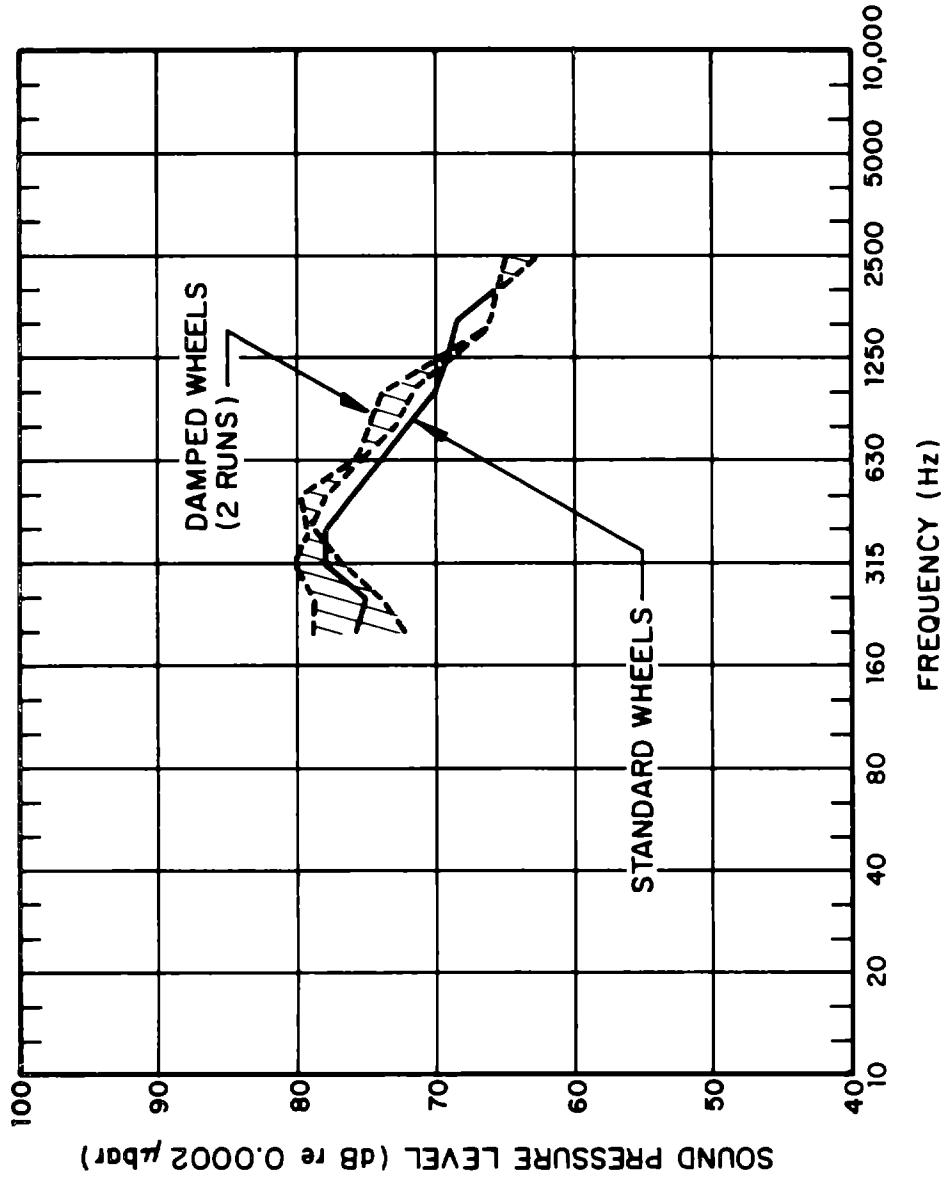

FIG. 3.4-14 WHEEL/RAIL NOISE, DAMPED AND STANDARD WHEELS AT 10 MPH (16 km/h) AT 3 FT (0.91 m) FROM THE WHEEL

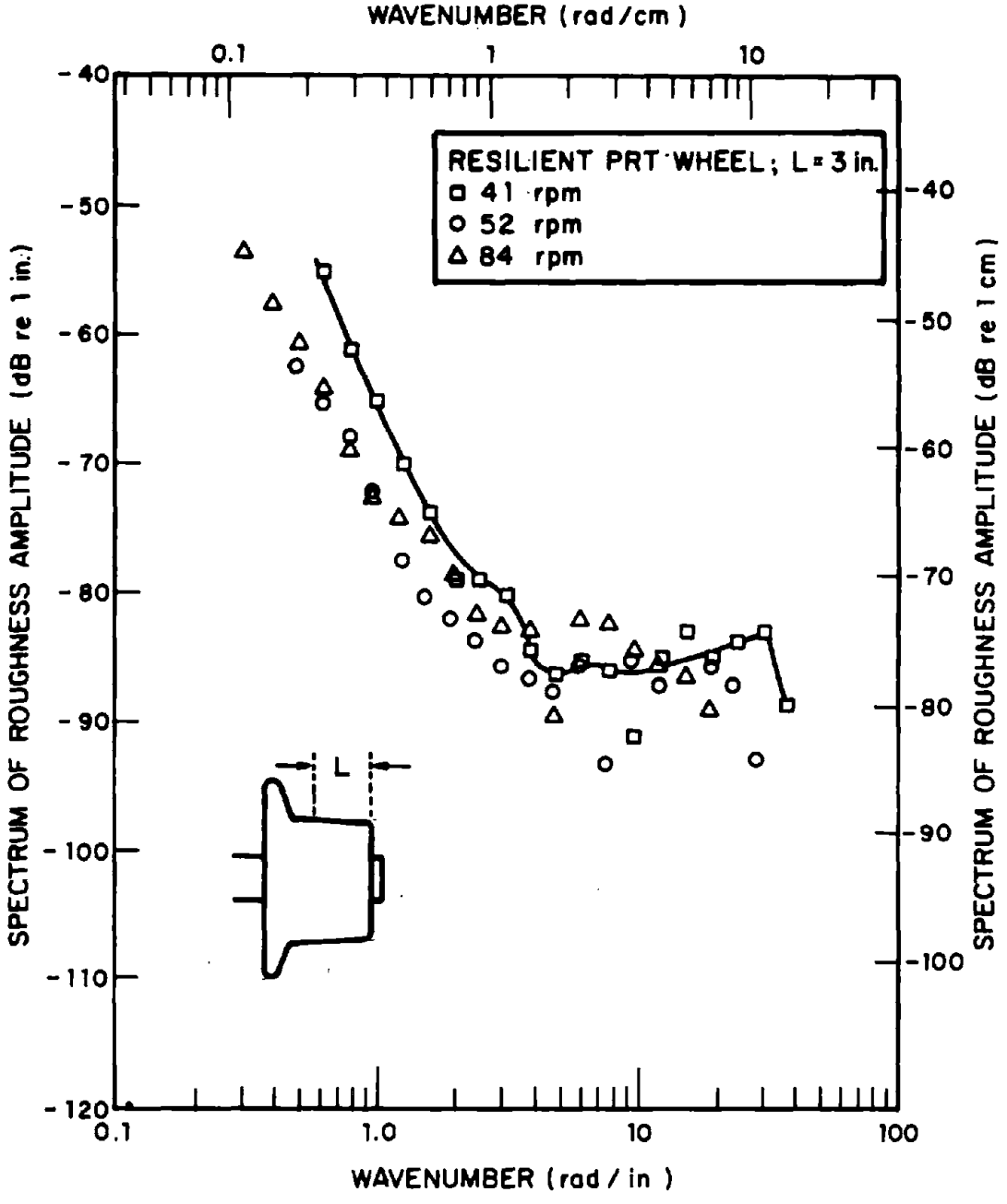

FIG. 3.4-15 RESILIENT WHEEL ROUGHNESS

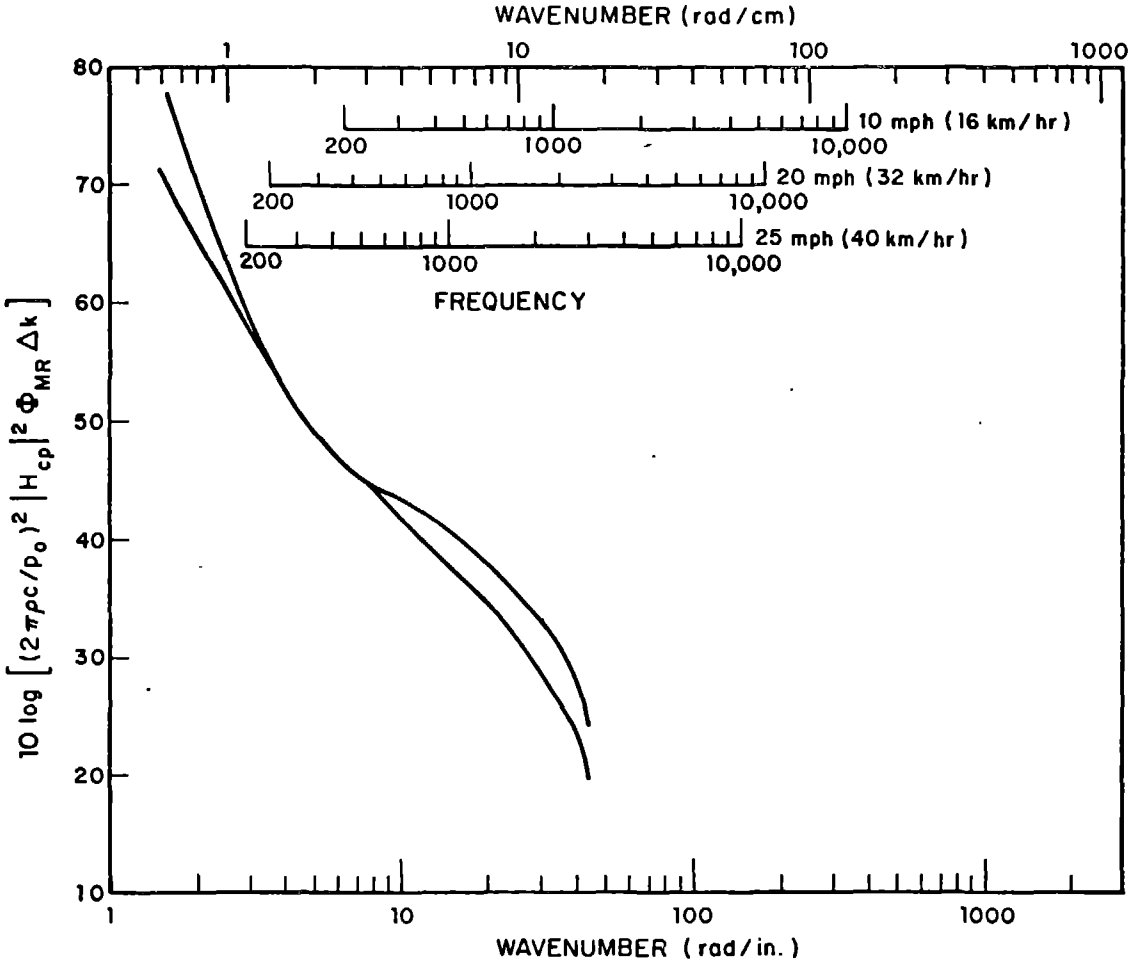

FIG. 3.4-16. WHEEL AND RAIL ROUGHNESS, RESILIENT WHEELS.

The radial impedance of one of the resilient wheels was measured by simply resting the wheel (unattached to an axle) on its hub and forcing it at the tread with an electromagnetic shaker in the same way used to measure the impedance of the 14 in. (35.5 cm) diameter standard wheel described in Sec. 2.1.1. The results of the impedance measurement are shown in Fig. 3.4-17 along with the predicted impedance of the 60 lb/yd (30 kg/m) rail used in the P-S test track. The wheel impedance was measured in 1/10-octave bands. In the figure, the dotted portions of the curve of impedance amplitude show that impedance data averaged in 1/3-octave bands.

The phase between force and velocity also shown in Fig. 3.4-17 was measured with a polarity coincidence correlator. It measured the phase angle between force and acceleration and obtained the phase angle between force and velocity by subtracting 90°. A difficulty is that this type of phase meter gives an angle between 0° and 180° and cannot tell whether force or acceleration is leading (i.e., a +5° or -5° phase shift between force and acceleration would both be measured as 5°). Thus, the sign of the real part of the impedance is uncertain. Ordinarily, this ambiguity causes no problems unless the wheel and rail impedance are nearly equal. In Fig. 3.4-17 this occurs around 500 Hz and around 1250 Hz. However, by reasoning physically we see that a negative real part of the impedance implies negative damping, which cannot occur in a passive system. As a result, the phase shown in Fig. 3.4-17 must be correct.

The resilient pads between the tread and web tend to isolate the web from excitation applied to the tread. To examine this isolation, we supported one of the resilient wheels at its hub as for the impedance measurement and used an electromagnetic shaker

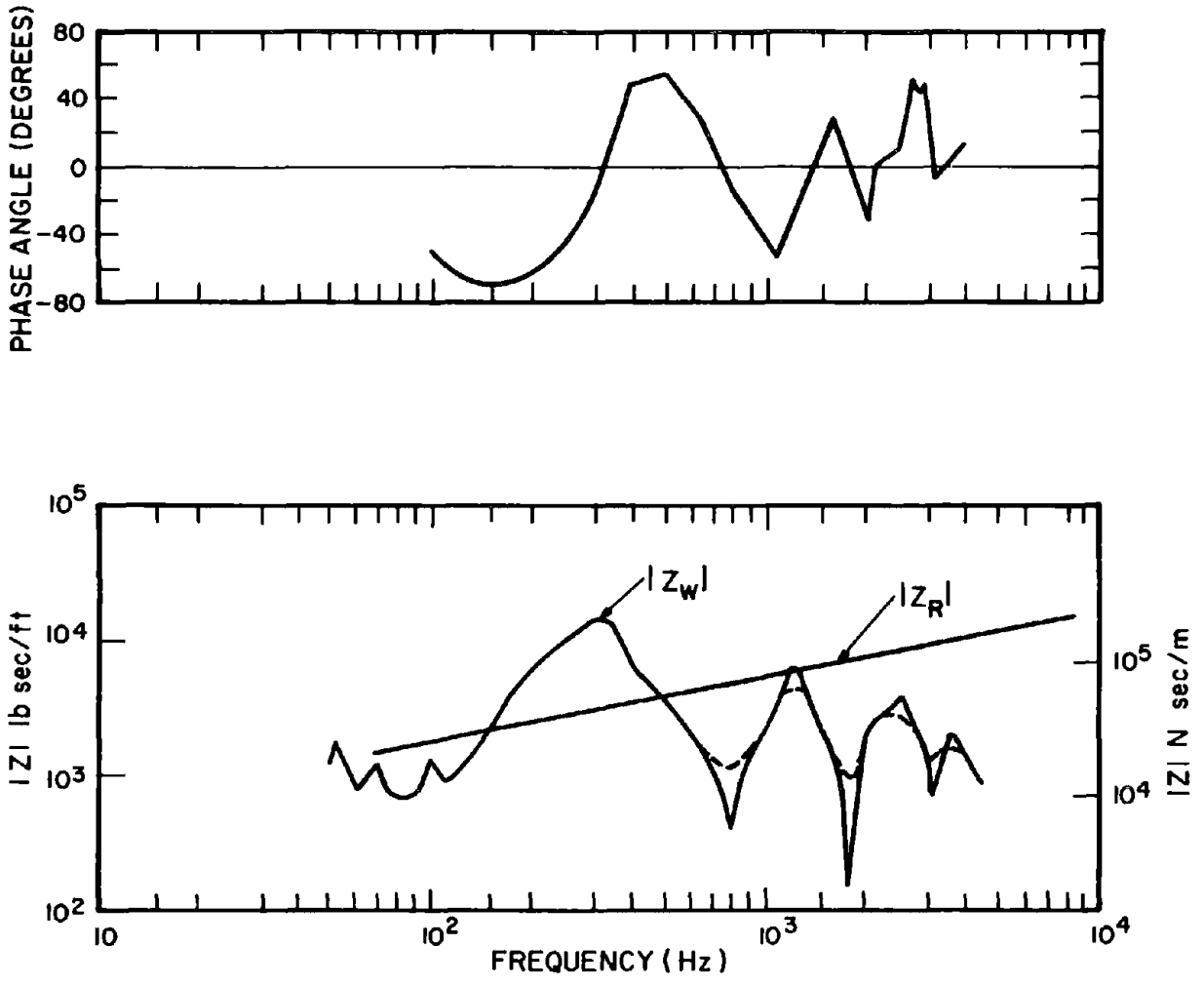

FIG. 3.4-17 PENN CUSHION RESILIENT WHEEL RADIAL IMPEDANCE

to excite the wheel in the center of the tread face in the radial direction. Acceleration measurements were then recorded at five positions around the tread and around the web using a B&K 4333 accelerometer through an Ithaco preamplifier into a Kudelski Nagra III tape recorder. The data were later reduced in the laboratory in 1/3-octave bands using a General Radio real time analyzer. The ratio of the tread acceleration (average of five points) to the web acceleration (average of five points) is shown in Fig. 3.4-18*. In what follows we will assume that the wheel radiates primarily from the web and use Fig. 3.4-18 to relate tread to web acceleration.

---

*The data in this figure were originally 10 dB higher, i.e., the web appeared to be 10 dB better isolated from the tread than shown. These data indicated that the resonance of the tread and web masses on the isolating pads separating the two was around 100 Hz. Measurements of the pad stiffness obtained by measuring the deflection of the tread relative to the web under the weight of the PRT vehicle gave a lower bound for the stiffness of $2 \cdot 10^6$ lb/ft ($2.9 \cdot 10^7$ N/m). With the tread mass at 60 lb (27.2 kg) and the hub (web) mass at 27 lb (12.3 kg) this stiffness implies an antiresonance (peak) in impedances at ~250 Hz and a resonance (minimum) in impedance at 300 Hz. Because the stiffness of the wheel is a lower bound, these frequencies are lower bounds. In fact, the impedance measurements suggest that these frequencies should be 300 to 400 Hz for the antiresonance and 800 Hz for the resonance, implying that significant attenuation would not occur until above 300 to 400 Hz. Based on this simple model and taking the antiresonance to occur at 400 Hz, the dotted curve in Fig. 3.4-18 shows what one would predict for attenuation with no damping. The damping introduced by the elastomer causes the discrepancy near 400 Hz. As a result, we conclude that there must have been a 10 dB error in recording one of the attenuation settings and we will use the corrected curve of Fig. 3.4-18 in the calculations that follow.

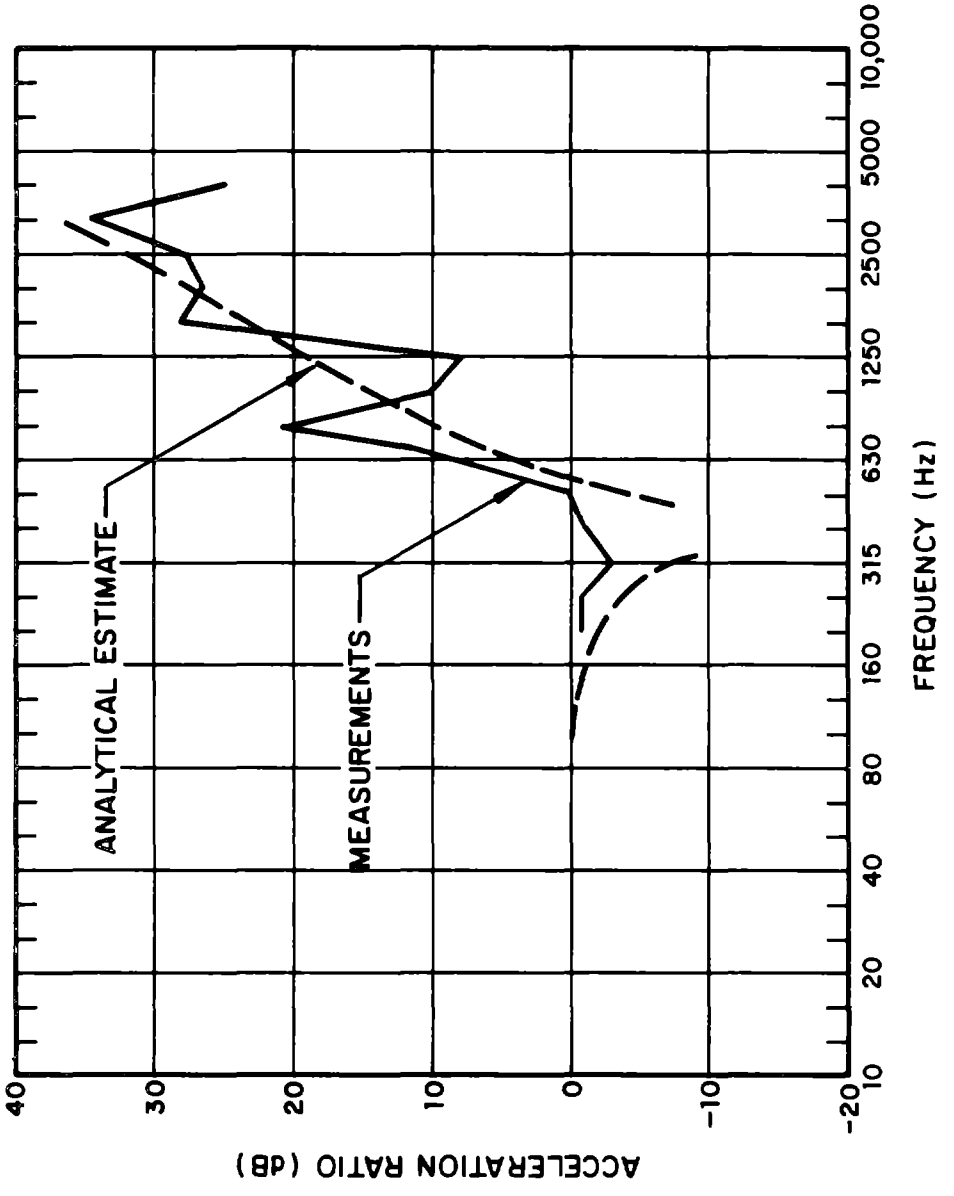

FIG. 3.4-18 RATIO OF TREAD TO WEB ACCELERATION FOR THE PENN CUSHION WHEEL UNDER RADIAL FORCING

At the Pullman Standard test track, the PRT vehicle was fitted with the four Penn Cushion resilient wheels and measurements of wheel/rail noise taken as with the standard wheels using the same section of track as a test section. The data are shown in Figs. 3.4-19 through 3.4-21 for vehicle passage speeds of 10, 20 and 25 mph (16, 32 and 40 km/h) along with the data from the standard wheel tests. The major differences that one notices are the strong dip in the noise at 800 Hz that correlates with the dip in wheel impedance at 800 Hz and the higher levels at high frequencies due to the higher roughness on the resilient wheels as compared to the polished standard wheels.

Using the same method we used for the standard wheels, we have combined Eqs. 3.4-1 and 3.4-2, the above roughnesses and impedances, the the radiation efficiency models of Sec. 2.1.3 to predict the sound radiated by the wheels and rails. These predictions are shown in Figs. 3.4-19 through 3.4-21. In general, the authors believe that the agreement between prediction and measurements is quite good, although in all cases we tend to predict noise levels that are too low at 800 Hz. The noise at the measurement position, 3 ft (0.91 m) from the lead wheel, is due primarily to the radiation from the lead wheel and to the rail vibration excited by that wheel.* At 800 Hz, the drop in wheel impedance causes the rail radiation to decrease and the fact that the web is well isolated from the tread causes the wheel radiation to drop. In all likelihood, radiation from other sources (drive motors, tread of the second wheel, etc.) keep the SPL from dropping as much as predicted.

*As with the standard wheels, radiation from the rail due to excitation by *both* wheels on the microphone side of the PRT contributes significantly to the total noise above 2000 Hz.

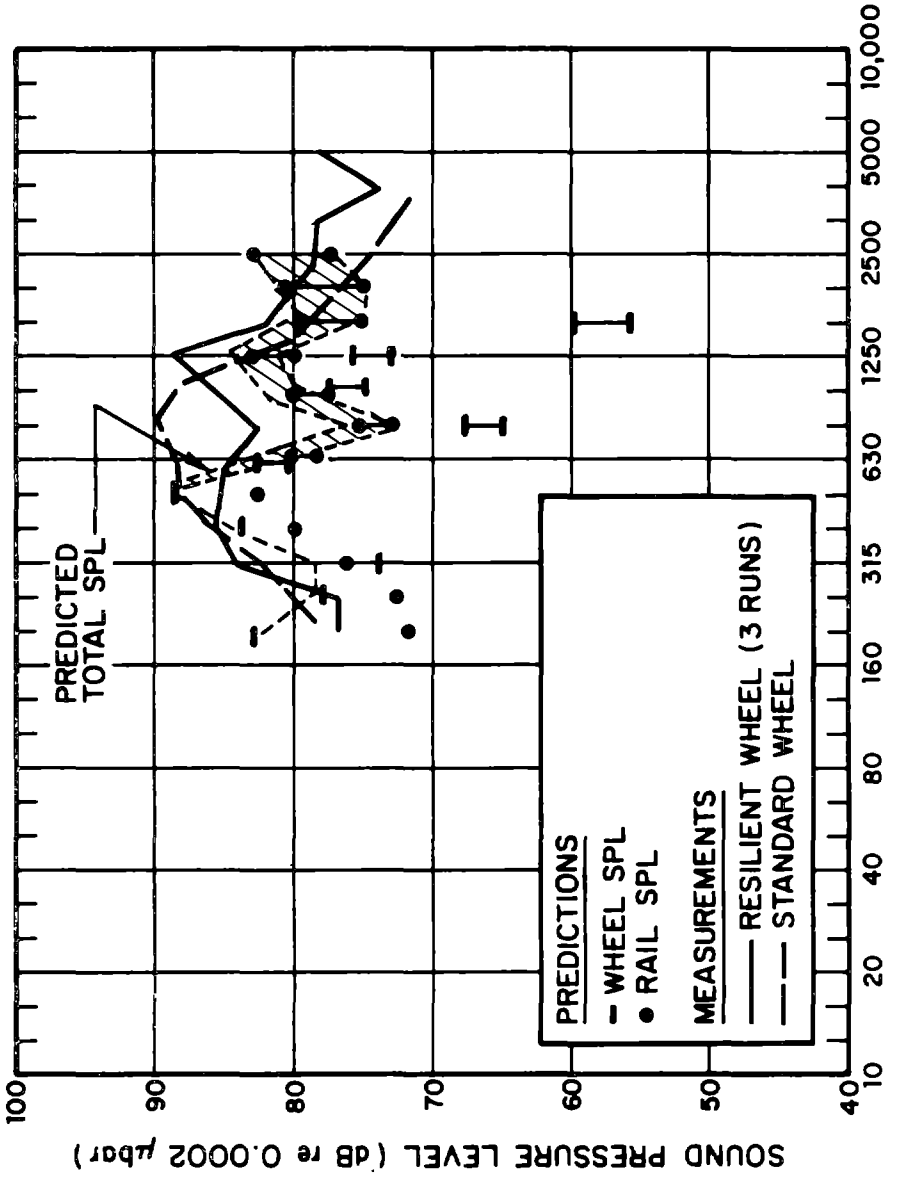

FIG. 3.4-19 WHEEL/RAIL NOISE, RESILIENT WHEELS AT 25 MPH (40 km/h) AT 3 FT (0.91 m) FROM THE WHEEL

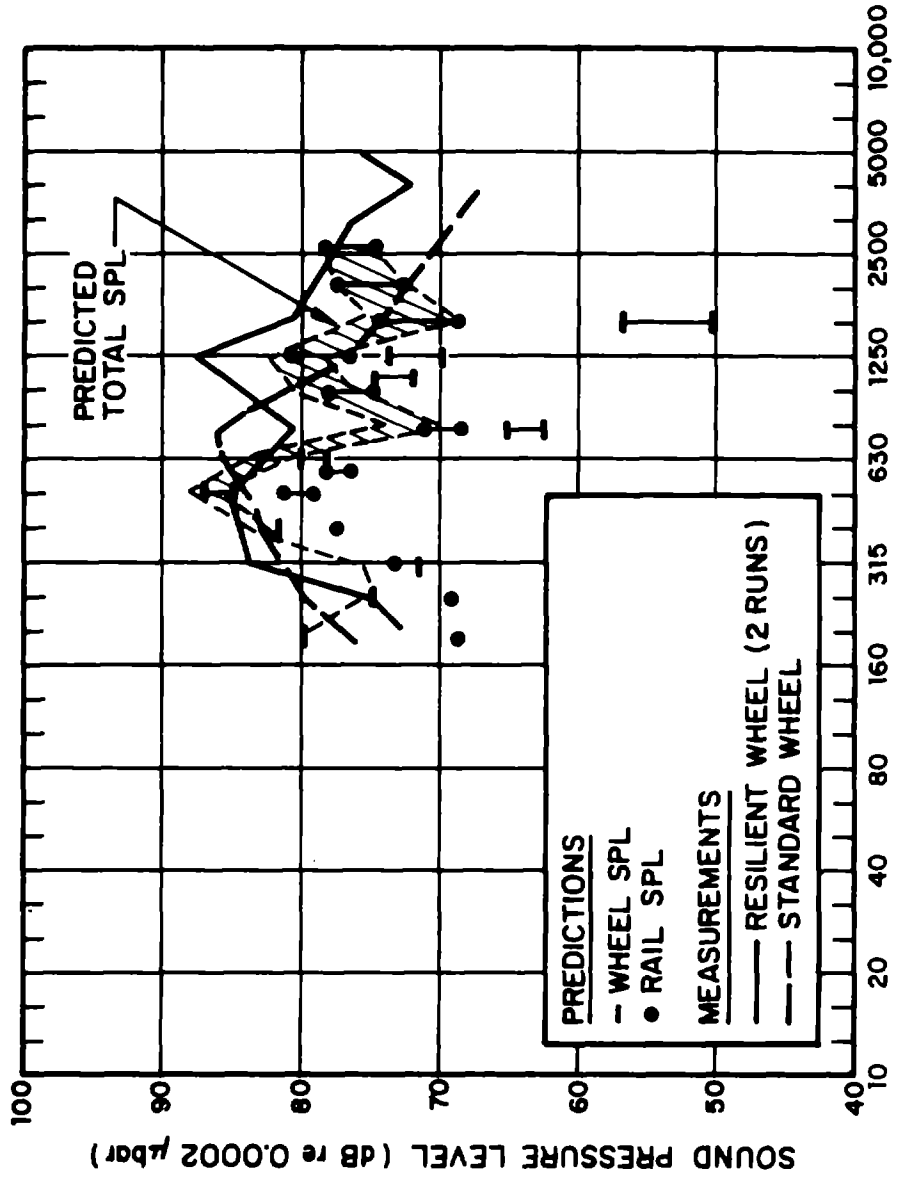

FIG. 3.4-20 WHEEL/RAIL NOISE, RESILIENT WHEELS AT 20 MPH (32 km/h) AT 3 FT (0.91 m) FROM THE WHEEL

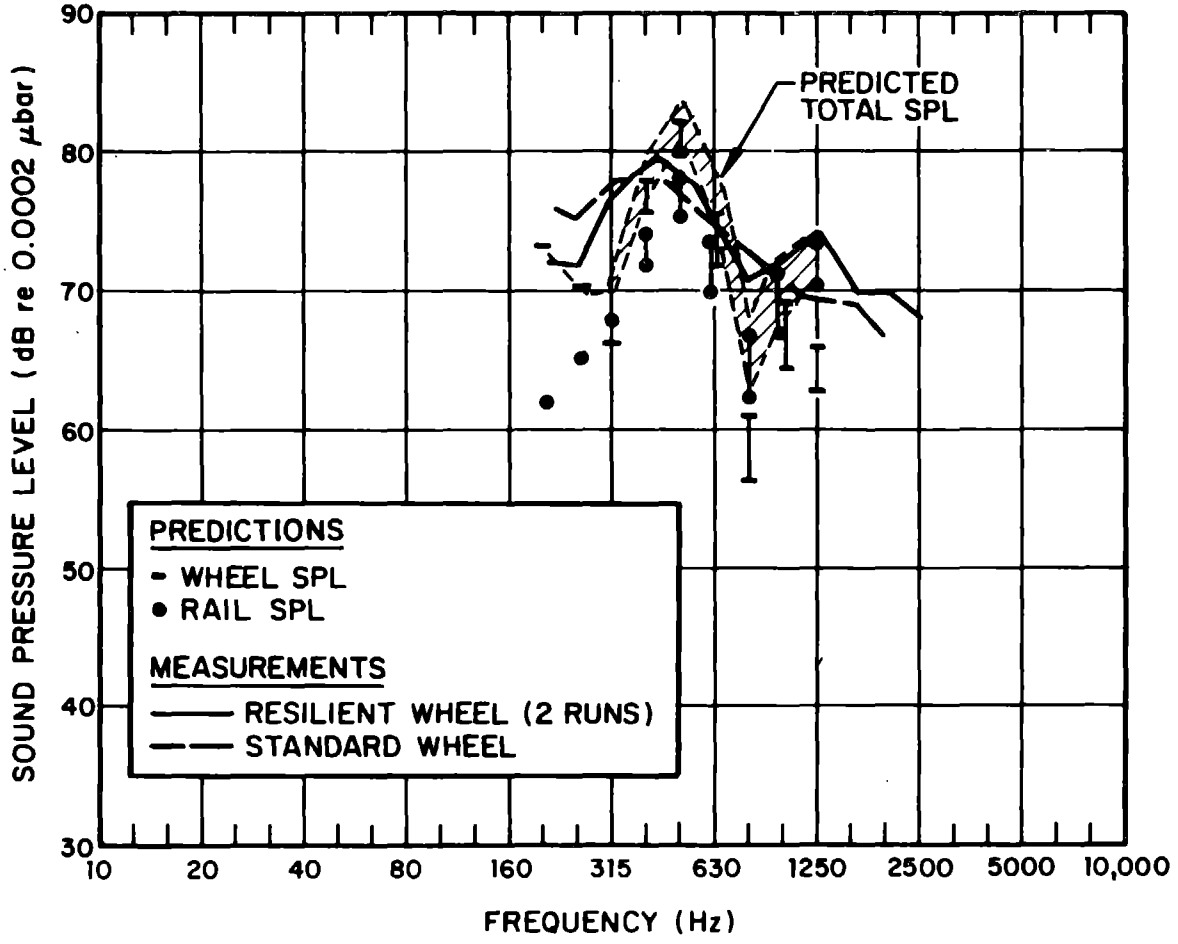

FIG. 3.4-21 WHEEL/RAIL NOISE, RESILIENT WHEELS AT 10 MPH (16 km/h) AT 3 FT (0.91 m) FROM THE WHEEL

4. TECHNIQUES FOR THE SUPPRESSION OF WHEEL/RAIL NOISE

The predictive formulas for wheel/rail noise verified with measured data provided considerable insight into various means by which wheel/rail noise may be controlled. Although it is apparent that some of the factors affecting wheel/rail noise cannot be modified, we have examined others that may be changed with beneficial results. In some cases, the suggested noise control techniques merit further study of their utility and practicality.

4.1 Suppression of Wheel Squeal Noise

4.1.1 Articulated trucks

Wheel squeal is caused primarily by the crabbing of the wheels of a truck in a curve. Thus, the most obvious technique for eliminating wheel squeal is to eliminate the crabbing of the wheels. One way of doing this is to use articulated trucks whose front and rear axles can pivot about a vertical axis. Such trucks could "steer" around curves. However, an articulated truck would be mechanically complex and may "hunt", or oscillate laterally at high speeds.

An alternative approach to eliminating crabbing would be to design the axle suspension to be compliant, so that the axles would naturally steer themselves around curves. The compliance might be achieved through the use of swing links and would have to be very carefully designed.

4.1.2 Short trucks

According to our model, the maximum curve radius at which wheel squeal can occur is about 100 times the truck length. Thus one can eliminate squeal on large radius curves by

employing shorter trucks. For example, a 5-ft (1.5-m) long truck would not squeal on a curve with a radius greater than 500 ft (153 m). This technique might be useful on a system such as BART where the tightest radius is about 525 ft (160 m). Of course, practical limitations, such as providing sufficient space for traction motors, may make the design of so short a truck difficult.

4.1.3 Reduced wheel loading

The wheel squeal stability diagrams in Sec. 2.2 showed that below a minimum wheel loading, squeal will not occur. Therefore, installing more wheels on a car and/or reducing the weight of the car will make squeal less likely.

Unfortunately, increasing the number of wheels by adding a third truck to a car or employing six-wheel trucks may increase cost and complexity to such an extent that such modifications would be impractical. Reducing the weight of cars may also be difficult, for in recent years there has been a weight reducing incentive in car design and additional significant reduction in weight may be difficult to achieve without going to smaller, lower capacity vehicles.

4.1.4 Damped wheels

The wheel squeal model requires that the negative impedance due to the stick-slip phenomenon must exceed, in magnitude, the positive damping due to acoustic radiation and internal mechanisms in the wheel for squeal to occur. Under this pro-

gram we were able to measure the natural internal damping of railroad wheels. At the squeal frequencies, we found a loss factor of 0.03%, a very small value. The radiation damping has a similar value. The negative impedance of stick-slip has a value about 100 times greater. Thus, one possible method of eliminating squeal is to increase the damping of the wheel greatly so that it exceeds the magnitude of the damping due to stick-slip.

Large amounts of damping material can be applied to the wheel to increase its loss factor. Since subway car wheels are very massive, the damping material cannot be simply sprayed or bonded onto the wheel, but must be *constrained* between a stiff ring and the wheel itself. The loss factor η required to prevent squeal is given by

$$\eta > \frac{P\nu}{m\omega V} .$$

Take typical values of wheel loading P = 10,000 lb (44,500 N), ω = 3,000 rad/sec, modal mass m = 200 lb (98 kg), and V = $\sqrt{aR}$ where a = lateral acceleration = 3% g and R = radius of curve in ft (m). Then

$$\eta > \frac{\nu}{2\sqrt{R}} .$$

Let us suppose arbitrarily that ν, the slope of the friction-creep curve, is given by

$$\nu = \frac{5R}{R_0 - R}$$

where R_0 is the maximum curve radius at which squeal can occur. Then $\nu = \infty$ at $R = R_0$ and $\nu = 1$ at $R = R_0/5$. Accordingly, to avoid squeal

$$\eta > \frac{5\sqrt{R}}{2(R_0 - R)}$$

where the curve radius is in feet. If we have a radius of 600 ft (183 m) [R_0 = 700 ft (213 m)], we require a loss factor of 60% to prevent squeal. However, a curve of 200-ft (61 m) radius requires a loss factor of only 6% and a 50-ft (15.3 m) radius curve requires a loss factor of only 2-½% to prevent squeal. The tighter curves need a lower loss factor to prevent squeal because the slope of the friction-creep curve decreases as the creep increases on the tighter curves.

Kirschner (1972) has reported the results of applying damping treatment to subway train wheels. The loss factor of the constrained damping treatment was between 10% and 20%, depending upon frequency and temperature. Kirschner observed that this damping treatment suppressed squeal on the tighter curves. However, it is unlikely that any such moderate damping treatment can suppress squeal on the larger curves. On the other hand, the intensity of the squeal noise on these larger curves will be lessened.

4.1.5 Resilient wheels

It has been found that resilient subway wheels rarely squeal. However, there is nothing in the model of wheel squeal which predicts that resilient wheels are any less likely to squeal than regular ones. The model does predict that the frequency of the squeal may be lower than with a regular wheel

since the resilient wheel is more compliant. However, measurements conducted under this program have determined that a resilient wheel has a loss factor of about 10% compared to .03% for a regular wheel. Indeed, this loss factor is comparable to that for the damped wheel mentioned above. Therefore, it is not surprising that a resilient wheel is nearly as effective as a damped wheel at suppressing squeal. The resilience itself is irrelevant; it is the damping associated with the resilience that is important.

4.1.6 Wheel damping ring

For many years London Transport has been using a damping ring loosely inserted into a groove on the inside of the wheel tread. When the wheel vibrates, the ring moves in the groove and produces damping by friction or air pumping. This technique is commonly used in helicopter gears to reduce vibration. Measurements were made under this program as to the effectiveness of this damping ring. The ring was found to increase the damping by a factor of three or so, but the loss factor was still only about 0.1%. This is not sufficient to suppress squeal and the damping ring is *not* considered effective to this end.

4.1.7 Wheel damping plate

The effectiveness of a wheel damping plate was investigated at the same time as the damping ring.* The damping plate is bolted to the face of the wheel. The damping produced by the

*The test involved bolting a 1/4 in. (6.3 mm) aluminum plate to the face of a 1/2-scale-model steel railroad wheel. Holes were drilled and tapped into the web of the wheel such that when the bolts holding the plate of the wheel were tightened, the plate pressed against the hub and the side of the tread.

plate was found to be greater and more reproducible than the ring. However, the plate produced a loss factor of less than 1% (even though it sounded very dead), and this is not generally enough to prevent squeal.

4.1.8 Rail lubrication

It is known that relative humidity above 60% reduces the static friction and the slope of the friction-creep curve and, consequently, will reduce the negative impedance of the stick-slip and suppress squeal. Hence, one method for suppressing wheel squeal is to increase the relative humidity by spraying water on the rails. However, this step has a severe side effect and that is that it substantially *increases* the wear on wheel and rail. This increased wear happens because the water breaks down the protective oxide layer on the steel, giving rise to metal to metal contact that enables particles of metal to be pulled out of the rail by the wheel and vice versa. Corrosive lubricants, such as soaps, have the same effect: they suppress squeal but increase wear greatly.

A remaining possibility is hydrodynamic lubricants, which are generally based on hydrocarbons. These lubricants can be applied to the rail just before the train traverses the curve. However, they have a different disadvantage, which is that when they contaminate the train wheels, they severely reduce the braking efficiency. One attempted solution has been to use a hydrocarbon of moderate vapor pressure, such as kerosene. Ideally, the lubricant will evaporate from the wheels soon after the train has traversed the curve.

4.2 Suppression of Impact Noise

Because impact noise is generated by discontinuities in the contact surface of rail and wheel, it could be virtually eliminated by perfect maintenance of the track and rolling stock. Observations made on the scale model as well as on well-maintained track indicate that the impact noise can be reduced to such an extent that it blends into the rolling noise and becomes indistinguishable from it.

Based on the results of our analytical and experimental studies, we have identified a number of promising measures for the control of impact noise; they are listed below in order of their relative importance. The implementation of any one of the listed noise control measures may have a substantial impact on the initial investment or cost of maintenance of rolling stock and track. Formerly untried measures may introduce new problems in installation and maintenance. Accordingly, the effect of each noise control measure contemplated for an existing or planned vehicle or track must be carefully studied by the design engineer, the maintenance specialist, and the acoustical consultant to assure that all aspects of cost, safety, and noise reduction benefits are considered.

4.2.1 Welded rail

Welded rail joints eliminate the largest rail surface discontinuities. Accordingly, if wheel flats are also eliminated or held to a minimum, impact noise can be virtually eliminated, except, of course, at switches and signal junctions.

4.2.2 Limit of vertical misalignment at rail joints

Both the analytical and experimental studies indicate that the vertical misalignment of the rail head at rail joints is one of the principal sources of impact noise. The gap between the adjoining rail ends has negligible effect on impact noise if the vertical alignment is perfect.

Tolerances for vertical misalignment should be chosen so that the joint is a step-down rather than a step-up joint for the principal direction of travel. With this specific choice of tolerances, the impact noise levels off above the critical train speed (typically 25 to 30 mph [40 to 48 km/hr]) and becomes masked by the rolling noise at high train speeds. Since most rapid transit tracks are traveled in one direction only, this noise and vibration control measure could be implemented on most rapid transit lines.

4.2.3 Limit of permissible wheel-flat height

The results of the analytical studies have indicated that flat wheels behave exactly like a step-down rail joint. Accordingly, wheel flats must be controlled to minimize impact noise. Since impact noise generated by wheel flats levels off above the critical train speed, the impact noise caused by them would be masked by the rolling noise at high train speeds. However, the impact producing properties of wheel flats with rounded "corners" have not been studied sufficiently to enable prediction of their behavior at high train speeds.

4.2.4 Resilient wheel

Scale-model experiments with a resilient wheel running on an essentially rigid rail indicated that the resilient wheel generates substantially less impact noise than does a rigid standard wheel. The decrease of the impact sound pressure generated at a rail joint was proportional to the ratio of the total mass of the solid steel wheel and the rim mass of the resilient wheel.

Based on the results of full-scale experiments reported in the literature, we expect that for resiliently supported rail the decrease in noise owing to use of a resilient wheel may be substantially smaller than for rigid rail.

4.2.5 Wheel radius and wheel mass

As indicated in Sec. 2.3, the impact noise caused by rail joints and by a wheel flat of the same height is proportional to the ratio $(h/a)^{\frac{1}{2}}$, where h is the height and a is the wheel radius. Accordingly, a larger wheel diameter would help to reduce impact noise. However, a wheel of larger radius usually is heavier than a wheel with smaller radius. The noise reduction gained by the larger wheel radius may then be compensated by the increase in wheel mass, so that no net reduction in impact noise is achieved. In addition, the allowable range in the wheel radius is relatively small compared with the possible variation in joint and wheel flat height. Thus, one can safely conclude that increasing wheel radius is not a promising measure for controlling impact noise.

4.2.6 Axle load

Above critical train speed, where the wheel separates from the rail and both the spring force F_0 acting on the wheel and the duration of separation t_s determine the total change in momentum $m\Delta v = F_0 t_s$, the impact noise increases with increasing axle load. However, axle load is usually determined by functional and economic considerations, and this parameter can be considered as unchangeable for the purposes of noise control.

4.2.7 Hertzian contact stiffness

It is widely assumed that the impact duration is controlled by the Hertzian contact stiffness. Accordingly, measures which would reduce the Hertzian contact stiffness (see the discussion of the resiliently treaded wheel in Sec. 4.3) would increase the impact duration and, consequently, would reduce the high-frequency components of the impact noise, which components contribute most strongly to the A-weighted sound pressure level.

4.2.8 Administrative measures

Since impact noise increases with increasing train speed, one can limit the level of impact noise by restricting train speed in critical areas situated near major impact producing rail irregularities, such as switches and frogs. Of course, measures such as this would only be applied on a temporary basis until noise control measures that do not limit system capacity could be installed.

4.3 Suppression of Roar Noise

Roar noise is produced when the microroughnesses on wheels and rails excite the wheels and rails which then radiate noise. The approaches that one might take to suppress roar noise can be placed in three categories: (1) to reduce the radiation of sound from wheels and rails, (2) to reduce the response of wheels and rails, and (3) to reduce the roughness on wheels and rails.

4.3.1 Reduction of radiation

Significantly decreasing the radiation of sound from wheels and rails by such simple approaches as reducing the radiating area through the use of spoked wheels or cutouts in the rails is usually unrewarding and may lead in some cases to excessive stresses and component failures. To achieve a 10-dB reduction in noise by reducing the radiating area so as to reduce radiated power requires a factor of 10 reduction in radiating area*, a goal that is generally quite difficult to achieve. There is one approach, the use of a low rail barrier, that might, however, be fruitful. Referring back to Sec. 3.4 (Figs. 3.4-6 to 3.4-8), we find that at the frequency at which the wheel/rail noise spectrum peaks, the rail is generally the dominant radiator. Modest reductions in the overall noise level (in excess of 6 dB) could be achieved by reducing radiation from the rail alone.

---

*Of course, by carefully reducing the radiating area in such a way as also to reduce the radiation efficiency, one can achieve additional reductions in radiation. For example, with spoked wheels one may achieve additional reduction in radiated sound due to the acoustic short-circuiting achieved by effectively putting holes in the web and thereby reducing its baffling effect.

Rail Barrier

One possible approach to controlling rear noise by reducing radiation from the rail would be the installation of a low barrier on each side of each rail in the track bed. The concept is shown graphically in Fig. 4.3-1, where barriers only slightly higher than the rail head, with absorptive treatment on the rail side, are attached to the ties. The barriers on the outer side of the rails would have to seal against the ballast and those on the inner side could either seal against the ballast or extend over the surface of the ties as shown. A barrier 1 ft (0.3 m) in height above the ties can lower the rail generated noise on the outside of the barrier by 10 to 15 dB in the 500 to 1500 Hz range. The two barriers on the inner sides of the rails could conceivably be eliminated, but the outer barriers would then have to be raised to about 2 ft (0.61 m) high to have the same noise reduction performance.

This type of low barrier, although considerably cheaper and more compact than a full barrier, may not be practical in some cases. For example, trolley brake systems that work by pressing a large shoe on the rail would be incompatible with the barrier on the inner side of the rail. Also, the barrier extends ~6 in. (0.15 m) above the rail head and, hence, there may be clearance problems with the inner barriers.

Absorptive treatments would be desirable on the inner surfaces of the barriers to prevent coherent reflections from increasing the noise levels inside transit cars. For example, a 1 ft (0.3 m) spacing between barriers might conceivably lead to an acoustic resonance when this spacing equals half an acoustic wavelength (or some multiple thereof). Absorptive treatments impervious to weather, oil, etc., are available,

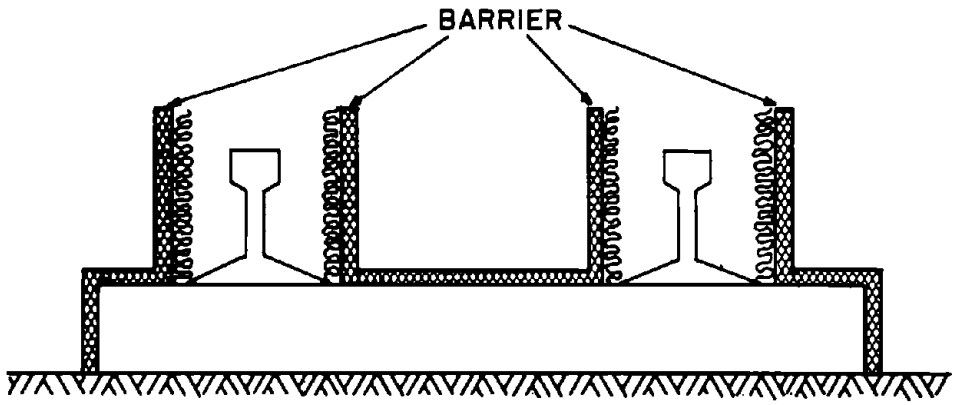

FIG. 4.3-1 LOW RAIL BARRIER

although occasional cleaning would probably be required to maintain good performance.

4.3.2 Reduction of response

One means by which the response of wheels and rails can be modified is to change the wheel and/or rail impedance. As a general rule, though, modifying impedance is not an effective technique for reducing wheel/rail noise. The reason for this is that for equivalent response levels the noise radiated by the wheels or by the rails is about the same, except at very low frequencies, where the rail radiation efficiency is low. Large changes in impedance simply change the primary responder from the wheel to the rail or vice versa. The resulting noise will in most cases change only a very few decibels. As an example, consider the situation in the frequency region between 400 and 1000 Hz where the wheel impedance Z_W is much greater than the rail impedance Z_R. Because the rail response is proportional to $Z_W/(Z_R+Z_W) \sim 1$ and the wheel response is proportional to $Z_R(Z_W+Z_R) \sim Z_R/Z_W << 1$, the rail radiation dominates. Reducing Z_W so that $Z_W << Z_R$ would simply reverse the situation and result in the wheel radiation dominating

Another approach to reducing response is to vibration isolate the primary radiating surfaces of the wheel or rail from the running surfaces where the excitation occurs. The Penn Cushion resilient wheel used in the P-S test provides isolation above 800 Hz by effectively isolating the web from the tread. Unfortunately, little noise reduction is achieved, because the rail remains a significant source. Clearly, for vibration isolation to be effective, it would have to be applied to both wheel and rail. One can conceive of a "resilient rail" analogous to the resilient wheel in which

the rail head is effectively isolated from the foot. The primary effect in the mid to high frequencies would be a reduction in the radiating area by a factor of 2 to 3. The resulting 3- to 5-dB improvement in noise seems to be a small gain when compared to the costs associated with the design, manufacture, and installation of new resilient rails.

Damping is another approach commonly used to reduce response. It is effective only if the response is resonant. The wheel response in the case of roar noise is nonresonant, and, as was seen in Sec. 3.4.2, no real change in radiated noise is achieved with damped wheels. Some reduction in the effective length of rail that radiates might be achieved by applying damping. The damping results in an effective increase in the decay constant η described in Secs. 2.1.4 and 2.4. If $\eta R > 1$, where R is the distance from the rail to the receiver, then the effective radiating length of rail is $1/\eta$. This relation implies that a 10-dB reduction in noise from the rail would require a tenfold increase in η. It may be quite difficult to achieve this increase, especially below 1000 Hz where the rail decay constant is already quite large.

The last means for reducing response that we will consider is the enlargement of the contact patch at the wheel/rail interface. In Sec. 2.4 we found that the wavenumber filtering of the contact patch produced significant reduction in wheel and rail response to roughness, especially at high wavenumbers. If the size of the contact patch could be increased, present roar noise levels could be reduced significantly. One suggested technique for doing this is to use a titanium treaded wheel. Using the simple formulas for the contact patch size in Timoshenko and Goodier (1951), one can show that a typical

dimension of the titanium wheel contact patch is increased over the same dimension of the steel wheel contact patch by the factor $\sqrt[3]{1/2\ (1 + E_S/E_T)}$, where E_T and E_S are the moduli of elasticity of titanium and steel, respectively. This implies a 14% increase in the contact patch size. For the wavenumber filter developed in Sec. 2.4, for $\alpha = 10$ one can derive the anticipated reduction in roar noise for a train with 30 in. (76 cm) diameter wheels passing at 50 mph (80 km/hr) under a loading of 10,000 lb per wheel (44,500 N).* The noise reduction is shown in Fig. 4.3-2. Using the range of noise spectra from the MBTA in Fig. 2.4-14, we calculate only a 1 dB(A) reduction in noise.

Resilient Treaded Wheels

A concept for attaining a highly compliant tread on a wheel and yet retaining good wear resistance of the tread surface is shown in Fig. 4.3-3. The wheel is in many ways similar to a resilient wheel in that a compliant layer is interjected between the running surface and the body of the wheel. The major difference here is that the metal ring forming the tread is much thinner than the tread of a typical resilient wheel.

Preliminary calculations have shown that if the tread is constructed from 1/2 in. (1.25 cm) thick steel and if the compliant material behind it (probably an elastomer with a low loss factor to reduce heating problems) is also about 1/2 in. (1.25 cm) thick with a modulus of around 10^4 psi ($6.65 \cdot 10^7$

*For a rail head radius of 12 in. (0.3 m), this gives a contact patch of ~0.32 × 0.26 in. (8 mm × 6.6 mm).

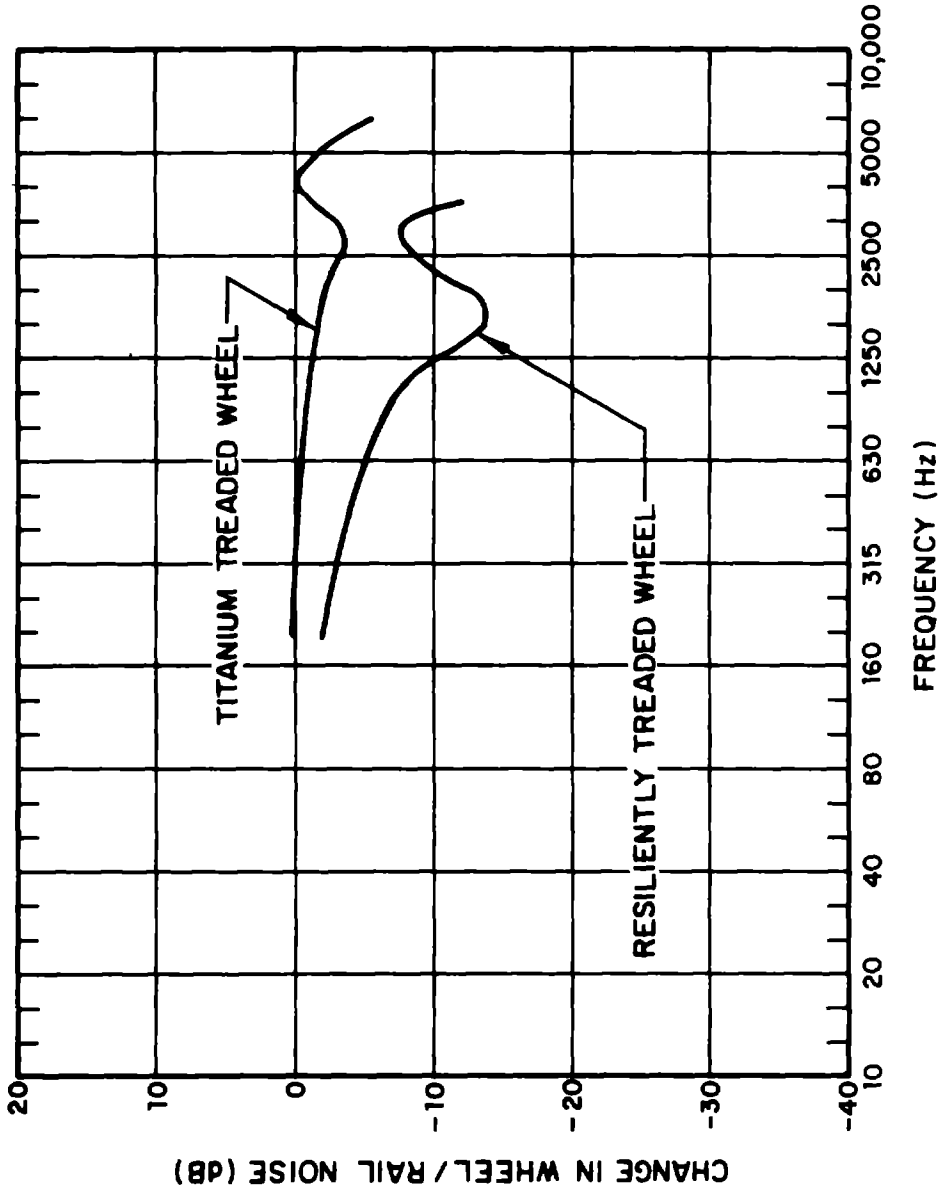

FIG. 4.3-2 ANTICIPATED NOISE REDUCTION WITH RESILIENTLY TREADED WHEELS AT 50 MPH (80 km/h)

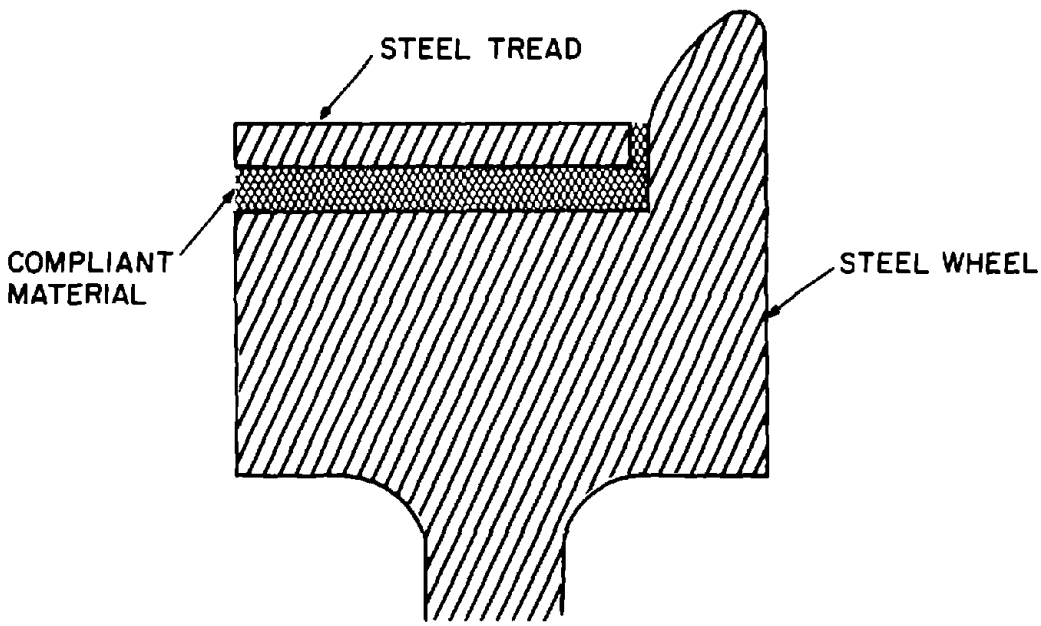

FIG. 4.3-3 RESILIENTLY TREADED WHEEL CONCEPT

N/m^2), a factor of 2 enlargement of the contact patch is possible. Figure 4.3-2 gives an estimate of the reduction in total wheel/rail noise for a train equipped with these resiliently treaded wheels operating under the same conditions as described for the titanium treaded wheels. Again, using the range of MBTA noise spectra in Fig. 2.4-14, we calculate a 7 dB(A) reduction in noise which is very encouraging. Also encouraging is the fact that one would anticipate strains placed on the elastomer by the 10,000 lb (44,500 N) wheel load to be less than 10%, which should pose no problems with regard to deterioration.

Safety considerations will probably require use of a mechanical constraint to ensure the ring remaining attached to the wheel should the elastomer fail. Interlocking teeth (or threads) similar to those in the Acoustaflex wheel, with elastomeric material between the threads, would retain the ring as well as provide side constraints to resist shear loads at the tread in the direction of the wheel axis. Braking presents a special problem that only in-service tests can resolve. Heating caused by tread braking has been known to cause deterioration of the elastomeric materials in existing resilient wheels. The thinner metal tread used here may worsen these problems. However, the use of disk brakes in place of tread braking is being seriously considered in new subway car construction. Disk brakes would eliminate the tread heating problem.

4.3.3 Reduction of roughness

Rail Grinding and Wheel Truing

Roughness on wheels and rails can be effectively reduced by turning the wheels or grinding the rails. Careful truing of the 14 in. (0.35 m) diameter wheels at Pullman Standard resulted

in up to 20-dB reduction in the roughness spectrum. Wheel truing carried out by the MBTA at their Everett Shop resulted in significant reduction in roughness at low wavenumbers, although the high wavenumber components were not reduced. The high wavenumber performance seemed to be caused by a tool chatter problem which can be corrected. Clearly, careful truing of wheels can produce significant reduction in their roughness. Reduction of roar noise requires that the rails also be ground. At the present time, there is no information available on the reduction of roughness through rail grinding. If it is comparable to the reductions achieved with wheel truing, then a combination of wheel truing and rail grinding could result in considerable (10 to 20 dB) reduction in roar noise.

Another unknown is at what intervals one must repeat the truing and grinding to maintain a given level of noise reduction. Also unknown is the effect of welded rail, antiskid braking systems, etc., on the proper intervals. If the intervals are too closely spaced, truing and grinding may not be economically feasible for controlling roar noise.

In any event, truing and grinding are *potentially* useful techniques for reducing roar noise. However, the economic feasibility of a regular schedule of truing and grinding needs to be examined.

5. SUGGESTED TESTING PROCEDURES FOR EVALUATION OF WHEEL/RAIL NOISE CONTROL MEASURES

For purposes of evaluation, it is essential that test procedures which give accurate, repeatable results be available for measuring the acoustic performance of measures for the control of wheel/rail noise. The insight gained from the analyses of Sec. 2 and the field testing of Sec. 3 has been valuable in designing such procedures, presented in this section.

A draft international standard, ISO/DIS 3095, "Measurement of Noise Emitted by Railbound Vehicles," from the International Organization for Standardization (ISO) is applicable in part to the measurements under consideration here. The following suggested procedures will reference articles in that standard when appropriate.

5.1 General

Here we discuss those elements of the testing procedures of general applicability to squeal, impact, and roar noise. In later sections we discuss those elements of specific applicability to each of the three types of wheel/rail noise.

Purpose

The intent of the testing procedures presented here is to provide a means for reproducibly evaluating the acoustic performance of devices and procedures for the control of squeal, impact, and roar noise.

Measured Quantities

Of particular interest here is the peak A-weighted sound pressure level during passage of a vehicle. For diagnostic work, 1/3-octave band spectra of the sound pressure level may also be of interest.

Measuring Equipment

See Article 5 of ISO/DIS-3095.

5.2 Evaluation of Squeal Noise Control Measures

Acoustical Environment

In general, Article 6 of ISO/DIS-3095 is applicable. However, because it has been found that conditions of high humidity may suppress squeal, it is recommended that no testing be carried out with ambient humidity in excess of 70%.

Track and Vehicle Conditions

The track and vehicle wheel surfaces must be in reasonably good condition. The surfaces do not have to be specially ground before the measurements, but they must be devoid of corrugations or flat spots. Since, for otherwise similar conditions, wheel squeal sometimes has been found to occur on worn rails, but not on freshly ground ones, it may be desirable to select a worn rail to test for squeal. Both rail and wheel must be clean and dry during the test.

Microphone Position

Wheel squeal is a highly variable phenomenon that occurs only intermittently. Thus, placing a microphone 7.5 m (25 ft) from the track, as recommended by ISO/DIS-3095 Article 9.1, would result in large uncertainty as to the distance of the train from the microphone at the exact moment of squeal. In order to overcome this difficulty two alternative microphone positions are recommended:

(a) Place the microphone at the center of curvature of the track. The train will thus be at a constant, and known, distance from the microphone as it traverses the curve. The sound level readings can be corrected to a standard distance by assuming inverse square spreading.

(b) Place a microphone 3 ft to the side of the car, on both sides, opposite the center of a truck. The sound levels are measured simultaneously on both sides of the vehicle. The higher of the two readings is taken.

Test Procedure

Tests may be performed on any curve where squeal is of concern. However, if a generalized set of measurements is required, tests should be conducted on the smallest radius curve encountered and a radius close to, but not greater than, 100 times the truck length. (Both radii are required, because elimination of squeal on the sharp curve does not necessarily entail elimination of squeal on the large curve.) During the tests the train should be loaded to its maximum operating weight.

Two sets of tests will be performed: baseline tests with the vehicle and track in their standard operating condition and noise control tests with the noise control package(s) installed on the vehicle and/or track.

The tests should be carried out at a range of speeds which will give a lateral acceleration of from 0.5% to 5% g. This should cover the range of speeds encountered in practice. The vehicle should be run in both directions down the track with a total of at least three runs at each speed. If the spread in peak A-weighted sound pressure level exceeds 3 dB(A) for any speed, the measurements at that speed should be repeated.

5.3 Evaluation of Impact Noise Control Measures

Acoustical Environment

See Article 6 of ISO/DIS-3095.

Track Conditions

Both rails on the track section opposite which measurements are to be made should be smooth, straight, level, and free of corrugations.

For those test cases in which a well-controlled wheel flat can be obtained on one of the wheels of the test vehicle, the track test section should be at-grade with smooth welded rail joints.

In those cases in which a track discontinuity, e.g., a rail joint with a height difference, is the impact noise source, any changes in the geometry of the discontinuity during vehicle passage should be noted. In addition, both rails should be free of all discontinuities to at least 18 ft (5.5 m) to each side of the discontinuity of interest.

Vehicle Conditions

If a rail discontinuity is the impact noise source, then the wheels of the vehicle should be smooth, round, and free of all flat spots.

If a flat spot on a single wheel is the impact noise source, the remaining wheels should be smooth, round, and free of all flat spots.

The test vehicle should be run through the test section loaded as in actual service with all auxiliary equipment turned off. In general, although impact noise will dominate propulsion

noise for electric-powered vehicles and may even dominate in some self-propelled vehicles, whenever possible, measurements should be performed with the vehicle coasting through the test section, especially when the noise control package(s) are installed, unless it can be shown that propulsion noise is at least 10 dB(A) below wheel/rail noise.

Microphone Position

Because of the localized nature of impact excitation, it is necessary to measure the impact noise in the vicinity of the surface irregularity causing it; i.e., to separate it from the rolling noise which is generated along the entire track. For the rail discontinuity measurement, position a stationary microphone at 5 to 6 ft (1.5 to 1.8 m) horizontal distance from the rail at a height corresponding to the center line of the wheel. To minimize the interference effects of ground reflections, line the ground with a 6 in. (15 cm) thick layer of fiberglass bats tied down by a chicken wire screen, or select a site where the ballast bed is carried on an earth berm and the relative geometry of source, receiver, and ground is such that there are no paths for geometric ground reflections.

To measure the impact noise generated by a wheel flat, mount the microphone on a boom fastened to the vehicle. This arrangement, which is especially convenient for experimental vehicles running on experimental tracks, enables the recording of many wheel impacts. The microphone distance from the vehicle should be the maximum allowed by sideway clearance and practicability of boom mounting. A wind screen should be used, and it may be necessary to vibration isolate the microphone.

Test Procedure

Two sets of tests will be performed: baseline tests with the vehicle and track in their standard operating condition and noise control tests with the noise control package(s) installed on the vehicle and/or track. For each set of tests, the vehicle will coast through the track test section at speeds in 10 mph (16 km/h) increments up to the maximum operating speed of the vehicle. The vehicle should be run in both directions down the track with a total of at least three runs at each speed. For the rail discontinuity test, there should be three runs in each direction, to allow examination of both step-up and step-down joints. If the spread in peak A-weighted sound pressure level exceeds 3 dB(A) for any speed in a given direction, the measurements at that speed and that direction should be repeated.

Wheel Drop Test

The good agreement between the impact noise measured by running the scale-model experimental vehicle over a step-down rail joint with that predicted from the wheel drop tests indicates that the wheel drop test may be a universal enough test to provide all the information needed to predict both the amplitude and spectrum of all type of impact producing rail and wheel irregularities, especially at train speeds above the critical train speed. It is most likely that the wheel drop test also can be used to evaluate the extent of impact noise reduction for any particular noise control measure contemplated without the need for a much more expensive rolling test, although more work is required to confirm this supposition.

5.4 Evaluation of Roar Noise Control Measures

Acoustical Environment

See Article 6 of ISO/DIS-3095.

Track Conditions

The rails in the track section opposite which measurements are to be taken should be smooth, straight, level, and free of corrugations, with smooth welded joints. The measurements should be performed at grade with the rail laid on tie and ballast.

Grinding of the rail or measurement of rail roughness is generally not required if the rail is smooth and free of discontinuities and if the section of rail to be tested is dedicated to the testing program, i.e., if the rail will remain unused between baseline tests and tests with the noise control package(s) installed. If the rail section is to be extensively used between baseline tests and tests with the noise control package installed, it should be ground smooth before each set of tests.

Vehicle Conditions

The wheels of the vehicle should be smooth and free from flats. If the running surfaces of the wheels are to be changed between baseline tests and tests with the noise control package(s) installed, the wheels must be turned smooth prior to each set of tests. The vehicle should be run through the rail test section loaded as in actual service with all auxiliary equipment turned off. In general, although wheel/rail noise will dominate propulsion noise for electric-powered vehicles and may even dominate in some self-propelled vehicles, whenever possible, measurements should be performed with the vehicle

coasting through the test section, especially when the noise control package(s) are installed, unless it can be shown that propulsion noise is at least 10 dB(A) below wheel/rail noise.

Microphone Positions

ISO/DIS-3095 Article 9.1 recommends that the microphone be placed 7.5 (25 ft) from the center of the track and 1.2 to 1.5 m (4 to 5 ft) above the running surface of the rail.

Test Procedure

Two sets of tests will be performed: baseline tests with the vehicle and track in their standard operating condition and noise control tests with the noise control package(s) installed on the vehicle and/or track. For each set of tests, the vehicle will coast through the track test section at speeds in 10 mph (16 km/h) increments up to the maximum operating speed of the vehicle. The vehicle should be run in both directions down the track with a total of at least three runs at each speed. If the spread in peak A-weighted sound pressure level exceeds 3 dB(A) for any speed, the measurements at that speed should be repeated.

6. CONCLUSIONS AND RECOMMENDATIONS

This report has presented the results of a comprehensive study of the noise generated when a flanged metal wheel rolls on a metal rail. Three very general categories of wheel/rail noise have been examined: squeal, impact, and roar. In this section we review the mechanisms that generate wheel/rail noise as well as methods for their control and then recommend further work to advance the state-of-the-art for wheel/rail noise control.

6.1 Review of the Wheel/Rail Noise Sources and Their Control

6.1.1 Squeal noise

Squeal, the intense noise composed of one or more tones and occurring when transit vehicles round short radius curves, is produced by the "crabbing" or lateral sliding of the wheels of a truck as that truck rounds a curve. The crabbing is caused by the fact that the finite-length wheelbase of the truck prevents the wheels from running tangent to the rails in the curve. This lateral sliding of the wheel on the rail results in a sticking and slipping motion that excites the resonance of the wheel, resulting in an intense narrowband noise. Analytically, this excitation can be modeled as a negative damping. Control of squeal noise is based primarily on preventing crabbing through the use of short-wheelbase or articulated trucks; eliminating the sticking and slipping through lubrication of the wheels and rails; and damping the wheels to overcome the negative damping due to the stick-slip excitation.

6.1.2 Impact noise

Impact noise is generated when the wheel encounters discontinuities on the rail or rolls over its own flat spots. When

the wheel encounters a discontinuity, its vertical velocity abruptly changes, resulting in an interactive force that excites both the wheel and the rail and causes them to radiate sound. Step-up rail joints are the most serious cause of impact noise, especially at high speed. Effective noise control measures involve the use of welded rail, wheel truing, contouring of the "run-on" rail end, and, in general, good maintenance procedures.

6.1.3 Roar noise

Roar noise is produced by microroughnesses on the running surfaces of wheels and rails that excite both structures to radiate sound. Sound radiation from the rail tends to dominate roar noise, the wheel contribution generally being important only at low frequencies. The contact patch at the interface between the wheel and the rail acts like a filter, attenuating the excitation produced by those components of roughness whose wavelengths are on the order of the size of the contact patch. Control of roar noise is accomplished primarily by grinding rails and truing wheels to reduce the roughness excitation; by increasing the size of the contact patch to increase the filtering effect; and by installing a low barrier along the rails to remove the sound contribution due to the rail.

6.2 Suggested Future Work

6.2.1 Squeal noise

Nature of the Stick-Slip Curve

One of the greatest uncertainties in the understanding of wheel squeal concerns the nature of the variation of the friction force with the slip velocity of the wheel. A very crude formulation, $x \exp(-x)$, was taken for the model, for want of any better

information. We know this formulation to be wrong, since it implies that the friction goes to zero as the sliding velocity goes to infinity, but, nevertheless, all predictions of the wheel squeal model are based upon this erroneous assumption. It appears that, as far as rough estimates are concerned, this error is not too important; however, if we are to make predictions with an accuracy of better than 20 or 30%, we must find out more about the stick-slip curve. The best way of obtaining this information is to employ a model three-axle truck, as did Friedrich (1971), yaw the center axle about a vertical axis, and then monitor the lateral force on this axle as a function of yaw angle and loading. The effects of rail surface finish, rail profile, and lubricants can all be investigated by this method.

Noise Control Techniques

The various noise control techniques mentioned in Sec. 6.1 need to be evaluated to determine which are the most effective and practical. A preliminary evaluation on paper can be performed based on the present theoretical model for wheel squeal, with more thought being given to the suitability of short trucks, to a tentative design for an articulated truck, and to available lubricants. Further attention should be given to rail grinding, which has sometimes been found to be an effective means of eliminating squeal, although the reason for this has not been fully understood.

Study of Noise Control Devices

A theoretical study of the various noise control devices suggested in Sec. 4 needs to be performed. These devices are articulated trucks, short trucks, reduced wheel loading, damped wheels, resilient wheels, and rail lubrication. The damped wheel

appears to be the most versatile method. However, it has two problems: the damping is temperature sensitive and current designs have dubious structural integrity. Articulated trucks and short trucks appear promising, except that they might give rise to "hunting" (lateral oscillations of the wheel).

The various noise control techniques should be compared systematically and tests of the most promising technique should then be performed on a small rapid transit vehicle, such as the PRT vehicle of Pullman Standard. The effectiveness of the noise control technique would be evaluated in accordance with the test procedures recommended in Sec. 5. In addition to tests of the acoustic effectiveness of the technique, its operational performance should also be evaluated, including such aspects as durability, maintainability, and cost. This program would lead to a practical method of greatly reducing, if not eliminating, wheel squeal.

6.2.2 Impact noise

The results of our analytical and experimental studies of wheel/rail impact noise, described in Secs. 2. and 3, have enabled us to predict the change in impact noise, given changes in wheel/rail geometry or transit vehicle operating parameters. This information has enabled us to suggest the noise control techniques described in Sec. 4.2.

One shortcoming in our newly gained knowledge of impact noise is uncertainty as to the duration and spectral content of the impact force. Further study is required to obtain a better understanding of this force, which would enable us to evaluate the relative magnitude of the contributions of wheel and rail to impact noise and allow us to develop additional innovative noise

control concepts. In addition, a number of the noise control measures suggested in Sec. 4.2 should be tried out in the field in order to examine their feasibility and optimize their design. Those topics requiring further study are discussed below.

Pulse Duration and Spectral Distribution of the Impact Sound

The analytical and experimental studies conducted within the framework of this investigation show that the peak amplitude of the impact sound caused by wheel and rail discontinuities is proportional to the total change in momentum of the impacting bodies. At the present time, we do not have enough detailed knowledge of the impact phenomena to predict the exact time history of the force pulse caused by the impacting bodies. Accordingly, we are not in a position to predict the spectral distribution of the impact noise or to determine if the wheel or the rail is the primary radiator. The limited experimental data collected during the scale-model studies seem to indicate that the duration of the acoustic pulse is not sensitive to the train speed or to the falling height. Consequently, it seems reasonable to assume that the impulse duration must be controlled by the Hertzian contact stiffness and by the mass of the impacting wheel and rail. However, we do not have sufficient information to support this hypothesis.

We recommend that further analytical and experimental work should be carried out to identify the major variables influencing the pulse duration and spectral content of the impact force in order to aid the development of innovative noise control measures.

Maximum Tolerable Size of Discontinuities

For imperfectly maintained track and rolling stock, the wayside noise is controlled by the impacts generated by rail joints

and flat wheels (Stüber, 1973). Accordingly, it is important to know the extent to which these discontinuities can be controlled by maintenance so that the wayside noise is reduced to the level of the rolling noise alone.

Since the established limits for wheel and rail discontinuities may strongly influence maintenance cost, detailed, analytical scale-model and full-scale experiments should be carried out to determine the net benefit and cost of the various limits.

Wheel Drop Test

Results of the limited scale-model experiments indicate that the wheel drop test may be the single most efficient way of: (1) testing the effectiveness of many planned noise control measures and (2) obtaining sufficient experimental data to predict both the amplitude and the spectral distribution of the impact noise generated by all characteristic impact-producing rail and wheel discontinuities.

Since the impulse response determines the steady-state response of the wheel/rail system, the wheel drop test may also be used to evaluate experimentally the effectiveness of various noise control measures (such as resilient wheel, damped wheel, damped rail, etc.) on rolling noise. In addition, wheel drop tests carried out under special controlled conditions could yield sufficient information to determine whether the radiated noise is due to the whole-body motion or to the elastic surface deformation of the wheel.

Because the wheel drop test is the simplest and most economical procedure for gaining needed information on wheel/rail noise, we strongly recommend that its use as a tool for predicting impact noise and as a test for the effectiveness of certain noise

control measures should be the subject of a detailed scale-model study followed by verification at full scale.

6.2.3 Roar noise

The analytical and experimental work described in previous sections has resulted in a fairly comprehensive analytical model of roar or rolling noise. The insight afforded by that model has resulted in a number of innovative concepts for the control of noise. Much further work could clarify several areas of uncertainty in the analytical model and, as a result, increase insight into means for the control of roar noise. However, at the present time, the most cost-effective approach is to begin development and testing of the innovative noise-control measures described in Sec. 4.3. As a result, our suggestions given below for further work heavily emphasize development and testing rather than further analysis.

Refinements to Analytical Model

One area of the analytical model that is somewhat in doubt is the microroughness spectrum, in particular, the spectrum of roughness in the horizontal direction across the head of the rail or in the axial direction across the tread of the wheel. This detail of the roughness spectrum is crucial to a complete understanding of the filtering effect of the contact patch between the wheel and rail and has significant noise control implications.

The railroad wheel is a mechanically very complicated structure. The details of the radial impedance of the wheel, especially its sudden drop in magnitude above 1000 Hz, have strong implications as to whether the wheel or the rail is the dominant radiator in various frequency bands. The reason for the sudden

drop in impedance is presently poorly understood. A finite-element computer study combined with an in-depth laboratory study could improve the understanding and possibly result in lowering the frequency at which the drop occurs, permitting development of an all metal resilient wheel. This type of resilient wheel would be more resistant than existing types to stresses at the wheel/rail interface. An additional bonus to lowering the frequency at which the impedance drops is that the wheel would probably become the dominant radiation source, which could then be controlled through the use of wheel skirts.

The rate of decay of vibration along the rail is not presently well understood. Limited data are available only for rail mounted on tie and ballast, and these data are not in good agreement in some frequencies. Additional damping data together with analytical studies of tie and ballast track and resiliently mounted track will be necessary to increase our understanding of the damping mechanisms. Although considerable increase in rail damping would be required to effect a significant reduction in wheel/rail noise, an improved understanding of the mechanism by which the rail foundation introduces this damping might make dramatic increases in rail damping possible, for example, through the use of highly damped resilient fasteners.

Resiliently Treaded Wheel

The resiliently treaded wheel concept of Sec. 4.3 appears highly promising. In-depth analytical studies are required to ensure the development of a mechanical design able to survive the stresses, fatigue, and heating produced by braking and running. These studies should be followed by inexpensive, small-scale, field testing (e.g., with the Pullman Standard PRT

vehicle) to examine the viability of the mechanical design and its noise control effectiveness. The construction of the small-scale wheels would, of course, require the cooperation of acoustic experts, railroad wheel manufacturers, and materials experts. After the design was refined on the small-scale vehicles (wheel loading would have to be properly scaled), full-scale wheels could be designed, built, and tested on a full-scale transit system.

Rail Barrier

For modest reductions in wheel/rail noise, the low rail barrier discussed in Sec. 4.3 presents an economically attractive approach. A simple plywood or chipboard barrier could be constructed and field tested very inexpensively on a small-scale rail system, such as the P-S PRT test track, or on the full-scale DOT test track at Pueblo, Colorado. More permanent barriers could then be performance tested on actual transit systems.

Rail Grinding and Wheel Truing

Rail grinding and wheel truing are generally accepted as effective techniques for the control of roar noise (and of impact noise from wheel flats), provided that in order to achieve the full noise control benefits, both procedures are performed at regular intervals. Two major areas of uncertainty remain:

1. What reduction in roughness (and, hence, in roar noise) is achievable through the use of existing techniques for grinding rails and truing wheels?

2. What maintenance intervals, i.e., for regrinding and retruing, are required to maintain the wheel/rail roughness at a sufficiently low level?

Item 1 could be fairly easily evaluated by measuring the roughness spectrum on wheels and rails (using the BBN roughness measuring device) before and after truing or grinding was done with existing devices. A natural by-product of such a study would be suggestions for improved grinding and truing practices, e.g., turning speed, depth of cut, grinding wheel coarseness, etc.

Item 2 requires a more expensive and time-consuming study, but one that is crucial to determining if rail grinding and wheel truing are economically viable noise-control techniques. A number of approaches are available. As a first step, one could true the wheels on a transit car (preferably two cars, one with antilock brakes and one without), run the car on an operating transit system, and monitor the change in the wheel roughness spectrum at regular intervals. Similarly, one could grind a section of rail on a transit line in regular revenue service and monitor the change in roughness with time. It would be necessary to monitor track sections representing different operating conditions, such as level tangent track, curved track, track in stations, track in tunnels, track exposed to the elements, track on elevated structures, and track with changing elevation. A study of this type could result in recommendations of grinding intervals for different track geometries. The final step in the study would be to determine whether, by truing the wheels of all the vehicles using a given line and grinding all the rails of that line, one can considerably increase the intervals between truing and grinding. Of course, the need for such an expensive final study would depend on the information gained in the earlier studies.

APPENDIX A: REVERBERANT CHARACTERISTICS OF PULLMAN STANDARD TENSILE TESTING MACHINE ROOM

The tensile testing machine room at the Champ Carry Technical Center of Pullman Standard is a large room [10^4 ft^3(280 m^3)] with painted concrete block walls. This room was used as a semi-reverberant room for measuring the radiation efficiency of a railroad wheel. A number of tests were performed in the room to determine its suitability for such measurements. With a standard ILG broadband source* used for calibration, the sound pressure level (SPL) was measured for three different source positions at six receiver positions to determine reverberant behavior throughout the room.

Figure A-1 shows the room, the ILG source positions, and the microphone positions all to an approximate scale of 1/4 in. equals 1 ft (2.1 cm equals 1 m). The measurement procedure was simply to mount the microphone [1/2 in. (1.25 cm) B&K 4134] in one position and record (Kudelski Nagra III single-track tape recorder) the level with the ILG source in each of its three positions. The microphone was then moved to a new position and the levels again recorded with the ILG source at its three positions.

The spread in levels at microphone position 6 resulting from the ILG source being moved through its three positions is shown in Fig. A-2. Above 200 Hz the spread is less than 4 dB and above 800 Hz the spread is less than 2 dB. Microphone positions 1, 3, and 4 have somewhat more spread. In all three cases, higher levels at these positions occurred when the source was nearby, suggesting that the microphone was in the direct rather than the reverberant field.

*ILG Industries, Chicago, Ill.

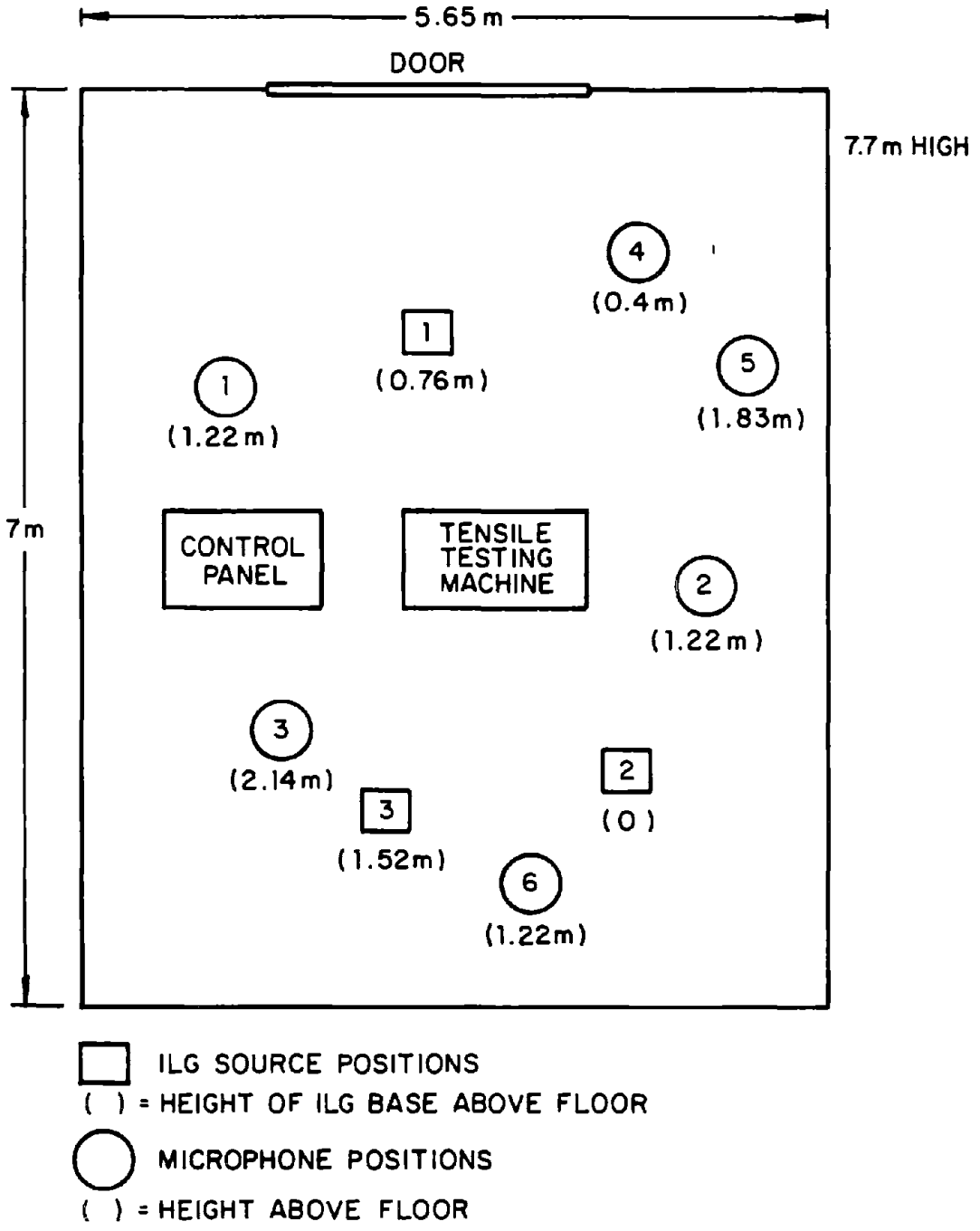

FIG. A-1 MICROPHONE AND ILG SOURCE POSITIONS IN SEMIREVERBERANT ROOM

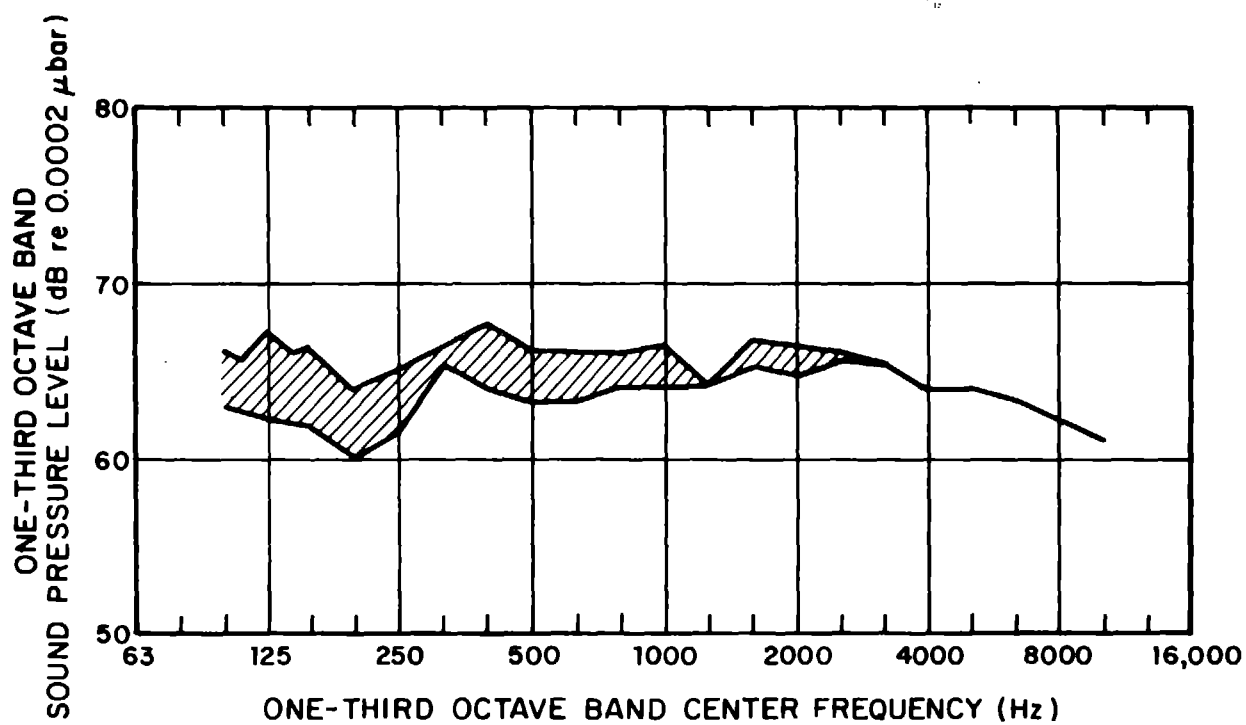

FIG. A-2 VARIATION IN LEVEL AT MICROPHONE POSITION 6 DUE TO MOVING THE ILG SOURCE

For ILG source position 1 (the position where the wheel was to be tested), Fig. A-3 shows the spread in levels at the six microphone positions. If we divide the six microphone positions into two groups, those farthest away (2, 3, 5 and 6) and those nearest (1 and 4), we find that the spread in the first group is small, less than 4 dB above 200 Hz. Levels at microphones 1 and 4 are consistently somewhat higher, suggesting that the microphones are close enough to the source to be in the direct field.

Although the above measurements suggest that the room is not ideally reverberant, by placing any source at source position 1 and measuring the SPL at microphone positions 2, 3, 5, and 6, we can get a measure of the power radiated by that source that is sufficiently accurate for our purposes.

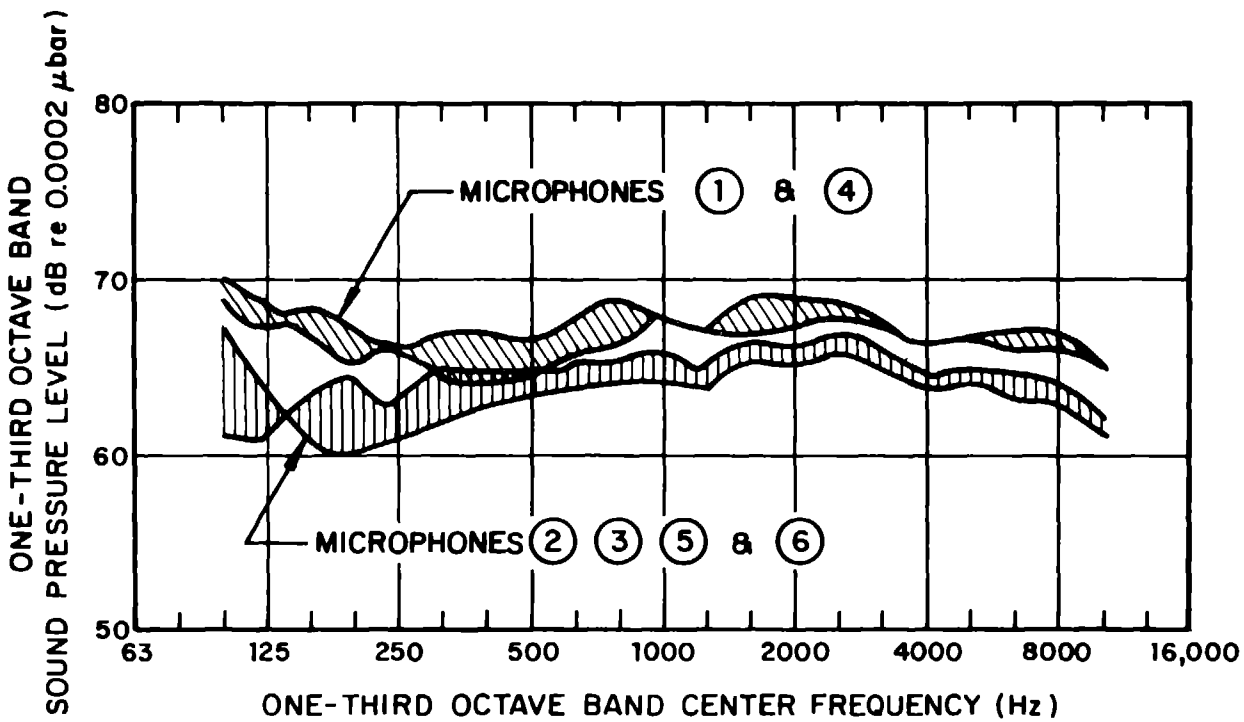

FIG. A-3 VARIATION IN MICROPHONE LEVEL FROM ILG SOURCE POSITION 1

APPENDIX B: CONTACT PATCH WAVENUMBER FILTER

For simplicity consider a circular region of radius b on a rail. Let x be the distance along the rail and let y be the distance across the rail. Let the patch sense and filter (or weight) the roughness r(x,y) on the rail such that the resulting sensed output $r'(\xi,\eta)$ when the patch is centered at (ξ,η) (see Fig. B-1) can be written

$$r'(\xi,\eta) = \int_{-\infty}^{\infty}\int_{-\infty}^{\infty} h(\xi-x,\eta-y)r(x,y)dxdy \quad , \qquad (B.1)$$

where $h(\xi-x,\eta-y)$ is a general weighting function that takes on finite values in the circle centered at (ξ,η) but is zero outside it. The function $h(\xi-x,\eta-y)$ is analogous to the impulse response function for a linear system in the time domain. Recall that the Fourier transform of the impulse response function is the frequency response of the linear system. In a completely analogous way, the Fourier transform of the function h(x,y) is the wavenumber response of, or the wavenumber filtering produced by, the contact patch in Fig. B-1, i.e.,

$$H(k_x,k_y) = \int_{-\infty}^{\infty}\int_{-\infty}^{\infty} h(x,y)\, e^{j(k_x x+k_y y)}\, dxdy \quad . \qquad (B.2)$$

For simplicity assume that the contact patch uniformly averages the roughness contained within it. The function h(x,y) becomes a pill box of radius b and height $1/\pi b^2$ centered at x = 0, y = 0. Equation B.2 then becomes

$$H(k_x k_y) = \frac{1}{\pi b^2}\int_{-b}^{b} dy \int_{-\sqrt{b^2-y^2}}^{\sqrt{b^2-y^2}} dx\, e^{jk_x x}\, e^{jk_y y} = \frac{2J_1(kb)}{kb} \quad , \qquad (B.3)$$

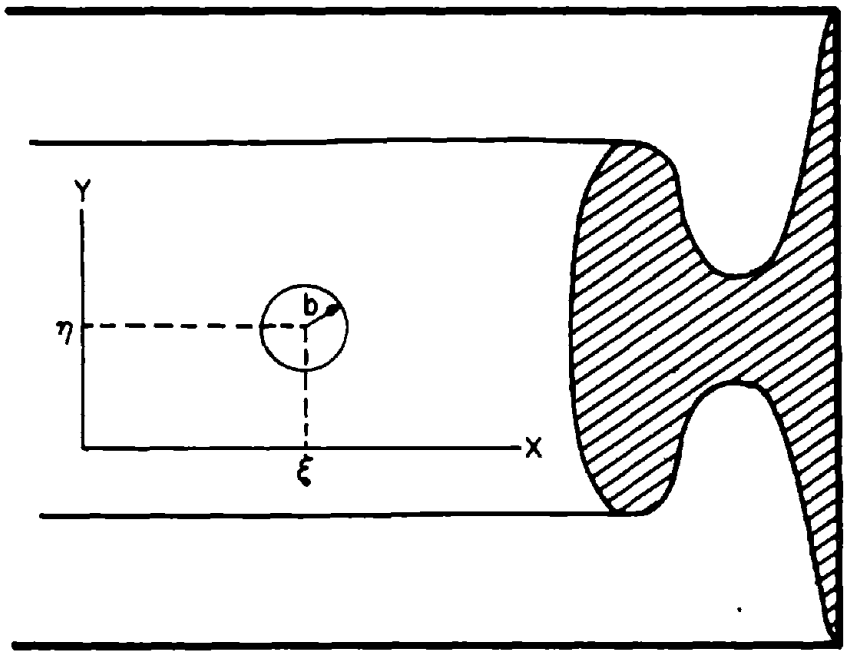

FIG. B-1 CONTACT PATCH FILTERING

where $k = \sqrt{k_x^2 + k_y^2}$. Under suitable assumptions of spatial averaging, the wavenumber spectrum sensed by the contact patch, $\Phi_{r'}(k_x k_y)$, is related to the actual wavenumber spectrum $\Phi_r(k_x k_y)$, (again in complete analogy with filtering of random signals in the time domain) by

$$\Phi_{r'}(k_x k_y) = \frac{4J_1^2(kb)}{(kb)^2} \Phi_r(k_x, k_y). \tag{B.4}$$

If when measuring the wavenumber spectrum, one uses a point sensor that moves along the rail in the x direction, the wavenumber spectrum that is sensed, $\Phi_r(k_x)$, is related to the actual spectrum by*

$$\Phi_r(k_x) = \int_{-\infty}^{\infty} dk_y \, \Phi_r(k_x, k_y) \quad . \tag{B.5}$$

By analogy the wavenumber spectrum sensed by the contact patch is

$$\Phi_{r'}(k_x) = \int_{-\infty}^{\infty} dk_y \, \frac{4J_1^2(kb)}{(kb)^2} \Phi_r(k_x, k_y) \quad . \tag{B.6}$$

---

*One can see this by assuming that the autocorrelation of the roughness $R(\delta_x, \delta_y)$ is measured on the rail along a line in the x direction yielding $R(\delta_x, 0)$. This is related by the Fourier transform to the wavenumber spectrum $\Phi_r(k_x k_y)$ or

$$R(\delta_x, 0) = \int_{-\infty}^{\infty} dk_x \, e^{jk_x\delta_x} \int_{-\infty}^{\infty} dk_y \Phi(k_x, k_y) = \int_{-\infty}^{\infty} dk_x \, e^{jk_x\delta_x} \, \Phi(k_x)$$

which implies that $\Phi(k_x) = \int \Phi(k_x, k_y) dk_y$.

To go any further requires a knowledge of the k_y dependence of the roughness spectrum. This has never been measured and so we make the assumption that

$$\Phi_r(k_x,k_y) = \Phi_r(k_x) \frac{1}{2\alpha k_x} \quad , -\alpha k_x < k_y < \alpha k_y$$

$$= 0 \quad , |k_y| > \alpha k_x \quad , \tag{B.7}$$

where $\Phi_r(k_x)$ is defined in Eq. B.5 and is the spectrum defined by running a point sensor along the length of the rail (or the circumference of the wheel). Equation B.7 implies a flat band-limited spectrum in k_y where the wavenumber above which no energy exists is a multiple of the wavenumber in the x direction. This implies that for a given wavenumber component in the x direction, k_x, the autocorrelation is of the form $\sin\alpha k_x\delta/\alpha k_x\delta$, which further implies a correlation length in the y direction proportional to λ_x/α where λ_x is the wavelength in the x direction. Substituting Eq. B.7 into Eq. B.6 and substituting $k_y = k_x \tan\theta$ for k_y, we have

$$\Phi_{r'}(k_y) = \frac{4\Phi_r(k_x)}{\alpha(k_x b)^2} \int_0^{\tan^{-1}\alpha} J_1^2(k_x b \sec\theta)d\theta \quad . \tag{B.8}$$

Equation B.8 is, of course, an estimate based on a guess at the k_y dependence of the wavenumber spectrum. Other guesses might be equally viable; for example, one might assume that $\Phi_r(k_x,k_y)$ is band limited at k_0, where k_0 is independent of k_x. This assumption implies a correlation length in the y direction across the rail head or the wheel tread proportional to $1/k_0$.

APPENDIX C: THE EFFECTS OF LOCAL DEFORMATION ON RESPONSE

If the local Hertzian contact stiffness of the wheel in contact with the rail is small, this could reduce the effective impedance of the wheel and rail and thus affect the response. We can examine the possibility in somewhat more detail by linearizing the contact stiffness and using the approximate model of Fig. C-1. In that figure the contact stiffness K_c is split between the wheel and the rail, and the motions on the surface of the wheel and rail are each split into two parts: those due to the contact stiffness, V_{cw} and V_{cr}, and those due to the impedance*, V_w and V_r. It is the latter motions that result in sound radiation from the wheel and rail, the motions at the contact point due to the contact stiffness being very localized.

Solving for V_w and V_r we obtain

$$V_w = \frac{Z_R}{Z_R + Z_W + 2Z_W Z_R/Z_c} \; V_{roughness} \qquad (C.1)$$

$$V_r = \frac{Z_W}{Z_R + Z_W + 2Z_R Z_W/Z_c} \; V_{roughness} \; , \qquad (C.2)$$

where $Z_c = 2K_c/j\omega$ and $V_{roughness}$ is the roughness velocity from the wheel and rail sensed as the wheels roll over the rail. Clearly, if $Z_c >> Z_W$ and $Z_c >> Z_R$, then the above equations simplify to the results in Eqs. 2.4-5 and 2.4-6 and Eqs. 2.4-14 and 2.4-16 are unaffected by the contact stiffness.

We know of no formula for calculating K_c for two cylinders in contact, i.e., a wheel and a rail; however, we can estimate

*This model implies that the impedances have been measured under circumstances where the impedance of the contact stiffness is much greater than Z_W or Z_R.

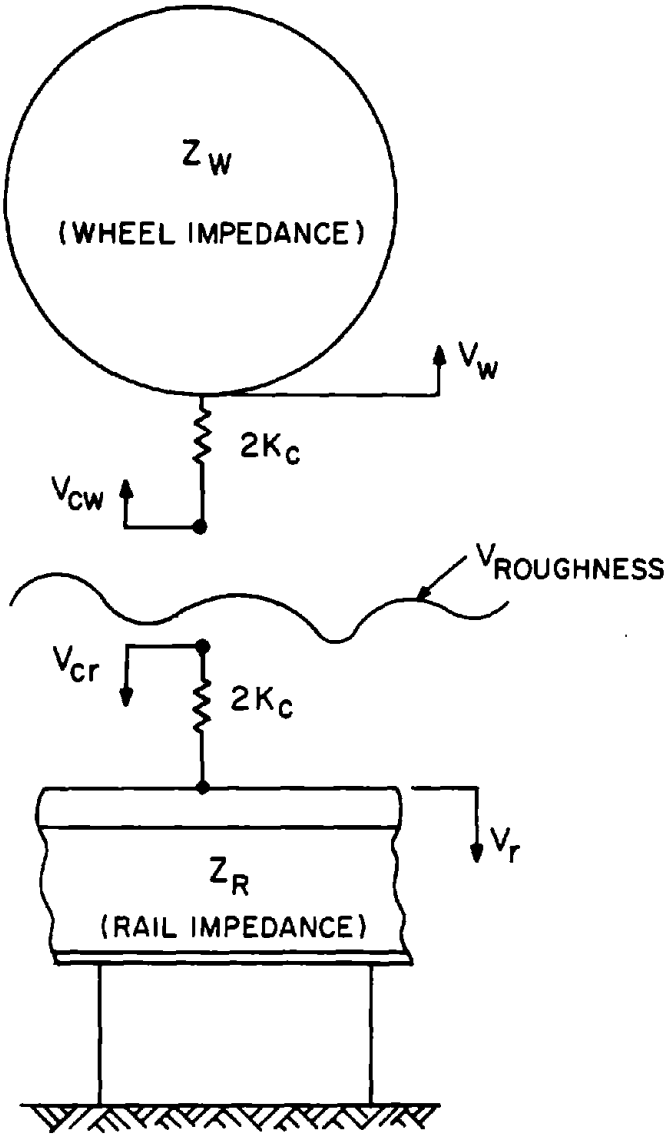

FIG. C-1 SIMPLE CONTACT STIFFNESS MODEL

K_c for an elastic sphere pressed into a half-plane as

$$K_c = 1.22(E^2aP)^{1/3},$$

where E is the modulus of the material, a is the sphere radius, and P is the load applied to the sphere. Simulating the parameters of the PRT vehicle and wheel, for a 14 in. (35.5 cm) diameter sphere (to simulate a wheel of similar radius) under 1750 lb (7800 N) load, we obtain $K_c = 3.3 \times 10^7$ lb/ft ($4.8 \cdot 10^8$ N/m). Figure C-2 compares this contact impedance to the analytical impedance models developed in Sec. 2.1 for the PRT wheel and the Pullman Standard test track rail [ASCE 60 lb/yd (30 kg/m)]. Above ~500 Hz the contact impedance becomes comparable to or less than the wheel impedance and some effect would be expected. Below 500 Hz little effect would be expected.

It is useful to distinguish two regions in Fig. C-2: the region where $Z_W >> Z_R$ and the region where $Z_R >> Z_W$. In those two regions it is possible to simplify Eqs. C.1 and C.2, as is shown in Table C.1. In region I the contact stiffness modifies

TABLE C.1. WHEEL AND RAIL RESPONSE INCLUDING CONTACT STIFFNESS.

Region	$V_W/V_{roughness}$	$V_R/V_{roughness}$
I ($Z_W >> Z_R$)	$\frac{Z_R}{Z_W}\frac{Z_c}{Z_c + 2Z_R}$	$\frac{Z_c}{Z_c + 2Z_R}$
II ($Z_R >> Z_W$)	$\frac{Z_c}{Z_c + 2Z_W}$	$\frac{Z_W}{Z_R}\frac{Z_c}{Z_c + 2Z_W}$

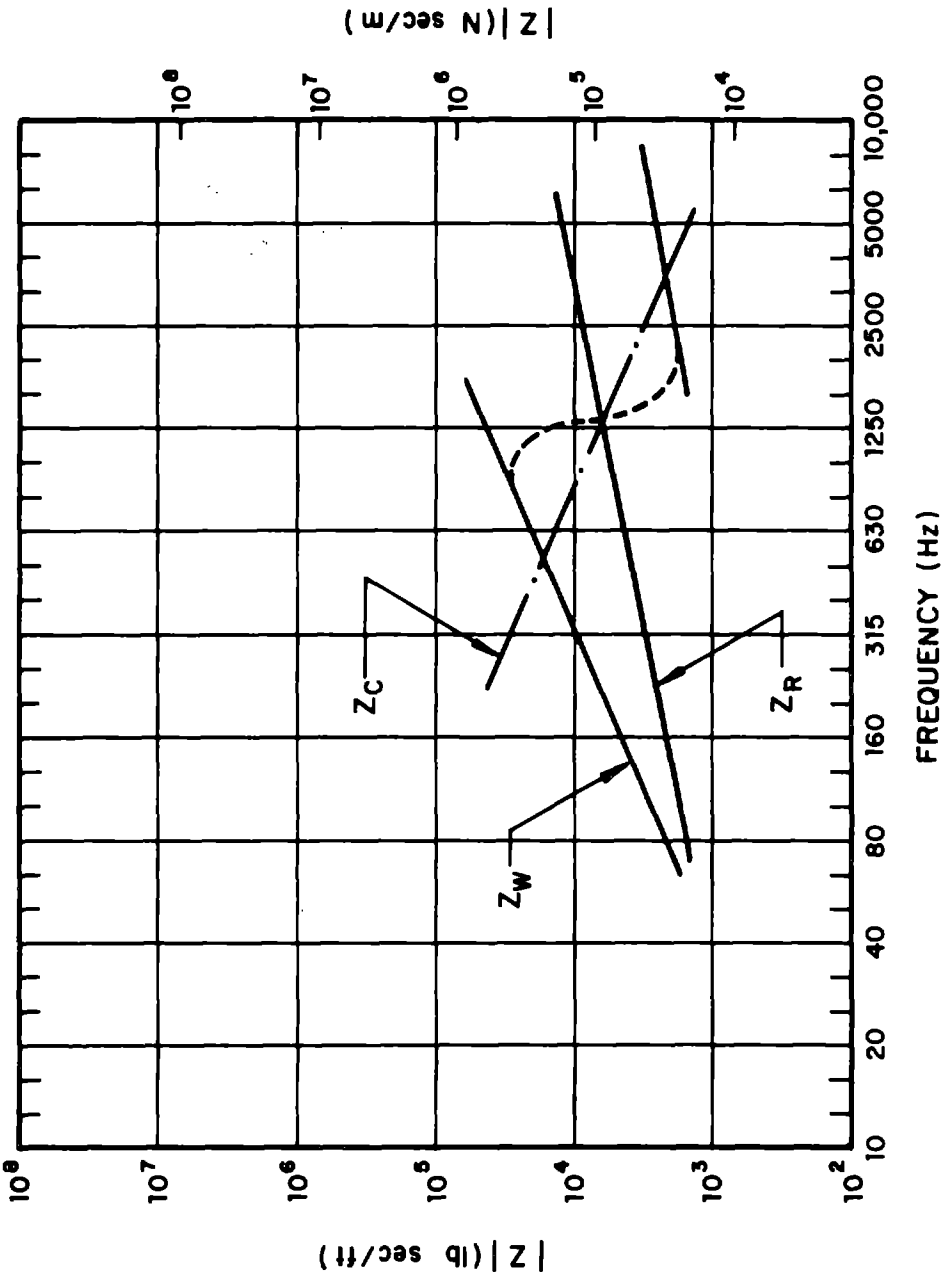

FIG. C-2. COMPARISON OF THE CONTACT IMPEDANCE WITH THE WHEEL AND RAIL IMPEDANCE.

the wheel and rail response by $Z_c/(Z_c + 2Z_R)$ and in region II the responses are modified by $Z_c/(Z_c + 2Z_W)$. Consequently, to examine the effects of the contact stiffness, one need only examine $Z_c/(Z_c + 2Z_R)$ in region I and $Z_c/(Z_c + 2Z_W)$ in region II. Using the analytical models of Sec. 2.1, we find that

$$Z_W \cong 10^3\left(\frac{f}{1000}\right)^{\frac{1}{2}} (1-j)\ \frac{\text{lb sec}}{\text{ft}} \qquad \text{(Region II)}$$

$$Z_R = 4 \cdot 10^3\ \left(\frac{f}{1000}\right)^{\frac{1}{2}} (1-j)\ \frac{\text{lb sec}}{\text{ft}} \qquad \text{(Region I)}$$

$$Z_c = j\ \frac{9.90 \cdot 10^5}{f}\ \frac{\text{lb sec}}{\text{ft}}\ . \qquad \text{(Regions I and II)}$$

Figure C-3 shows the resulting effects of the contact stiffness in the two regions.

In Sec. 2.4, all calculations were performed assuming that $Z_c \to \infty$. As a result, in all these calculations

$$\frac{Z_c}{Z_c+2Z_R} = \frac{Z_c}{Z_c+2Z_\omega} = 1$$

and Fig. C.3 shows the correction factor that should be added to all the roar noise predictions in Secs. 2 and 3 to correct for the contact stiffness. Only at very high frequency (> 4000 Hz), where Z_c is much less than both Z_W and Z_R, is this correction significant.

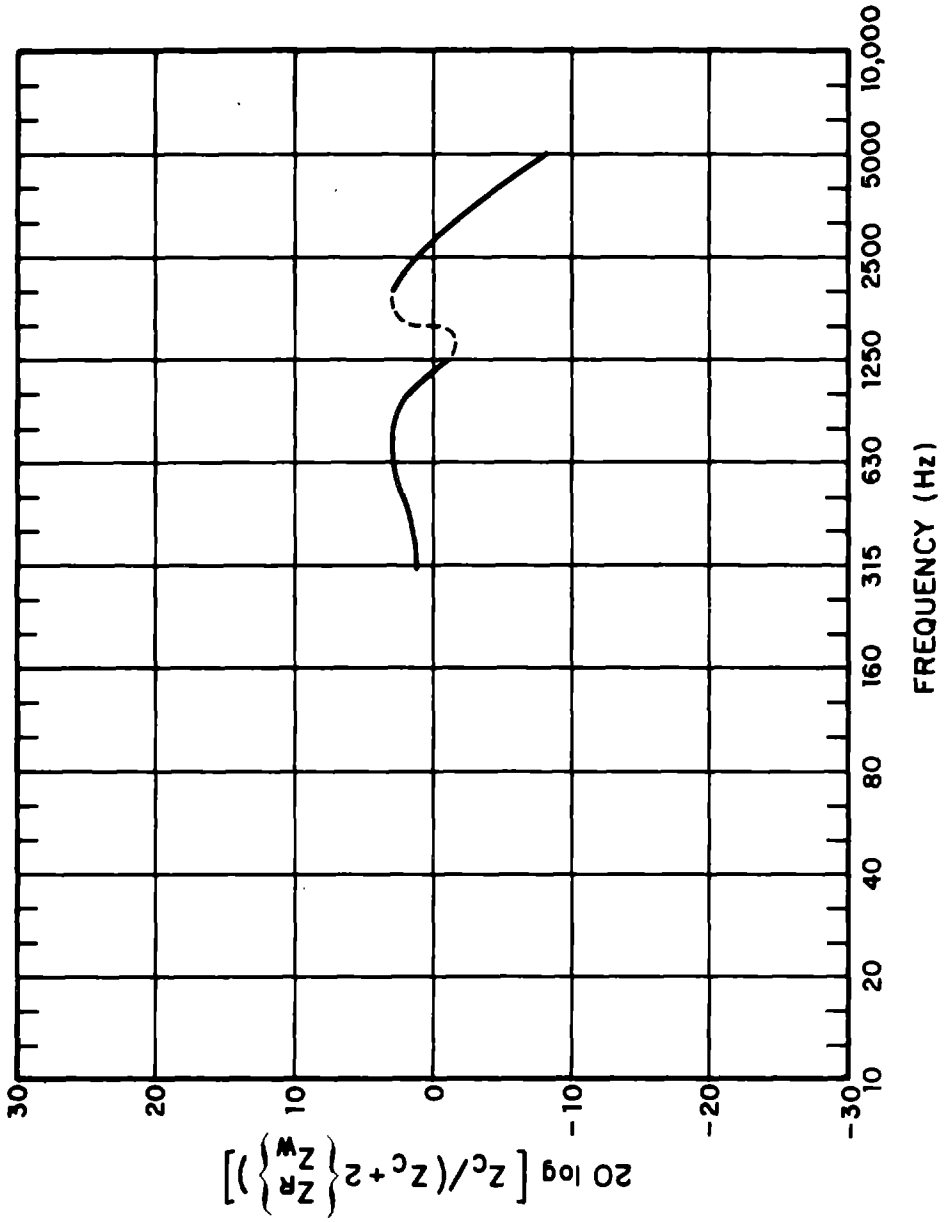

FIG. C-3 EFFECT OF CONTACT STIFFNESS

APPENDIX D: EVALUATION OF THE ROUGHNESS MEASURING DEVICE

To ensure that the roughness measuring device properly measures surface roughness at the wavelengths of interest, we performed a detailed evaluation of its operation. In this appendix we describe these measurements and the resulting conclusions.

D.1 Isolation of the Probe

A schematic of the measuring device is shown in Fig. D-1. The total signal as registered by the accelerometer when the carriage is in motion is given by

$$S_p = H_{rp}S_r + H_pS_c + S_b + S_e \quad , \qquad (D.1)$$

where S_r and S_c are the accelerations of the rail surface and carriage, respectively, as recorded in an inertial frame moving at a uniform speed u along the rail. S_b is mechanical background noise, S_e is electrical noise, and H_p, H_{rp} are the carriage-to-probe and rail-to-probe transfer functions. The useful quantity S_r must be "filtered" out from the rest of the terms.

Through proper design of the carriage and carriage-to-probe coupling, we obtained $|H_{rp}| \approx 1$ and $|H_{rp}S_r| >> |H_pS_c|$ over a large portion of the range of interest, which allows us to ignore the second term of Eq. D.1. In particular, we polished the carriage track to reduce S_c and applied strips of damping and vibration insulation material along the transmission path (Fig. D-1) between the carriage and probe to reduce the magnitude of H_p.

The last two terms, S_e and S_b, of Eq. D.1 are very small most of the time and can be neglected, except at very low frequencies, where the actual signal S_r becomes increasingly weaker for

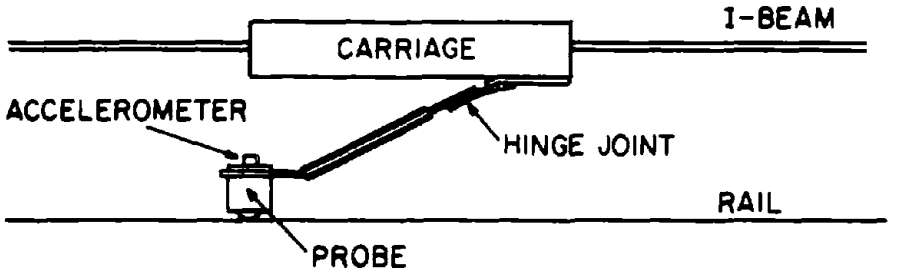

(a)

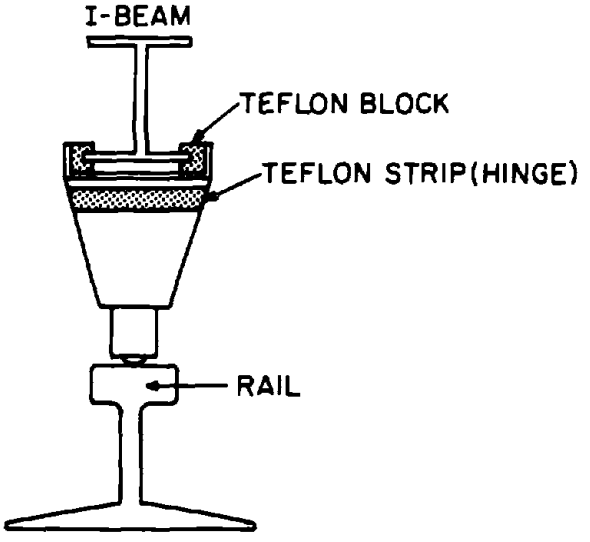

(b)

FIG. D-1 ROUGHNESS MEASURING DEVICE

a given speed u and is finally lost into the background level S_b. This subject of signal-to-noise ratio will be discussed further in subsequent sections.

D.2 Details of the Test Setup

The main structural details of the final carriage design are illustrated in Fig. D-1. We repeatedly changed the carriage shape, teflon blocks, amount of damping, and accelerometer holder in an effort to achieve a satisfactory signal-to-noise ratio. The final carriage design is basically an aluminum channel segment partially coated with damping material; it is coupled to the I-beam by means of teflon blocks. The probe consists of two pieces joined together with a soft teflon strip (hinge) which serves as a low-pass filter. The arm containing the probe is coated with damping material and its coupling to the accelerometer holder includes two layers of vibration insulation material.

The accelerometer holder (Fig. D-2) has two threaded pieces, H_1 and H_2, that hold a 1-in. diameter ball bearing B. An accelerometer A is attached to the upper piece H_2. The accelerations registered by the accelerometer and the ball bearing will differ as a result of some finite compliance in the A to H_1 and H_1 to B couplings, but the difference is negligible in the low-frequency range of interest.

This particular holder design also solves the problem of "spragging" resulting from an excessively worn-out surface of contact. Whenever the worn-out patch exceeds 1/10 (0.25 in) of an inch, one can obtain a new clean spherical contact surface by unscrewing H_2 and rotating the ball bearing to a new position.

One of the basic assumptions made in this project is that the carriage speed remains constant throughout an entire run.

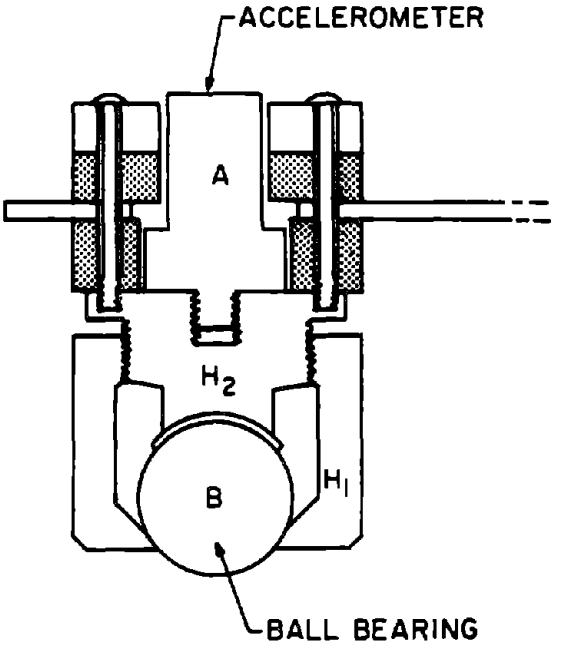

FIG. D-2 ACCELEROMETER HOLDER

To achieve constant carriage speed, we used a high impedance motor drive and occasional oil lubrication of the track. However, we omitted this type of lubrication during our second field trip because the first field trip established that its results were detrimental at low temperatures.

We sometimes measured the carriage speed by recording the time spacing of pulses corresponding to 2 ft (0.61 m) intervals. The carriage had a soft shimstock arm on one end which when it made contact with track extensions [spaced 2 ft (0.61 m) apart] closed momentarily a circuit that gives a 6.7 volt pulse. In most cases, however, we measured the speed by using a stopwatch to measure the time it took the carriage to traverse 8 ft (2.44 m).

D.3 Measurement of H_p

The extent to which noise caused by contact between the carriage and the I-beam is transmitted to the probe can be determined by the test setup of Fig. D-3a. When the I-beam is shaken, the acceleration levels S_p at the probe and S_c at the carriage are measured simultaneously to yield the transfer function H_p defined by

$$H_p = \frac{S_p}{S_c} \Bigg|_{S_r = S_b = S_e = 0} .$$

It should be noted that during this test the shaker, the beam, and the probe are all isolated from the ground and each other to ensure that $S_r \approx 0$. In all cases S_e and S_b were found to be negligible compared to S_c and S_r.

The response of both accelerometers to the pink noise used as the driving signal is shown in Fig. D-3b. It is clear that with the exception of the 31.5 Hz and 315 Hz bands, vibration

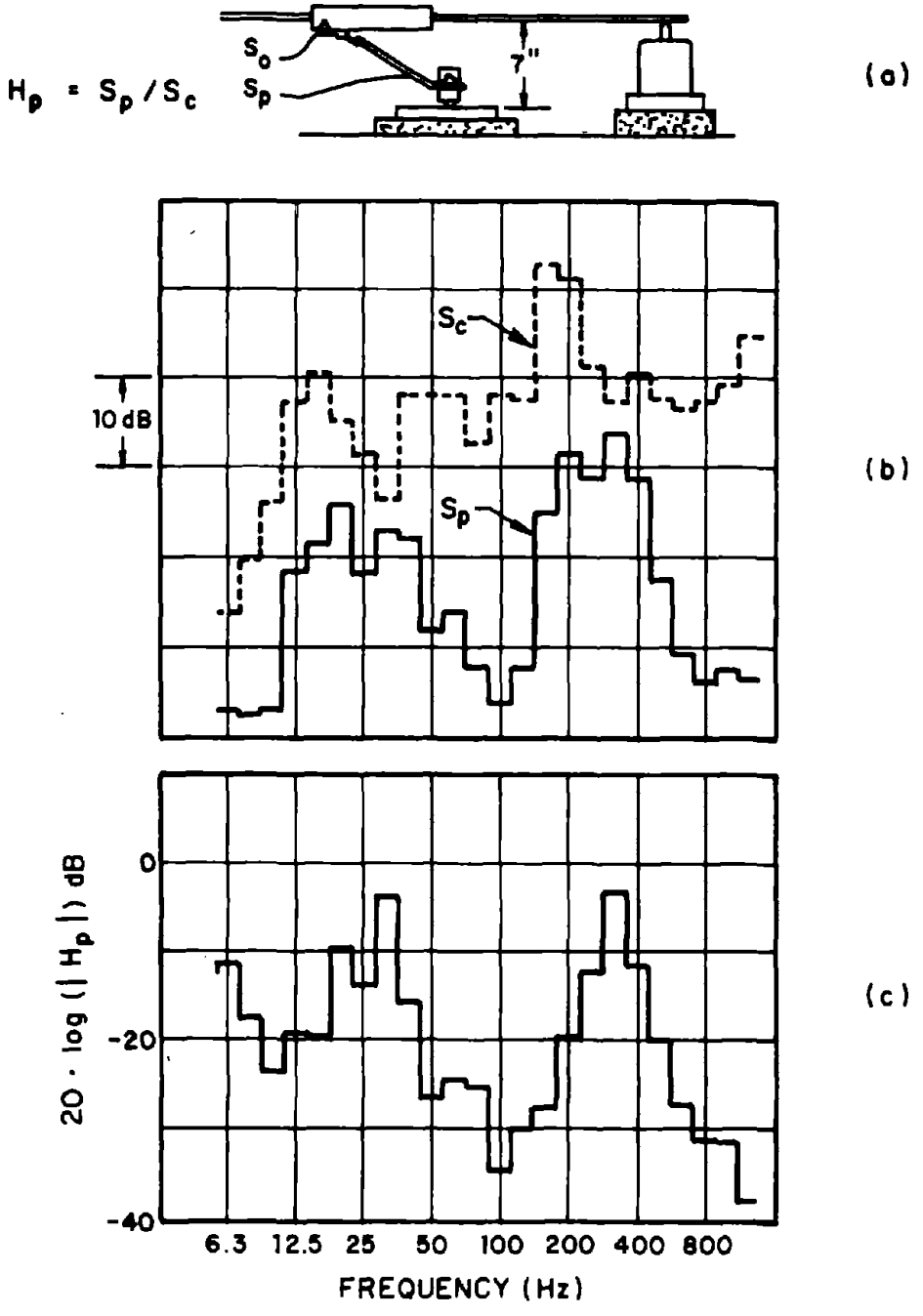

FIG. D-3. TRANSFER FUNCTION $H_p = S_p/S_c$.

originating at the carriage is attenuated by at least 10 dB on its way to the probe. Furthermore, for typical metal strips that were tested, the "rail" roughness in the above two bands was much higher than the carriage roughness; therefore, there is always a very good signal-to-noise ratio in all bands.

A better picture of the behavior of H_p is shown in Fig. D-3c which plots 20 log ($|\bar{H}_p|$) vs frequency, where $\bar{H}_p$ is the average over 4 runs defined by

$$\bar{H}_p = \frac{\sum_i S^{(i)}}{\sum_i S_c^{(i)}} \quad , \; i = 1,2,3,4 \; . \qquad (D.2)$$

D.4 Measurement of H_{rp}

The validity of the entire roughness measurement procedure presented here is based on the assumption that the probe and rail maintain good contact while the carriage moves. However, this assumption does not always hold true. On very rough surfaces or at very high carriage speeds, the probe lifts off the rail and then bounces off a few times before resuming smooth contact, thus leading to erroneous results. It is quite important, then, to determine some basic methods for maintaining good contact.

The arrangement used to determine the threshold for lift-off as well as the transfer function H_{rp} is shown in Fig. D-4a. The probe is shaken by an impedance head and the readings of the probe and impedance head accelerometers are recorded simultaneously. At each frequency (1/3-octave band tones), the level was increased until lift-off occurred, i.e., until the signal developed a substantially distorted form accompanied by an audible rattle. Subsequently, the level was decreased until the

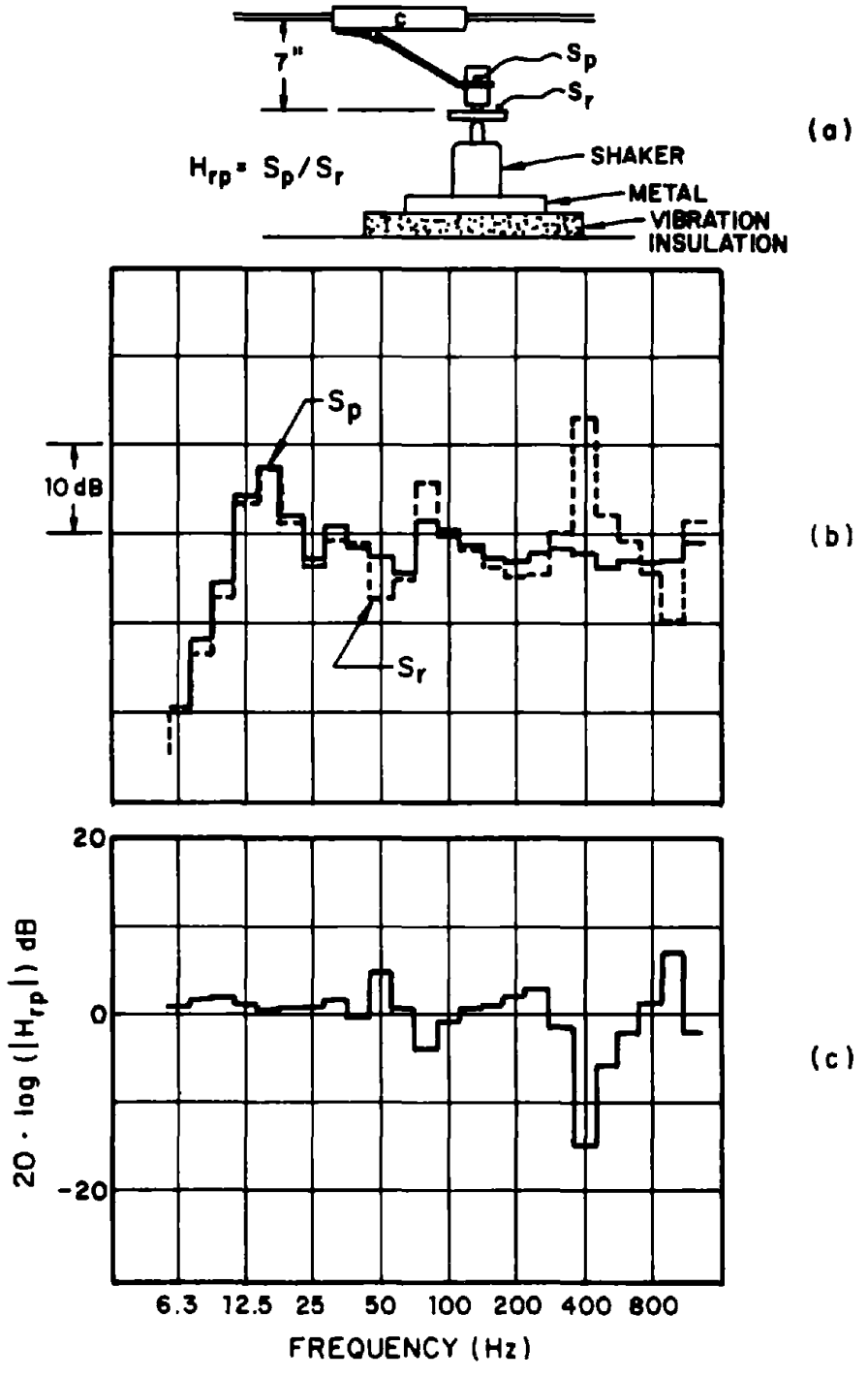

FIG. D-4. TRANSFER FUNCTION $H_{rp} = S_p/S_r$.

rattle disappeared and the signal assumed its undistorted form.

The level at which lift-off commences (i.e., increasing levels) was consistently higher than the level at which lift-off stopped (decreasing levels). The driving acceleration of the latter case was defined as the threshold of lift-off and found to be always larger than g/5.

In all measurements that follow, the signal was first tested to ensure the absence of lift-off before any data were acquired.

The test setup of Fig. D-4 was also used to determine the transfer function H_{rp} defined by

$$H_{rp} = \left.\frac{S_p}{S_r}\right|_{S_c = 0} . \qquad (D.3)$$

During the lift-off test, heavy pieces of metal were supported from the carriage to ensure that $|S_c| \approx 0$, and the acceleration of the Wilcoxon impedance head and probe were recorded simultaneously. The results of this test also appear in Fig. D-4. It is noted that $|S| \approx |S_r|$ with a better than ± 5 dB accuracy until $\omega = 400$ Hz, beyond which the accelerometer response becomes very irregular due to coupling resonances. The reduced version of H_{rp} is shown in Fig. D-4c where we have plotted

$$20 \log |H_{rp}| .$$

We used the detailed form of the transfer function H_{rp} in reducing all our roughness data.

D.5 Reference Rough-Surface

The tests just described for the measurement of H_{rp} and H_p have been carried out with the carriage at rest. To make sure that this method does work, we constructed and tested a surface of (approximately) known roughness.

We constructed a sinusoidal surface by epoxying a 2½ in. (6.35 cm) wide and 0.006 in. (0.152 mm) thick shimstock strip over an array of ¼ in. (0.635 cm) wide strips of the same shimstock spaced 2 in. (5.1 cm) apart. Consequently, the peak-to-peak roughness amplitude was

$$H = 6 \text{ mils } (0.152 \text{ mm}) \quad .$$

For a roughness wavelength $\lambda = 2$ in. (5.1 cm), the acceleration at a speed $V_0 = 4$ ft/sec (1.22 m/sec) from the shimstock would be

$$a = \omega^2 H \simeq 0.176 \text{ g} \quad ,$$

or -18 dB re 1 g rms amplitude.

The measured spectrum is shown in Fig. D-5. There is a distinct spike at 25 Hz of -10 dB re 1 g, which is lower than our prediction. Note that in addition to the peak at 25 Hz, there is another distinct peak at 50 Hz, the first harmonic. Its substantial level is explained by the irregularities of our handmade wavy surface, which is periodic but not perfectly sinusoidal. The -8 dB discrepancy can be easily explained in terms of the expected increased effective amplitude of the corrugation resulting from the use of glue in the construction of the wavy surface. A 4- to 5-mil layer of glue would account for this difference, which is a not an unreasonable possibility.

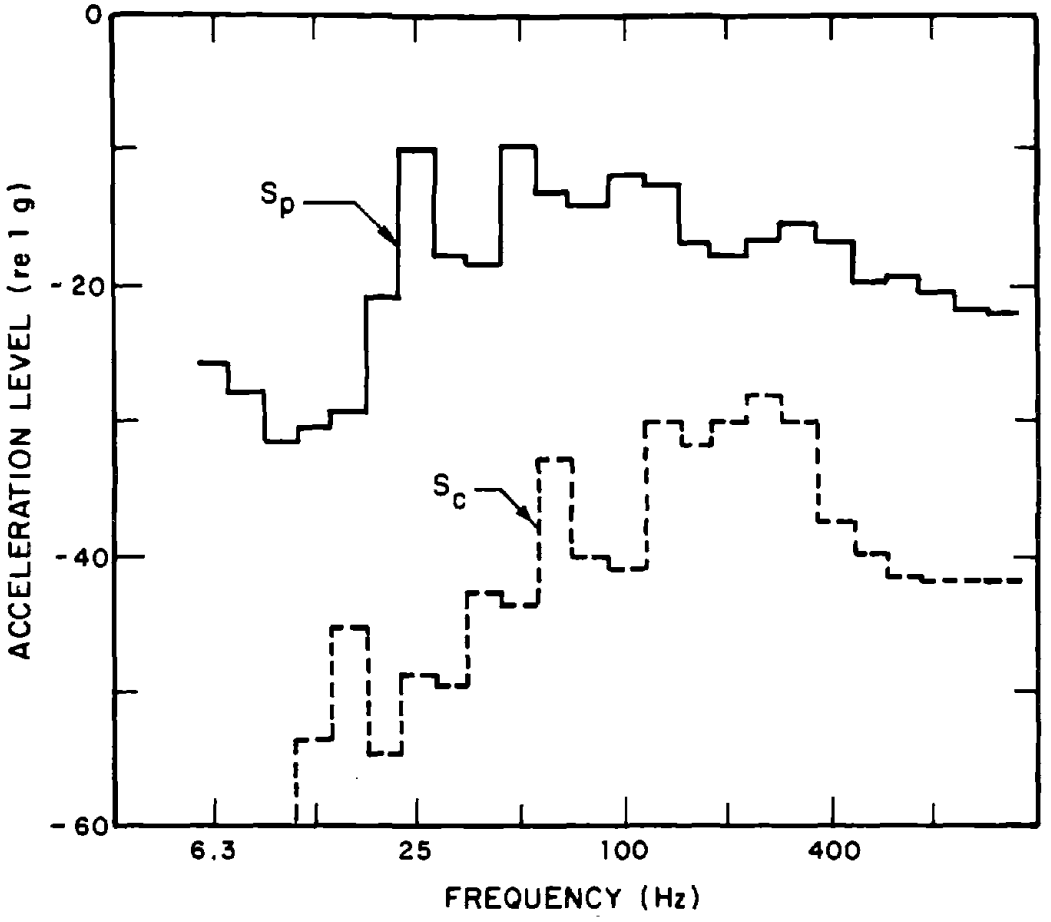

FIG. D-5 SPECTRUM FOR WAVY SURFACE

D.6 Conclusion

The above measurements show that the roughness measuring device operates properly, and that data produced by it in the 6- to 200-Hz range are reliable. In addition, the measured transfer functions can be used to reduce the new data, up to about 200 Hz. Above that frequency, there is a strong resonance or antiresonance at 400 Hz that makes data taken near that frequency of questionable validity.

The operating range in frequency can be easily translated to the operating range in wavelength by

$$\lambda = \frac{u}{f} \quad ,$$

where u is the carriage velocity. For a carriage velocity of 3 ft/sec (0.91 m/sec), the 6-to 200-Hz frequency range implies a 6 in. (15.2 cm) to 0.015-in. (0.38-mm) wavelength range. For a transit vehicle traveling at 50 mph (80 km/hr) this would give a frequency range of ~140 Hz to ~6000 Hz, well in the range of interest.

APPENDIX E: REPORT OF INVENTIONS AND INNOVATIONS

The following inventions and innovations were made during the course of the program described in this report:

- A device for the measurement of wheel/rail roughness, pp. 133 to 147 and Appendix D.
- The resiliently treaded wheel, pp. 257 to 260.
- The low rail barrier, pp. 252 to 255.
- The constrained layer damped wheel, pp. 161 to 164.

REFERENCES

Bailey, J.R. and Fahy, F.J. (1972). "Radiation and Response of Cylindrical Beams Excited by Sound," *ASME Trans. J. of Engineering for Industry*, **94**, Series B, No. 1, pp. 139-147.

Barwell, F.T. and Woolcott, R.G. (1963). "The N.E.L. Contribution to Adhesion Studies," *Proc. Instr. Mech. Engrs.*, **178**, pp. 145-160.

Bender, E.K. and Remington, P.J. (1974). "The Influence of Rails on Train Noise," *J. Sound and Vibration*, to be published.

Crandall, S.H. (1959). "The Timoshenko Beam on an Elastic Foundation," AMFDC-TR-59-8, pp. 79-106.

Dörr, J. (1948). "The Dynamics of a Resiliently Supported Infinite Beam," *Z. Ing. Archiv.*, XVI, No. 5 and No. 6, pp. 287-298 (in German).

Frederich, F. (1970). "Viraftschlussbeanspruchungen am Schrägrolenden Schienfahrzeugrad" (Interaction Forces in Wheels of Rail Vehicles Rolling Obliquely), *Glas. Ann*, **94**, pp. 86-94.

Gramse, H.E. and Spence, J.H. (1974). "Noise and Vibration of a Steel Wheel/Steel Rail Personalized Rapid Transit System," U.S. Department of Transportation, Urban Mass Transportation Administration, Report No. UMTA-MA-06-0027-74-1.

Jenkins, H.H. *et al* (1974). "The Effect of Track and Vehicle Parameters on Wheel/Rail Vertical Dynamic Forces," *Railway Engineering J.*, **94**, No. 1, pp. 2-26.

Kirschner, F. (1972). "New Developments in the Control of Railroad Wheel Screech Noise," The Soundcoat Company, Presented at Internoise 1972 Conference.

Morse, P.M. and Ingard, K.U. (1960). *Theoretical Acoustics*, McGraw-Hill Book Co., New York.

Naake, H. (1953). "Experimental Investigation of the Vibration of Railroad Rails" (in German), *Acustica*, **3**, pp. 139-147.

Remington, P.J. *et al* (1974). "Wheel/Rail Noise and Vibration Control," U.S. Department of Transportation, Urban Mass Transportation Administration, Report No. UMTA-MA-06-0025-74-10, PB 237-012/AS.

REFERENCES (continued)

Rickley, E.J. and Quinn, R.W. (1972). "MBTA Rapid Transit System (Red Line) Wayside and In-Car Noise and Vibration Level Measurements," DOT Report No. DOT-TSC-OST-72-31.

Schultz, T.J. (1974). "Development of an Accustic Rating Scale for Assessing Annoyance to Wheel/Rail Noise in Urban Mass Transit," U.S. Department of Transportation, Report No. UMTA-MA-06-0025-74-2.

Stappenbeck, H. (1954). "Street Car Curve Noise" (in German), *Z. VDI*, **96**(6), pp. 171-175.

Timoshenko, S. (1926). "Method of Analysis of Statistical and Dynamic Stresses in Rail," *Proc. 2nd Int. Congress for Technical Mechanics*, Zürich.

Timoshenko, S. and Goodier, J.N. (1951). *Theory of Elasticity*, McGraw-Hill Book Co., Inc., New York, p. 91.

Ungar, E.E. *et al* (1970). "An Investigation of the Generation of Screech by Railway Car Retarders," BBN Report No. 2067.